

UNIVERSITY OF TWENTE
&
ARCADIS NEDERLAND

MASTER THESIS

**The Effects of Planimetric and
Altimetric Changes on Tidal
Amplification in Coastal Plain
Estuaries**

Author:
Marc T. M. WARMERDAM,
BSc

Supervisors UT:
Dr. Ir. Pieter C. ROOS
M.Sc. Pim W. J. M. WILLEMSEN

Supervisors Arcadis:
Dr. Jelmer CLEVERINGA
Dr. Nathanael GELEYNSE

*A thesis submitted in fulfillment of the requirements
for the degree of Master of Science
in the*

Chair group of Marine and Fluvial Systems
Water Engineering and Management
Faculty of Engineering Technology

January 4, 2018

Abstract

Estuaries are unique coastal features that occur all over the world. Many estuaries are surrounded by densely populated areas and are very important to the local economy, because they provide easy access to shipping ports inland. At the same time they often contain abundant and vibrant ecosystems with unique flora and fauna which are threatened by the expansion of shipping routes in estuaries. Dredging operations are performed to guarantee access to ports for larger ships by widening and deepening the main channels. Recent studies have shown that the structural widening and dredging of main channels in funnel-shaped coastal plain estuaries leads to an increase of the tidal amplification. The increased tidal range is often accompanied with decreased water levels during low tide, endangering shipping access. Additionally, the increased water levels during high increase the risk of flooding and endanger the ecosystem.

The goal of this research is to increase understanding of the processes behind the amplification of the tidal wave in a tidal basin caused by changes in planimetry and altimetry, to predict the effects of certain interventions on the tidal ranges in estuaries.

To this end, an idealized hydrodynamic model has been designed using Delft3D-FLOW to analyze the tidal dynamics in a simplified funnel-shaped estuarine tidal basin. The model has been set-up using the Scheldt Estuary in the Netherlands and Belgium as a case study. This estuary has a typical exponentially decreasing width profile. It also subject to heavy dredging operations to allow access to the port of Antwerp.

A systematic analysis of several planimetric and altimetric characteristics has been performed to assess their influence on the tidal range profile in a tidal basin. Results from the analysis show that the amplification and damping of the tidal wave depends on a combination of the rate of convergence, the length of the converging tidal basin and the depth of the prismatic part upstream of the converging basin. These characteristics influence the tidal range through three basic processes: 1) Amplification through width convergence; 2) amplification through shoaling; 3) damping through bottom friction.

Analysis of historic bathymetric profiles and several artificial interventions has shown that it is possible to increase or reduce the tidal amplification in a tidal basin through human interventions. However, in order to significantly reduce the tidal range large scale interventions are necessary. Additionally, the results show that local increases of bottom elevation hardly reduce the water levels during high tide.

The results of this study show that it is possible to estimate the general effects of planimetric and altimetric changes caused by human interventions in a strongly simplified 2DH hydrodynamic model. The model designed in this study could be used for additional research of the effect of the channel-shoal system on tidal amplification and assess the effects of more detailed and localized interventions.

Foreword

This thesis has been written for the completion of the Master of Civil Engineering and Management at the University of Twente. Over the last 10 months I have had the great opportunity to perform my research as an internship at Arcadis. The motivation of this research stems from the increasing trend of tidal amplification that has taken place over the last decades in the Western Scheldt and the Sea Scheldt located in the Netherlands and Belgium.

During my time at Arcadis I have met many great people and have learned an incredible amount on the subject of estuarine management and numerical modeling. I have had the pleasure of taking a look at the practical side of river and coastal engineering and have seen many new and interesting projects during my time in Zwolle. I have been inspired by the many friendly, open and welcoming people at Arcadis making my internship a period I will remember fondly. In this regard I would like to thank Jos van der Baan, Wessel van der Zee, Sjoerd van Til, Jessica Bergsma and Rufus Velhorst for inviting me to the social drinks and showing me the city of Zwolle.

However, without the help of my supervisors I would not have made it through the project. During my times in need of help, they would provide me with the necessary support by giving great feedback and taking time out of their day. I want to thank Nathanael Geleynse for his positive attitude and great advice and feedback related to both the modeling software and theory behind the research. I would like to thank Jelmer Cleveringa for his incredible practical and critical insights, but always with an undertone of witty humor. I would also like to thank Pim Willemsen for his incredibly fast responses and insightful feedback on the structure of the report and the theory and methods used in the study. Finally, I would like to thank Pieter Roos for introducing me to the subject of marine dynamics and for bringing me into contact with Arcadis. His drive and enthusiasm has inspired me to conduct my final project in this area of expertise.

With this I implore you to dive into the culmination of 10 months of hard but satisfying work,

Marc Warmerdam,

16-11-2017

Contents

1	Introduction	1
1.1	Estuaries	1
1.2	Theoretical background	2
1.2.1	Estuarine characteristics	2
1.2.2	Classification	3
1.2.3	General estuarine processes	5
1.2.4	Hydrodynamic processes	5
1.2.5	Tidal amplification	9
1.2.6	Morphology	11
1.3	Problem definition	11
1.4	Research questions and objective	12
1.5	Outline	13
2	Methods	15
2.1	Study site	16
2.1.1	Physical characteristics	16
2.1.2	Human interventions	18
2.2	Data analysis	19
2.2.1	Water level data	19
2.2.2	Bathymetric data	21
2.3	Model description	23
2.4	Model set-up	24
2.4.1	Model parameters	25
2.4.2	Numerical grid design	26
2.4.3	Model output	28
2.4.4	Calibration and validation of model	30
2.4.5	First set-up with Van Rijn's model	30
2.5	Systematic model analysis	33
2.5.1	Step A: Lateral boundaries	35
2.5.2	Step B: Uniform depth	36
2.5.3	Step C: Longitudinal slope	37
2.5.4	Step D: Channel-shoal system	37
2.5.5	Step E: Interventions	38
3	Results: Data Analysis	41
3.1	Water level analysis	41
3.1.1	Tidal range profile	41
3.1.2	Tidal deformation	43
3.2	Bathymetry analysis	44
3.2.1	Longitudinal profile	46
3.2.2	Cross-sectional hypsometry	48

4	Results: Systematic Model Analysis	51
4.1	Step A: Lateral boundaries	51
4.2	Step B: Uniform depth	54
4.3	Step C: Longitudinal slope	56
4.4	Step D: Channel-shoal system	58
4.4.1	Without longitudinal slope	58
4.4.2	With longitudinal slope	60
4.5	Step E: Interventions	62
4.5.1	Historical analysis	62
4.5.2	Intervention scenarios	64
4.6	Validation underlying processes	67
5	Discussion	69
5.1	Uncertainty in data	69
5.2	Bathymetric analysis	69
5.3	Channel-shoal design	69
5.4	Order of systematic analysis	70
5.5	Hydrodynamic processes	70
6	Conclusion	73
7	Recommendations	75
	Bibliography	77
	Appendices	79
A	Estuary Classifications	81
B	Dredging volumes	85
C	Van Rijn Model Validation	87
D	Sedimentation and erosion maps	91
E	Bathymetric cross-sections	93
F	Cross-sectional depths	95
G	Model output	103

List of Figures

1.1	Example of an estuary, The Thames estuary, UK	1
1.2	Simplified representation of a funnel-shaped estuary	2
1.3	Schematic representation of an alluvial estuary	4
1.4	System of physical processes in the estuarine system, also known as the morphological loop	5
1.5	Curve of a tidal wave	6
1.6	Shoaling of tidal wave	8
1.7	Deformation of tidal wave	9
1.8	Damping of tidal wave	9
1.9	Examples of channel-shoal patterns typical for alluvial estuaries	11
1.10	Historical evolution tidal amplification in Scheldt estuary	12
2.1	The Scheldt estuary	15
2.2	Overview plates Western Scheldt	16
2.3	Vertical tide Western Scheldt	17
2.4	Historic HW and LW Western Scheldt	18
2.5	Example of a relative tidal range profile	20
2.6	Western Scheldt cross-sections	21
2.7	Example of channel-shoal schematization	22
2.8	Model geometry of idealized basin	24
2.9	Example of rectangular numerical grid	27
2.10	Example of curvilinear numerical grid	28
2.11	Jump in lateral boundary of computational grid	28
2.13	Prismatic basins Van Rijn	31
2.14	Converging basins Van Rijn	32
2.15	Tidal range profile of reference model	33
2.16	Overview systematic analysis	34
2.17	Changing of planimetric variables	35
2.18	Changing of uniform altimetric variables	36
2.19	Changing of slope variables	37
3.1	Tidal range profile Scheldt estuary around 1900	42
3.2	Tidal range profile Scheldt estuary around 1955	42
3.3	Tidal range profile Scheldt estuary around 2000	42
3.4	Tidal curves in Scheldt estuary at spring tide	43
3.5	Tidal curves in Scheldt estuary at neap tide	43
3.6	Bathymetry Western Scheldt 1955	44
3.7	Bathymetry Western Scheldt 2005	44
3.8	Evolution of bathymetry in Western Scheldt	45
3.9	Hypsometry of Western Scheldt	45
3.10	Western Scheldt cross-sections	46
3.11	Longitudinal depth and width Western Scheldt	46
3.12	Rate of convergence along Western Scheldt	47

3.13	Longitudinal cross-sectional flow area Western Scheldt	47
3.14	Depth profile cross-section 7	48
3.15	Depth profile cross-section 14	48
3.16	Depth profile cross-section 28	48
3.17	Cross-sectional hypsometries for 1955 and 2005 of the Western Scheldt	49
3.18	Comparison total hypsometry against cross-sectional hypsometry	49
3.19	Characteristic cross-sectional depth profile	49
4.1	Modeled tidal ranges for different basin geometries	51
4.2	Computational grid of optimal geometry	53
4.3	Modeled tidal ranges for varying uniform depth	54
4.4	Tidal ranges of different slope scenarios	56
4.5	Tidal ranges of different slope scenarios	56
4.6	Top-down view of an example of channel-shoal bathymetry	58
4.7	Cross-sectional profiles model cases D1, D2 and B6	58
4.8	Comparison tidal range profiles of models with and without a channel-shoal system	59
4.9	Tidal range output for models D3 and D4	60
4.10	Longitudinal bottom profiles of Scheldt estuary used in model schematization	62
4.11	Modeled relative tidal range profiles based on historic bathymetric data	63
4.12	Altimetric profiles short interventions	64
4.13	Altimetric profiles long interventions	64
4.14	Tidal range short interventions	64
4.15	Tidal range long interventions	65
4.16	Tidal range interventions with channel profile	65
4.17	Water levels interventions with channel profile	66
4.18	Deformation of tidal wave in model A14	67
4.19	Phase lag along estuarine basin for case A14	68
4.20	Flow velocity curve at multiple locations in modeled basin	68
4.21	Flow speed profile A14	68
A.1	Examples of different types of estuaries	82
A.2	Types of mixing and water circulation	83
B.1	Historicity of dredging in Sea Scheldt	85
B.2	History of dredging in Western Scheldt	85
C.1	Van Rijn prismatic cases modeled tidal range profiles	87
C.2	Van Rijn prismatic cases tidal range outcome	87
C.3	Van Rijn converging cases modeled tidal range profiles	88
C.4	Van Rijn converging cases tidal range outcome	89
D.1	Deepening of Scheldt Bathymetry 2005	91
D.2	Shallowing of Scheldt Bathymetry 2005	91

List of Tables

1.1	Overview of estuary classifications	4
1.2	Major tidal constituents	6
1.3	Wave characteristics	7
1.4	Wave characteristic relationships	7
2.1	Geometric and tidal data of Scheldt estuary	17
2.2	Sources of tidal range data Scheldt estuary	19
2.3	Model geometry parameters	25
2.4	Parameters related to the model boundary conditions	25
2.5	Parameters related to computational grid	26
2.6	Temporal model parameters	27
2.7	Physical parameters used in Delft3D	27
2.8	Prismatic tidal basins	31
2.9	Converging tidal basins	31
2.10	Reference model parameters	33
2.11	Geometry parameters used for sensitivity analysis	36
2.12	Slope cases and their parameters	37
2.13	Channel Cases implemented for sensitivity analysis	38
2.14	Intervention scenarios	38
3.1	Tidal range profile characteristics Scheldt estuary	41
3.2	Ebb and flood phase duration in Scheldt estuary	44
4.1	Step A models maximum tidal range values	52
4.2	Step A relative tidal range peak locations	52
4.3	Validation of spatial geometry	52
4.4	Tidal range output and validation uniform depth changes	55
4.5	Step C: Slope - Model output and validation results	57
4.6	Tidal range characteristics and validation results channel-shoal no slope	59
4.7	Step D: Channel-shoal - Model output and validation results	60
4.8	Tidal range characteristics and validation results for historic and present bottom profiles of Scheldt estuary	63
4.9	Flood/ebb durations model A14	67
C.1	Results prismatic models Van Rijn at mouth of basin	88
C.2	Results converging models Van Rijn at mouth of basin	89
E.1	Bathymetric data cross-sections 1955	93
E.2	Bathymetric data cross-sections 2005	94

1 Introduction

1.1 Estuaries

Estuaries are common coastal features located all over the world. They are unique systems that form at locations where a river flows into the ocean (Figure 1.1). This creates a complex transitional zone between riverine and marine environments. The basic definition of an estuary is described by [Cameron and Pritchard \(1963\)](#):

“An estuary is a semi-enclosed body of water having a free connection with the open sea and within which seawater is measurably diluted with fresh water derived from land drainage.”

The complexity of estuaries stems from both their physical characteristics and processes, and the environmental and human functions it fulfills. The areas surrounding tidal basins are often densely populated and have high economic value, while being home to abundant ecological systems ([McDowell and O’Connor, 1977](#); [Levinton, 1995](#); [US Department of Commerce and NOAA, 2008](#)). This creates a set of interests that tend to be in conflict with each other, causing tensions between functions and users within the estuary ([McDowell and O’Connor, 1977](#); [Perillo, 1995](#)). Economic values are generally the main driver for interventions in estuaries ([Perillo, 1995](#)). Economic growth causes the expansion of inland ports, increasing both the number and size of ships passing through the estuary. To guarantee shipping access and allow safe navigation through estuaries, deepening and widening operations of the main channels are performed. Other interventions, such as land-reclamation and embankment, are driven by population growth and flood safety ([NOAA, 2017](#)).

In the past, an integral approach to implementing such interventions and policies was missing ([Perillo, 1995](#); [Taal, Meersschaut, and Liek, 2015](#)). It remains difficult to predict the effects of interventions in the estuarine system and many unexpected side-effects have been observed in estuaries around the world. Although short-term economic and social goals are met, long-term effects and stability of the estuarine system has not been considered in policy making until recently ([McDowell and O’Connor, 1977](#); [Perillo, 1995](#); [Taal, Meersschaut, and Liek, 2015](#)).

With the rise of an integral approach, there is an ongoing effort to improve understanding of all aspects of the estuarine system. From the many problems that require



FIGURE 1.1: Example of an estuary, The Thames estuary, UK

further study, this thesis will focus on the process of tidal amplification in alluvial funnel-shaped estuaries in connection with planimetric and altimetric changes caused by interventions such as dredging and dumping operations. The Scheldt estuary in The Netherlands is an example of an estuary with these characteristics and will be used as a case study in the research.

1.2 Theoretical background

Estuaries have been subject to extensive research in the past decades. This section will introduce relevant concepts related to estuaries and tidal amplification. The focus will be on the physical description and classification of estuaries, the hydrodynamics processes and the morphological characteristics of an estuarine basin.

1.2.1 Estuarine characteristics

As stated in the definition by [Cameron and Pritchard \(1963\)](#), an estuary is a semi-enclosed basin with an opening to the sea, receiving fresh water from river discharge upstream (Figure 1.2). Estuaries come in many shapes and sizes and have numerous characteristics that define their appearance and physical behavior ([McDowell and O'Connor, 1977](#)). A description of some important characteristics is given below:

Shape The shape of an estuary is defined by (semi-)rigid boundaries imposed by the elevation of the surrounding land. This can range from very mountainous banks to sandy sedimentary deposits. The boundaries of an estuary can evolve due to erosion and sedimentation, but the temporal scale of this process is in the order of centuries and millennia, which is significantly longer than that of other processes ([Van der Wegen, Wang, et al., 2008](#); [Van der Wegen and Roelvink, 2012](#)). The shape of the tidal basin plays an important role in the circulation of water throughout the estuary and on the propagation and deformation of the incoming tidal wave.

Size The size of an estuary is an important aspect to tidal wave propagation and morphological evolution. The length and width of estuaries can range from tens to hundreds of kilometers. The exact size of an estuary can be up for debate as the upstream limit is hard to define. Generally, the length of the estuary is defined as the area where a oscillatory motion of water is observed. This motion is damped by bottom friction and river discharge ([McDowell and O'Connor, 1977](#); [Savenije, 2001](#)). At some point upstream, the oscillatory motion will disappear and river dynamics become dominant, which is called the tidal limit ([McDowell and O'Connor, 1977](#)).

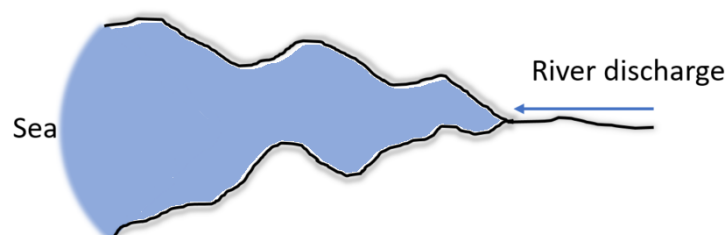


FIGURE 1.2: Simplified representation of a funnel-shaped estuary

Climate The climate in which an estuary is located has implication for the temperature of sea and river water. It also influences ecological processes and defines the types of fauna and flora within an estuary (Levinton, 1995). Different types of plants can influence the hydraulic roughness of the bed profile, or act as a sediment sink for material in suspension.

Tidal regime The tidal regime is the shape of the incoming tidal wave at the mouth of the estuary. It is described by the fluctuations in water level (vertical tide) and flow velocity (horizontal tide). An important indicator is the tidal range, which is the difference between high water (HW) and low water (LW) (Hayes, 1975). The tides on open ocean are relatively small, but due to shoaling, funneling and resonance of the tidal wave some basins experience tidal ranges of 12 m or higher, such as the Bay of Fundy, Canada and the Severn Estuary, between Wales and England (NOAA, 2017).

River discharge The river discharge and the volume of sediments carried into the tidal basin play an important role in many physical processes. The ratio between river discharge and tidal currents define the type of mixing of salt and fresh water. The amount and type of sediment from upstream can significantly influence the morphological evolution in the estuary.

Salinity Water in estuaries is a mix of salt seawater and fresh river discharge. The type of mixing profile in estuaries are dependent on the salinity of incoming seawater and the ratio between the strength of tidal currents and river flow (Appendix A). Estuaries often experience a gradual change from salt to fresh water in landward direction. This gradient in salt concentration can influence water circulation and sediment transport processes. On average, seawater has a salinity of approximately 3.5% (35 g salt per liter water) and has a higher density than fresh water.

Type of sediment Sediments in estuaries influence the development of bed forms and channels in the alluvial plain. Sediment grain size is an important aspect in the suspension and transport of material through water motion. In general, the material transported by water can be divided in three groups (McDowell and O'Connor, 1977):

- Clay-sized particles ($< 2\mu m$)
- Silt-sized particles (between $2\mu m$ and $60\mu m$)
- Coarse sand and gravel ($> 60\mu m$)

1.2.2 Classification

The complexity and large variety of estuarine systems around the world makes it difficult to generalize problems and solutions across multiple estuaries (Perillo, 1995). To tackle this problem and to streamline research efforts, classifications have been made based on similarities in physical characteristics and certain physical behaviors (Perillo, 1995). Three basic classifications still used today, have been defined (Pritchard, 1967; J. L. Davies, 1964). According to them, estuaries can be grouped based on geologic features, water circulation processes and tidal regime (Table 1.1).

Although many different types of estuaries exist, the most common type of estuary is found around the world is the coastal plain estuary (Pritchard, 1967; Perillo, 1995). As described in appendix A, this type of estuaries are inundated river valleys

Geologic Features	Water Circulation	Tidal Regime
Coastal plain	Salt-wedge	Micro
Tectonic	Partially mixed	Meso
Bar-built	Well-mixed	Macro
Fjord	Fjord-type	

TABLE 1.1: Overview of estuary classifications (Pritchard, 1967; J. L. Davies, 1964). For detailed explanation see Appendix A

originating from the previous ice age. These types of estuaries are relatively shallow and show a steady bottom slope with a deep wide mouth and shallow narrow landward boundary. Coastal plain estuaries evolve due to processes of infilling and erosion and depending on the initial shape of the coastal plain several stages of evolution can be recognized (Cameron and Pritchard, 1963). Young coastal plain estuaries show a significant average bed slope throughout the tidal basin and no significant channel-shoal systems are developed yet. Over centuries to millenia, the processes of sedimentation and erosion cause the bed slope and geometry to evolve to a typical shape observed in many older coastal plain estuaries (Savenije, 2005). This is supported by several morphological studies by Hibma, Vriend, and Stive (2003) and Van der Wegen, Wang, et al. (2008). The process of infilling causes the average bed slope to become less pronounced in the lower and middle regions of the estuary. Additionally, erosion of the lateral boundaries creates a characteristic funnel-shape with an exponentially decreasing width in landward direction (Figure 1.3). This type of late stage coastal plain estuaries is called alluvial estuaries (Savenije, 2005). The name stems from the presence of an alluvial plain with a dynamic system of channels and shoals observed in many of these estuaries. Alluvial estuaries show great similarities in processes regarding hydrodynamics and sediment transport (Savenije, 2005; Savenije, 2001; Van Rijn, 2010).

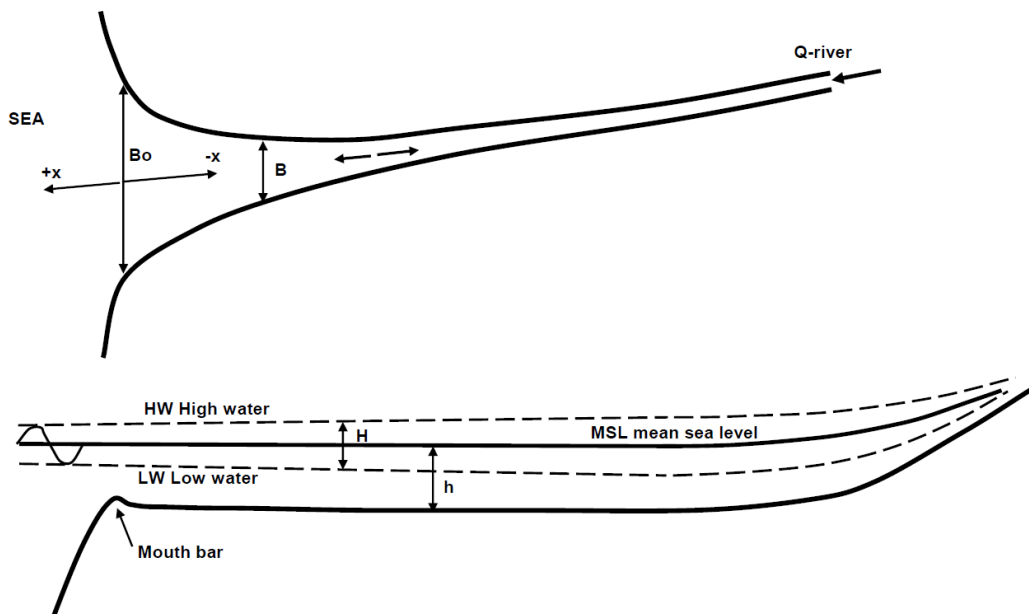


FIGURE 1.3: Schematic representation of an alluvial estuary with a top-down view (upper picture) and side-view (lower view). Source: Van Rijn (2010, p.9)

1.2.3 General estuarine processes

The behavior of an estuary is governed by the processes in the estuarine system. There are many different processes such as, ecological, morphological, hydrodynamic, chemical, and sediment transport processes. The individual processes are well understood, but the interaction of different aspects of the estuarine system create a complex system. By focusing on the physical processes, [McDowell and O'Connor \(1977\)](#) mention that the physical behavior of an estuary can be schematized as a loop of three distinct categories, namely hydrodynamics, sediment transport processes and morphodynamics (Figure 1.4).

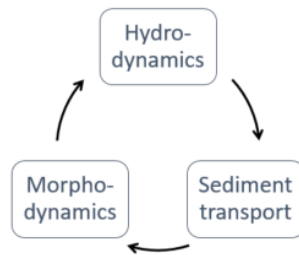


FIGURE 1.4: System of physical processes in the estuarine system, also known as the morphological loop

Tidal motion and river flow are external forces acting upon the estuarine system. Water movement caused by tidal and river currents can pick up sediments and bring them in suspension, transporting the material to other locations. The transport processes depend several hydrodynamic aspects and on the characteristics of the available sediments in the tidal basin. Additionally, river discharge can bring new sediment material into the estuary from upstream creating a source of sediment material. The picking up and deposition of sediments in suspension causes an evolution of the bed, which in turn influences the water circulation in the tidal basin. This creates a feedback loop between the different processes, causing an indefinitely evolving estuarine system. It also means that any intervention related to a single process will inadvertently have effects on other physical aspects in the ([McDowell and O'Connor, 1977](#)).

1.2.4 Hydrodynamic processes

Hydrodynamic processes describe the movement of water in an estuary. It is driven by tidal motion coming from the ocean and from river discharge upstream. River discharge is considered as a uni-directional flow of fresh water in seaward direction, whereas tidal motion cause a periodic in- and outflow of water (flood and ebb flow). Tidal dynamics play a dominant role in the lower regions of an estuary, while river dynamics can play a dominant role in the upper regions of an estuary ([McDowell and O'Connor, 1977](#)). This division of processes strongly depends on the relative strength of the tidal currents compared to the strength of river flow. This comparison can be made based on the ratio between the tidal prism¹ and the total river discharge during one tidal cycle. When river discharge per tidal cycle is in the same order of magnitude as the tidal prism, estuaries experience a distinct upstream and downstream part with riverine and marine processes respectively. When river discharge is small compared to the tidal prism, tidal dynamics can dominate most of the estuarine basin. In some

¹The volume of water that leaves or enters an estuary between high and low tide

cases no riverine processes are observed in the tidal basin due to the presence of a solid obstacle, such as a sluice.

Another aspect influenced by the ratio tidal prism and river discharge is the mixing profile of salt and fresh water throughout an estuarine basin. Gradients in salt concentration cause density differences in the water profile, which create a force in the direction of decreasing salt concentration. In an estuary with strong stratification, this can lead to complex vertical and lateral flow structures (McDowell and O'Connor, 1977).

With the focus on tidal amplification, it is important to understand the basic tidal wave dynamics. This entails the forcing caused by astronomical forces, propagation of a tidal wave and the deformation of the wave as it approaches and travels along the coastline. The next few sections will explain the basic theory behind tidal wave dynamics in deep and shallow water.

Tidal wave generation

A tidal wave is the rise and fall of water levels in seas and oceans around the world. This is caused by the gravitational pull of the sun and the moon acting on the body of water on earth, known as the vertical astronomical tide. Due to the rotation of the earth around the sun and the moon around the earth, this creates a propagating wave around the globe. The crest and trough of the wave are known as high water (HW) and low water (LW) and the difference between them is called the tidal range.

Tidal waves have long wave lengths, in the order of hundreds or thousands of kilometers. Usually, the period of a tidal wave is about 12.42 hours, known as a lunar semi-diurnal tide (M_2). In some locations the tide is asymmetrical, causing the tidal wave to have a period of 24 hours, known as a diurnal tide. Although the rise and

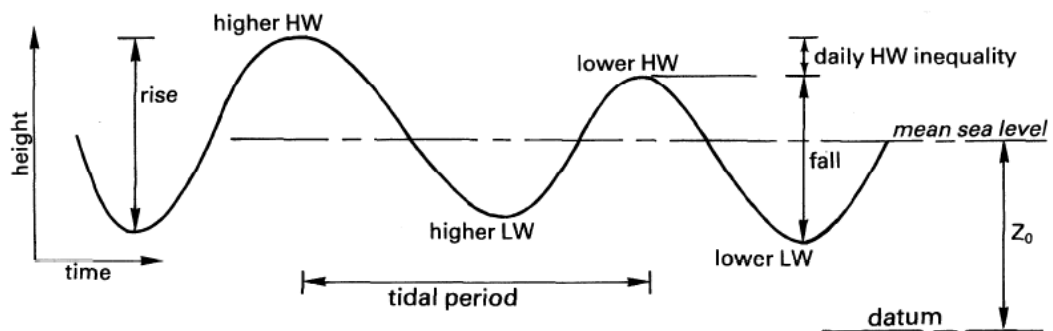


FIGURE 1.5: Curve of a tidal wave. Source: Van Rijn (2010, p. 3)

Origin	Symbol	Period (hours)
Main Lunar, semi-diurnal	M_2	12.42
Main Solar, semi-diurnal	S_2	12.00
Lunar Elliptic, semi-diurnal	N_2	12.66
Lunar-Solar, semi-diurnal	K_2	11.97
Lunar-Solar, diurnal	K_1	23.93
Main Lunar	O_1	25.82
Main Solar	P_1	24.07

TABLE 1.2: Major tidal constituents

fall of the tide is periodic, successive tidal cycles have different HW, LW and tidal ranges due to the complicated motion of the sun and the moon. This is known as the daily inequality and is shown in figure 1.5.

The tide generating forces can ultimately be expressed using harmonic constituents. The astronomical harmonic constituents each describe a separate motion of a relevant astronomical body. Each constituent has its own period and relative strength on the body of water on earth. Because the harmonic constituents all have different periods and relative strengths, this creates a very complicated tidal signal. Table 1.2 shows the 7 major astronomical constituents that account for 83% of all tide generating forces on earth (Van Rijn, 2010). An additional tidal signal not shown in table 1.2 is the well known spring-neap cycle. This cycle has a period of 14.8 days and is generated due to the interaction of the sun and the moon. Spring tide happens when the sun and moon are in alignment, while neap tides occur when the sun and moon have right angles (Van Rijn, 2010).

Tidal wave propagation

Assuming a monochromatic wave in deep water, the propagation of the wave is formulated as follows:

$$\zeta(x, y, t) = \hat{\zeta}(y) \cos(kx - \sigma t + \phi_{\zeta}) \quad (1.1)$$

Angular velocity	σ	[rad/s]	Temporal structure of the wave
Wave number	k	[rad/m]	Spatial structure of the wave
Elevation amplitude	$\hat{\zeta}(y)$	[m]	Wave amplitude in y direction
Phase constant	ϕ_{ζ}	[rad]	The wave state at $x = 0$ and $t = 0$
Wave speed	c	[m/s]	Celerity of the wave (σ/k)

TABLE 1.3: Wave characteristics

In reality, a tidal wave is a combination of many wave constituents and is subject to drag forces caused by bottom friction and reflection due to obstacles, such coastlines of continents.

Tidal waves on deep open ocean are generated by astronomical forces described in the previous section. These forces define the wave period T and the elevation amplitude $\hat{\zeta}$. The other wave characteristics can be derived using these characteristics and depend on the water depth through which the wave is moving. These relations are derived from linear wave theory and are shown in table 1.4.

Deep water ($kh \gg 1$)	Shallow water ($kh \ll 1$)
$\sigma^2 = gk$	$\sigma^2 = gk^2h$
$c = \frac{gT}{2\pi}$	$c = \sqrt{gh}$
$L = \frac{gT^2}{2\pi}$	$L = \sqrt{gh}T$

TABLE 1.4: Relationships between wave characteristics, where g is gravitational acceleration [m/s^2], T the wave period [s], h the average water depth [m]

As a tidal wave enters shallow waters and approaches coastal areas it experiences deformation effects. According to Van Rijn (2010) there are four basic phenomenon that cause this to happen:

- Reflection
- Amplification
- Deformation
- Damping

The propagation and shape of a tidal wave in coastal areas and tidal basins depends on the shape of the incoming tidal wave from the ocean and the four processes mentioned above. Astronomical forces do not play a significant role in the propagation and shape of a tidal wave in these areas and can be neglected.

A tidal wave can be **reflected** by sudden obstacles in the path of the tidal wave. A reflected wave travels in the opposite direction of the incoming tidal wave and will interfere with the tidal signal causing deformation and generation of the higher harmonic components mentioned before. A tidal wave can be partially reflected when it travels over a sudden obstacle or completely reflected when it travels against a vertical boundary. In a tidal basin such as an estuarine basin this can create a standing wave and resonance may occur if the length of the tidal basin is in the same order of magnitude as a quarter of the wave length of the tidal wave. In case of partial reflection the transmitted wave has a shorter length than the incoming wave, but a larger height, which is known as shoaling.

Amplification is the increase in wave height caused by shallowing (changes in altimetry) and gradual convergence of lateral boundaries (changes in planimetry). The former is called shoaling and is explained in this section. The latter process is explained separately in section 1.2.5. When the depth slowly decreases, the wave height increases as it propagates in direction of the shallowing. This phenomenon can be explained with Green's Law which uses definition of the energy flux of a wave. This consists of the following equations:

$$E = \frac{1}{8} \rho g b H^2 \quad (1.2)$$

$$F = E c \quad (1.3)$$

Where E is the energy per unit length of the tidal wave [N], ρ is the water density [kg/m^3], b the channel width [m], H the wave height [m], h the water depth (in relation to the mean water level) [m] and F the energy flux [Nm/s].

In the ideal case that there is no reflection and loss of energy through bottom friction the energy flux remains constant:

$$E_0 c_0 = E_x c_x \quad (1.4)$$

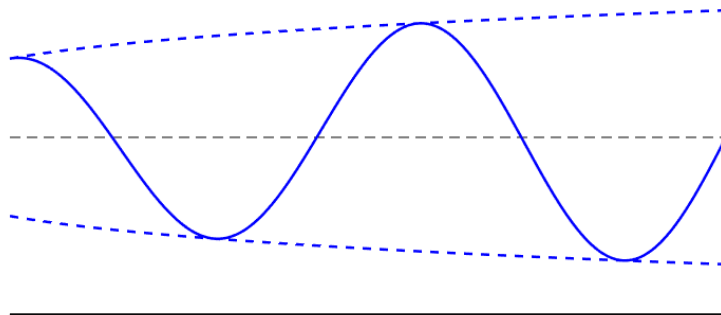


FIGURE 1.6: Amplification caused by shoaling

This shows that when the depth decreases, the wave height has to increase to satisfy equation 1.4.

Deformation of a tidal wave is caused by non-linear effects. Flow velocities in the water column have a vertical gradient caused by bottom friction. Water flow faster at the surface and slower near the bottom of the water column. Consequently, the top of a wave moves faster than the water in the troughs of a wave. The wave peak will 'overtake' the troughs causing a deformation of the sinusoidal wave profile (figure 1.7). Other processes causing skewness of the wave profile are higher harmonics generated from by (partial) reflection and shoaling.

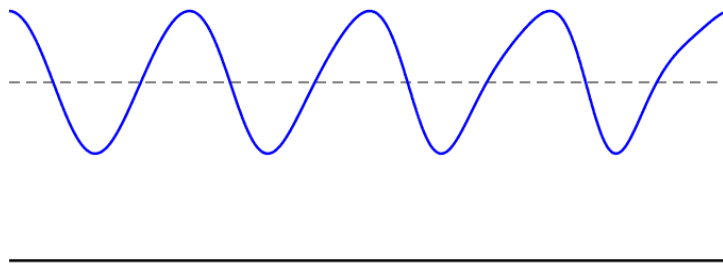


FIGURE 1.7: Deformation of the sinusoidal wave profile caused by higher harmonics and non-linear processes

Finally there is the process of damping. **Damping** of the tidal wave means that wave height is reduced as it progresses over shallow bed elevations. This reduction in wave height is caused by dissipation of wave energy through friction with the bed and between moving water layers. (figure 1.8).

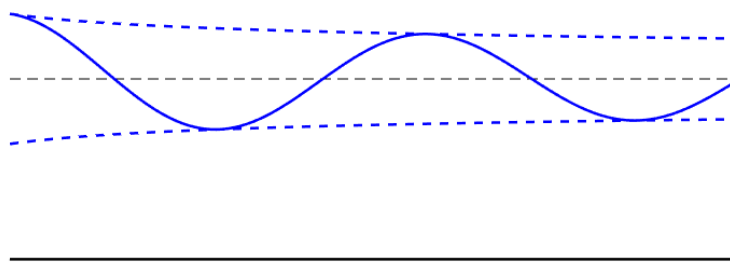


FIGURE 1.8: Reduction of tidal amplitude caused by dissipation of energy

1.2.5 Tidal amplification

As explained by the processes in the previous section, a tidal wave entering an estuary will start to deform. Assuming an open landward boundary and an elongated profile (Figure 1.3), the amplification of the tidal range fully depends on the rate of convergence of the lateral boundaries, shallowing and the average water depth (Savenije, 2001). When shoaling by reflection and convergence is stronger than energy dissipation, amplification will occur. When these processes are in perfect balance the tidal

range will remain constant throughout the estuary. According to Van Rijn (2010), this means three categories of estuaries can be recognized:

1. Amplified ($H/H_0 > 1$)²
2. Damped ($H/H_0 < 1$)
3. Equilibrium ($H/H_0 = 1$)

Savenije (2001) found an analytical solution to describe tidal amplification in an idealized tidal basin with an exponentially decreasing width profile. This exponential profile is typical for alluvial estuaries (section 1.2.2) and can be described by:

$$b(x) = b_0 \exp(-x/\gamma) \quad (1.5)$$

With $b(x)$ is the width at location x [m], b_0 is the width at the mouth [m], x the longitudinal distance from mouth [m] and γ the width decreasing e-folding length scale [m]. Savenije (2001) suggests that this profile is characteristics for any estuary and deviations from this shape are either caused by non-erodable outcroppings and bottom layers or because the estuary has not fully developed yet. The analytical solution by Savenije (2001) uses several dimensionless parameters to describe tidal amplification. These parameters can be led back to simple physical parameters that describe bottom friction, water depth, tidal asymmetry and convergence of the geometry. The analytical solution is shown in equations 1.6, 1.7, 1.8 and 1.9.

$$\frac{dy}{dx} = \frac{\alpha}{\beta} \frac{H_r el}{(\alpha + H_r el)} \quad (1.6)$$

$$H_r el = \frac{H}{H_0} \quad (1.7)$$

$$\alpha = \frac{2c\nu \sin \epsilon}{gH_0} \quad (1.8)$$

$$\frac{1}{\beta} = \frac{1}{\gamma} - \frac{fg \nu \sin \epsilon}{C^2 ch} \quad (1.9)$$

Where $H_r el$ is the dimensionless tidal amplification, α the dimensionless tidal Froude number, β the tidal damping scale [m], H_0 the tidal range at the basin mouth [m], ν the amplitude of the tidal velocity [m/s], ϵ the phase lag between HW and HW slack [rad] and f a friction factor accounting for difference in average water depth during ebb and flood flow. The solution states that whether a section of the tidal basin is damped or amplified depends on the ratio of β/α :

- $\beta/\alpha > 0$ is an amplified basin
- $\beta/\alpha < 0$ is a damped basin

Vandenbruwaene et al. (2013) performed an analysis on tidal amplification on four alluvial estuaries and found reasonable results using the analytical solution compared to measured amplification factors. However a shortcoming of the analytical solution is that it does not account for exponential friction and complex bathymetric profiles. Van Rijn (2010) expanded on the analysis of tidal amplification by comparing the analytical results to numerical outcomes. For basins with an open landward boundary the results were comparable. Unfortunately, in basins with a closed landward boundary the complete reflection causes the analytical solution to fall apart in the upper regions of the estuary.

² H_0 is the tidal wave height (or tidal range) at the seaward boundary of a specified domain

1.2.6 Morphology

The morphology in an estuary depends on the available sediments and the water circulation (Figure 1.4). In estuaries with an alluvial bed the to-and-fro motion of the tide creates complex channel-shoal systems. Ahnert (1960) found that estuarine meanders are distinctly different from river meanders. This is caused by the ingoing and outgoing tidal flows. The reversal of flow during a tidal cycle creates separate flood- and ebb-channels that evade each other. Both Ahnert (1960) and Van Veen et al. (2005) noticed that the channel-shoal system shows a repeating pattern over the length of tidal basins. Figure 1.9 shows two channel patterns observed in Chesapeake Bay, US and the Western Scheldt, The Netherlands.

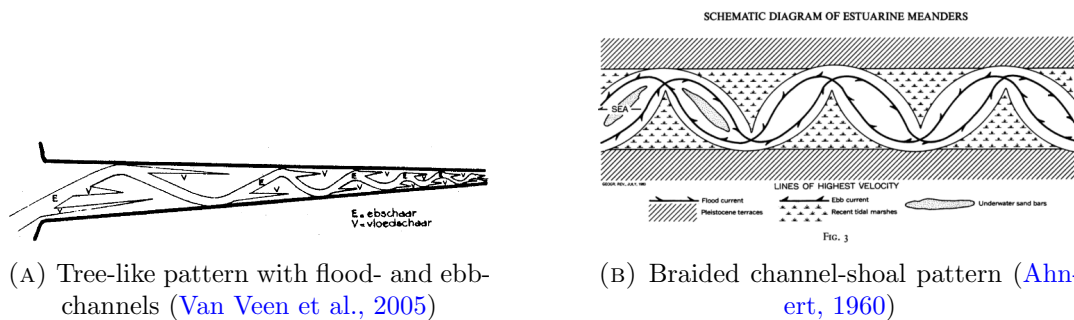


FIGURE 1.9: Examples of channel-shoal patterns typical for alluvial estuaries

The channel shoal pattern influences the deformation of the tidal wave. In a tidal cycle the intertidal areas are flooded during the flood phase and lay dry during the ebb phase. This means that the average depth and surface area of the flow cross-section are significantly different during the flood and ebb stages. J. M. Brown and A. G. Davies (2007) state that the ebb- and flood-dominance in an estuary can be attributed to the relative extent of the channels and shoals. The frictional drag on the water column decreases as the water level increases. This serves to reduce the time between LW and the subsequent HW and increases the time between HW and the following LW. This creates a relatively short, but strong flood phase and a longer weaker ebb phase. A tidal wave can be ebb-dominant at the mouth of an estuary, due to reflection and creation of higher harmonics. But, can turn flood-dominant upstream as it flows over the channel-shoal system. This has implications for the net sediment transport (J. M. Brown and A. G. Davies, 2007).

1.3 Problem definition

Many estuaries around the world experience some form of amplification of the incoming tide. This is in principle caused by the relationship between the average bottom depth, the rate of convergence of the lateral boundaries and the tidal characteristics (Section 1.2.5). There is strong evidence that human interventions have made an impact on the tidal amplifications in some estuaries. Historic water level data, in conjunction with data on bathymetry, shows that the tidal amplitude has increased significantly in several estuaries (Peters, 2002; Taal, Meersschaat, and Liek, 2015; Winterwerp, 2013). Figure 1.10 shows the historic tidal range profiles for the Western Scheldt, which is an example of an estuary coping with problems of tidal amplification. Many interventions that alter the planimetry and altimetry of an estuary have an influence on the tidal ranges throughout an estuary. Embankments and land

reclamation change the shape of the lateral boundaries increasing the narrowing of an estuary. Winterwerp (2013) found that dredging also has a significant influence on the tidal propagation and amplification. Dredging operations have increased the depth and width of main channels in many estuaries around Europe and change the hydraulic resistance of the bed by bringing fine sediments in suspension.

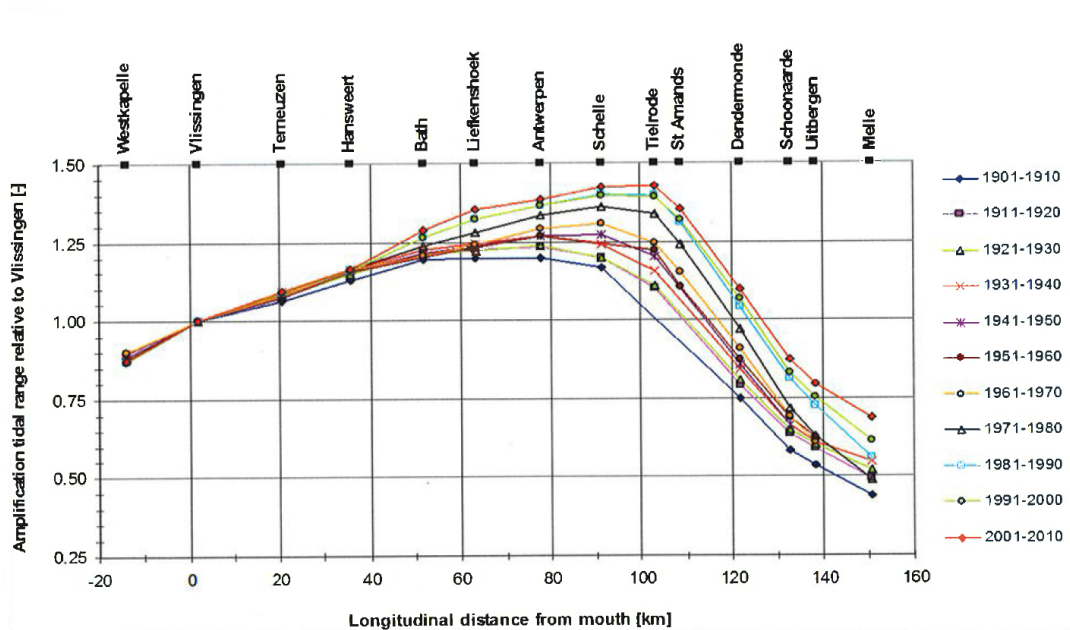


FIGURE 1.10: Historical evolution of the amplification of the tide along the Scheldt estuary (Source: Taal, Meersschart, and Liek (2015))

Unfortunately, dredging and dumping operations are a necessity in many estuaries due to economic and flood safety reasons. In order to keep performing deepening and widening through dredging, a better understanding of the effects of these operations on the tidal dynamics in an estuary is required. This will lead to a better ability to predict the effects of such interventions and possibly allow to design strategies of sediment management to keep tidal amplification under control.

Currently, studies have shown that the planimetry and altimetry are important parameters in tidal amplification. But the effects of different channel configurations is still unknown. Additionally, the sensitivity of the system to local interventions is also still an aspect that is not well understood. Therefore this study will attempt to analyze the effects of planimetric and altimetric changes of the tidal basin on tidal amplification.

1.4 Research questions and objective

Based on existing theory and the problem definition, the following research objective has been formulated:

“To determine the effects of planimetric and altimetric changes on the tidal propagation and amplification in a well-mixed macro-tidal coastal plain estuary.”

To realize the objective, the Scheldt estuary is used as a case study in this research. The following research questions will be addressed in this research:

1. How have the tidal and morphological characteristics of the Scheldt estuary evolved over the last century?
2. How can the hydrodynamic system and morphology of the Scheldt estuary be modeled using an idealized process-based model in Delft3D?
3. How do planimetric and altimetric changes affect the tidal propagation and tidal amplification in a tidal basin?
4. How does the channel-shoal pattern and local interventions influence the hydrodynamic processes in a tidal basin?

1.5 Outline

First the methods used in the study are explained in chapter 2. A description will be given of the study area used as a case study in this research. Additionally, the set-up of the hydrodynamic model and subsequent analysis with the model are explained in this chapter. In chapter 3 and 4 the results of the study are presented. Chapter 5 will give a detailed discussion of the used methods based on the obtained results and experience gained throughout the research. Finally, chapter 6 and 7 give the conclusion and recommendations of the study.

2 Methods

This chapter contains the research methods used in this study. For this research, a process-based model has been designed to model hydrodynamics in an idealized tidal basin. This model is used to analyze the behavior of the system to changes in planimetry and altimetry caused by dredging and dumping operations. The Scheldt estuary has been used as a case study (Figure 2.1). The study can be divided in three sections:

1. Data analysis
2. Model set-up
3. Systematic model analysis

Firstly, data analysis will be performed on the hydrodynamic and morphological characteristics of the Scheldt estuary. Secondly, the model is set-up using Delft3D modeling software based on existing literature. Finally, the model is used to systematically analyze relevant hydrodynamic processes in coastal plain estuaries by implementing step-wise changes of planimetry and altimetry in the idealized model. Calibration and validation of model results is done iteratively for each step in the systematic analysis, based on observed data of water levels, tidal ranges and bathymetry.



FIGURE 2.1: The Scheldt estuary on the border of The Netherlands and Belgium, located at 51°N , 4°E

This chapter will introduce the study area in section 2.1. The method of data analysis is described in section 2.2. In sections 2.3 and 2.4 a description of the model is given, the model set-up is explained and the relevant model parameters are described. Section 2.4.4 will describe the calibration and validation methods used and finally, section 2.5 will give a detailed explanation of the systematic analysis of planimetry and altimetry on the tidal amplitude.

2.1 Study site

The Scheldt estuary is located in South of the Netherlands and partly in the North of Belgium (see figure 2.1) and is divided in two parts: the Western Scheldt (Dutch part) and the Sea Scheldt (Belgium part). As specified below, it is a well-mixed, coastal plain estuary with a macro-tidal regime and receives a river discharge from the Scheldt river originating from the North of France. The basin is situated in a densely populated area with Antwerp (~500,000 inhabitants (FOD Economie België, 2011)) being the largest city along its banks. The estuary has always been of great economic importance to the region and allows access to many inland ports. Coincidentally, the most important harbor in the estuary is the port of Antwerp. It is the second largest freight and cargo port in Europe and is still expected to grow in the coming years (Eurostat, 2017).

2.1.1 Physical characteristics

The Scheldt estuary is a coastal plain estuary with a macro-tidal regime (See Appendix A). Its mouth is located at Vlissingen and the basin continues until Gent where sluices interrupt the incoming tide, for a total length of approximately 180 km. The estuary has a characteristic funnel-shaped geometry (section 1.2.2 & section 1.2.5) and is relatively shallow. At Vlissingen the estuary has a width of about 6 km with a width average depth of 15 m, which decreases to less than 200 m wide and 3 m at its head (Bolle et al., 2010). The alluvial plain of the estuary contains a complex meandering multi-channel system. It shows a repetitive pattern of flood- and ebb-channels separated by shoals and sills as described by Van Veen et al. (2005). A few significant shoals found in the Western Scheldt are shown in figure 2.2. The boundaries of the estuary consist naturally of peat and sedimentary deposits, such as clay and sand, which are prone to erosion. However, dikes and bank-protection measures prevent bank erosion, creating semi-rigid lateral boundaries (Bolle et al.,

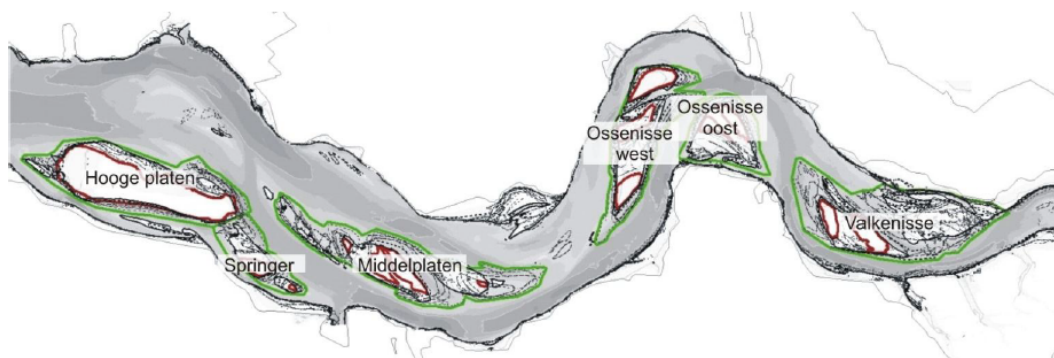


FIGURE 2.2: Overview of plates in Western Scheldt for the bathymetry of 2010 (Cleveringa, 2013)

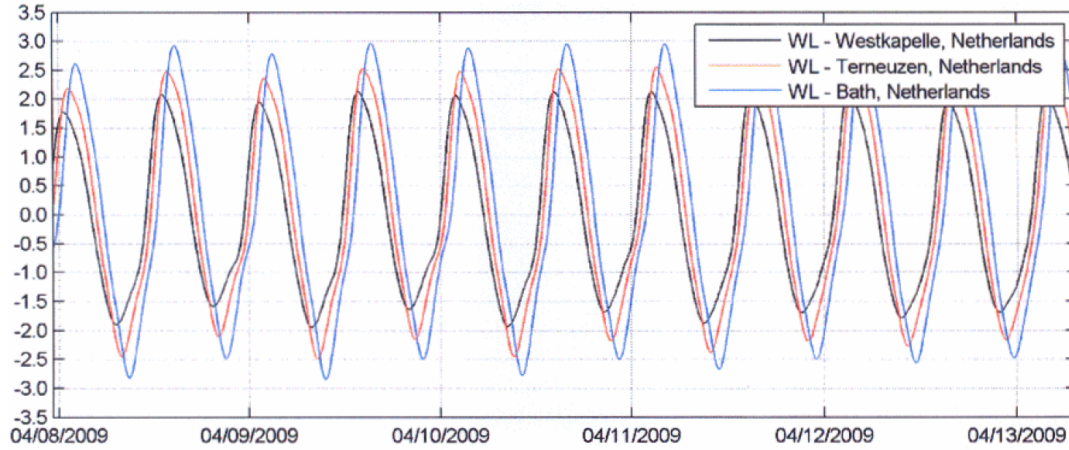


FIGURE 2.3: Vertical tide in the Western Scheldt at three locations (Van Rijn, 2010, p.37)

2010). This is supported by the fact that the configuration of channels and position of lateral boundaries of the estuary have remained the same since 1930 (Bolle et al., 2010).

Many ports and cities are situated along the banks of the Scheldt estuary. Several important locations are shown in table 2.1. These locations also contain measurement stations that continuously monitor water levels in the estuary. Additional bathymetric analysis has also been performed at these location by Pieters (2002). In table 2.1, the locations in the estuary are defined relative to the mouth at Vlissingen, with a positive value in landward direction and a negative value in seaward direction. This convention is often used in studies of the Western Scheldt (Taal, Meersschant, and Liek, 2015; Pieters, 2002) and will be used also in this study.

The tidal regime in the Western Scheldt is semi-diurnal with an amplitude between 1.7 m and 2.1 m at Westkapelle depending on neap- or spring-tide (Pieters, 2002). The main tidal constituent is M_2 , and some asymmetry of the tidal signal can be seen at Westkappelle (see figure 2.3), caused by higher harmonics M_4 and M_6 (Bolle et al., 2010). Throughout the estuary tidal dynamics play a dominant role over river dynamics. The reason is that river discharge is very small compared to the volume of water displaced during a tidal cycle. The mean tidal prism at the mouth is 2.2×10^9

Stations	Distance	Width
	[km]	[km]
Westkapelle	-12	25
Vlissingen	0	6
Terneuzen	18	6
Hansweert	33	6
Bath	51	3
Antwerpen	83	0.8
Rupelmonde	98	<0.5
Temse	103	<0.5
Dendermonde	118	<0.5
Gent	148	<0.5

TABLE 2.1: Geometric and tidal data (annual mean spring tide) of Scheldt estuary around 2000 (Van Rijn, 2010)

m^3 (Bolle et al., 2010), while the average fresh water discharge of the Scheldt is $120 \text{ m}^3/\text{s}$. Leading to a total fresh water discharge in a tidal cycle that is less than 1% of the tidal prism (Van der Wegen and Roelvink, 2012).

2.1.2 Human interventions

In order to satisfy the demands of population growth and economic growth, the Western Scheldt (Dutch part) and the Sea Scheldt (Belgian part) have been subject to many human interventions over the years. Embankment, dredging and land-reclamation have been executed both by the Dutch and Belgian governments. In recent history the most notable projects have been the deepening operations in 1970's and 2000's, performed to allow more and larger ships to reach the port of Antwerp. The depth of the main channel is generally sufficient, but sills form at locations where flood and ebb channels meet, possibly blocking shipping access. The deepenings involved dredging these sills specifically. Currently, the minimum depth to be maintained in the main channels is set at 14.5 m below LAT (Vlaams Gewest - Afdeling Maritieme Toegang, 2011). Large dredging operations were set-up both in the Dutch and Belgian part of the estuary. Consequently, the total volume of dredged material increased from $<5.5 \text{ Mm}^3/\text{year}$ in 1955, to $9\text{-}16 \text{ Mm}^3/\text{year}$ between 1995-2003 (haecon, 2006) (See Appendix B). Both the Netherlands and Belgium decided to keep the dredged material in the estuarine system and have performed many dumping activities on intertidal areas or very close to the original dredging location at the sides of the main channels. Only through large sand mining operations have been the cause of sediments being taken out of the Scheldt estuary in the order of $2\text{Mm}^3/\text{year}$ (Coen and Plancke, 2015; Pieters, 2002). Presently, sand mining activities in the estuary have been reduced as it was found to be correlated to scouring/deepening and disappearance of intertidal area (Winterwerp, 2013; Taal, Meersschaut, and Liek, 2015).

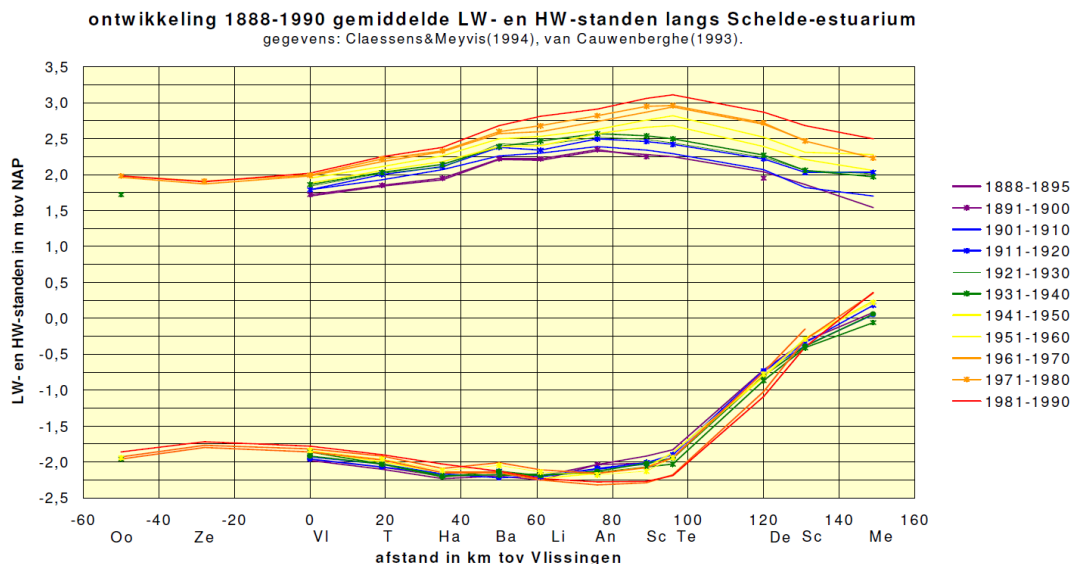


FIGURE 2.4: Historical evolution of the high and low water levels in the Western Scheldt (Pieters, 2002, p.52)

2.2 Data analysis

The data gathering and analysis in this study focuses on water levels and bathymetry of the Scheldt estuary. Both the historic situation and the present situation have been evaluated and used for calibration and validation of the hydrodynamic model. Furthermore, the comparison of historic and present data provide a means to test model behavior and determine the processes related to bathymetric changes and water level changes.

2.2.1 Water level data

Several characteristics of the hydrodynamic system in the Scheldt estuary have been determined. This has been done using results from literature and by collecting available water level data from online databases. As mentioned in section 2.1.1, the mouth of the estuary ($x = 0$) is defined at Vlissingen. However, as will be explained in section 2.4, the designed hydrodynamic model sets its seaward boundary at Westkapelle. This means the area of interest runs from Westkapelle to Gent.

In order to calibrate and validate model data the following data has been gathered:

Tidal range profile The tidal range profile is the tidal range as a function of the distance along the estuary relative to Vlissingen (Figure 2.5). The data is gathered from reports by [Van Rijn \(2010\)](#), [Pieters \(2002\)](#) and [Taal, Meersschant, and Liek \(2015\)](#). The data of tidal range profiles is extracted from figures from existing field studies using a plot digitizer. This is because exact data could not be obtained. Both present and historic data is gathered as shown in table 2.2. A comparison has been made between the data sources and a choice for a single dataset is made based on the reliability of the data source. This is done by looking at the description of how and when the data is obtained and the values compared to other data sources.

Source	Period
Pieters (2002)	1888-1895
	1951-1960
	1981-1990
Taal, Meersschant, and Liek (2015)	1901-1910
	1951-1960
	2001-2010
Van Rijn (2010)	2001-2010

TABLE 2.2: Sources and periods of time used for the data gathering of the tidal range profile in the Scheldt estuary

The gathered data have been processed and analyzed using Matlab. The data by different sources use different measurement locations, therefore a linear interpolation of the data is performed (`griddedInterpolant`) to be able to compare the same locations (Table 2.1) within the boundaries of the dataset. In order to determine the relative amplification of the tide throughout the estuary, the tidal range profile is normalized using the tidal range at the mouth at Vlissingen H_0 , according to equation (2.1). This also allows the comparison of different

tidal range profiles from different sources even if the amplitudes at the mouth might vary.

$$H_{rel}(x) = \frac{H(x)}{H_0} \quad (2.1)$$

Where $H_{rel}(x)$ is the relative tidal range at x [-], $H(x)$ the measured tidal range at x [m] and H_0 the measured tidal range at Vlissingen. Two characteristics will be extracted from the obtained relative tidal range profile (Figure 2.5):

1. Location of maximum relative tidal range $x_{H_{rel,max}}$
2. Value of maximum relative tidal range $H_{rel,max}$

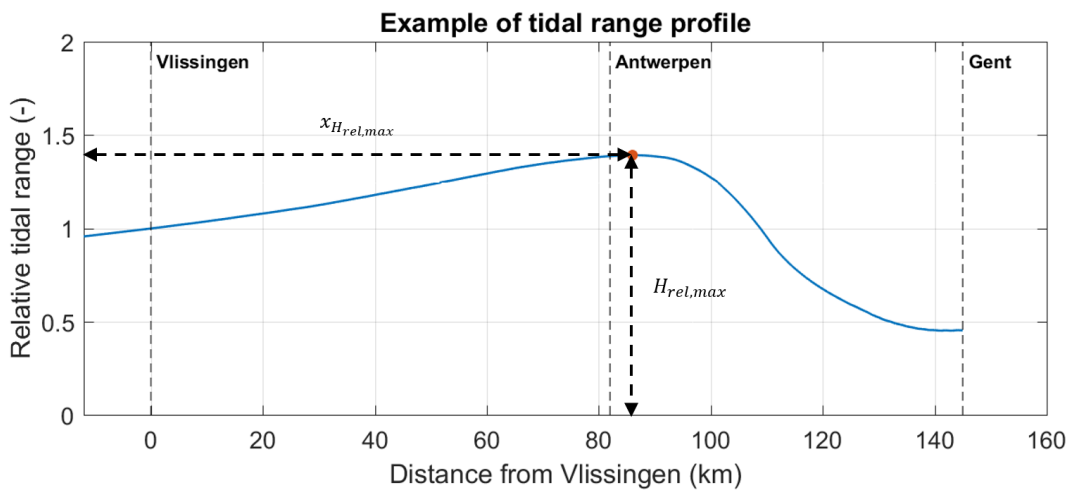


FIGURE 2.5: Example of a relative tidal range profile. The red dot marks the peak of the relative tidal range profile

Tidal deformation The incoming tidal wave at Westkapelle has already experienced some deformation effects due to the shallow coastal shelf and higher harmonics created by reflection from the estuary (Pieters, 2002; Bolle et al., 2010). Using tidal data provided online, the shape of the tidal wave at multiple measurement locations (See table 2.1) along the estuary can be determined. By comparing these profiles the ebb-dominance and flood-dominance of the estuary can be determined. The tidal curves have been analyzed at the following stations and for both spring and neap tide situations:

- Westkapelle ($x = -12km$)
- Bath ($x = 51km$)
- Antwerpen ($x = 83km$)

Wave celerity The celerity of the wave moving through the estuary has also been gathered from literature and data analysis. Using the tidal information from the three stations in the previous step the propagation speed of the peak of the tidal wave has been determined.

2.2.2 Bathymetric data

Bathymetric data is provided by measurements (also known as 'vakkodingen') from Rijkswaterstaat and is obtained through an open database (openDAP). The earliest complete bathymetric dataset of the Western Scheldt is 1955 which is chosen as the historic reference point (before the major deepening operations in 1970's, 1990's and 2010). The water level analysis by Pieters (2002), Bolle et al. (2010) and Taal, Meerschaert, and Liek (2015) was performed on data between 2000 and 2010. Therefore the bathymetric profile of 2005 will be chosen as the 'current' morphological state of the Western Scheldt. Bathymetries of the Sea Scheldt were not directly available and are therefore not analyzed in this report. It is assumed that the channel bathymetry in the Western Scheldt can be used to represent the Sea Scheldt. The bathymetric data has been analyzed using elevation maps and cross-sections of the flow profile along the length of the estuary. 29 cross-sections have been defined manually using Matlab (Figure 2.6).

The bottom elevation of the estuary contains a complex channel system. To use the bathymetry data in the idealized model, the bathymetric profile has been simplified to fit the idealized estuarine basin. Starting from a uniform bed, several grades of complexity will be included step-by-step. To this end, the following aspects have been determined:

Average basin depth The simplest form of the Scheldt bathymetry is a uniform bed with a depth equal to the system wide average depth. This is determined both by values used in literature and values found by averaging bathymetric charts from 1955 and 2005. The data from the bathymetric charts is defined with a structured spatial grid of 20m x 20m. The cells that lie without measurements have a default value of *NaN*. These cells are excluded from the analysis. The average depth is obtained using equation (2.2).

$$d_{avg} = \frac{\sum_{i=1}^N \sum_{j=1}^N d_{i,j}}{N} \quad (2.2)$$

Where d_{avg} is the average basin depth [m], N the number of cells with a valid depth value, i and j the rows and columns of the structured grid and $d_{i,j}$ the depth of cell (i, j) [m].

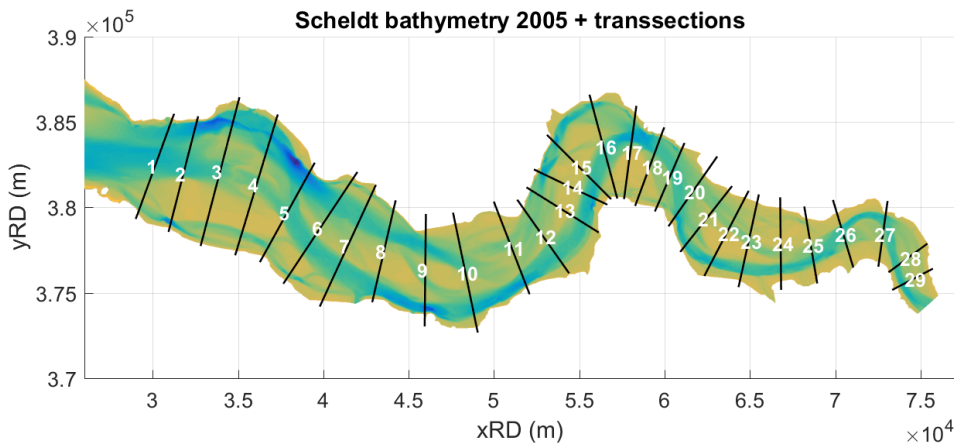


FIGURE 2.6: Overview of defined cross-sections in the Western Scheldt estuary

Longitudinal bed slope The longitudinal bed profile is determined based on values from literature and using the manually defined cross-sections depicted in figure 2.6. The width-averaged depth is calculated for each cross-section using linear interpolation. This is done as follows:

1. The cross-section is evenly divided in 250 sections
2. The x and y coordinates of each node are calculated
3. Query the depths for each node
4. Nodes with value *NaN* are removed
5. Take average of depths across the cross-section

Secondly, the distance between the center points of the cross-sections is determined using a straight line from cross-section to cross-section. The distance is defined relative to the location of Vlissingen.

Estuary width The geometric shape of the estuary is determined by calculating the width of each cross-section. This is done by calculating the distance between the two outer points with a numeric value. The converging length scale γ between each cross-section is then determined using the following equation:

$$\gamma(x) = -\frac{x_{n+1} - x_n}{\ln(b_{n+1}/b_n)} \quad (2.3)$$

Where γ is the converging length scale [m], x_n the distance to Vlissingen of the n^{th} cross-section and b_n the width of the n^{th} cross-section.

Characteristics cross-sectional bottom profile The channel-shoal system of the Scheldt estuary will be schematized to fit the idealized basin. This is done by determining the characteristic cross-sectional flow area of the Western Scheldt estuary. The aim of the characteristic cross-sectional bottom profile is that it resembles a channel with shoals on the side, while retaining the width-averaged depth and cross-sectional flow area of the estuary. This has been done using the following method:

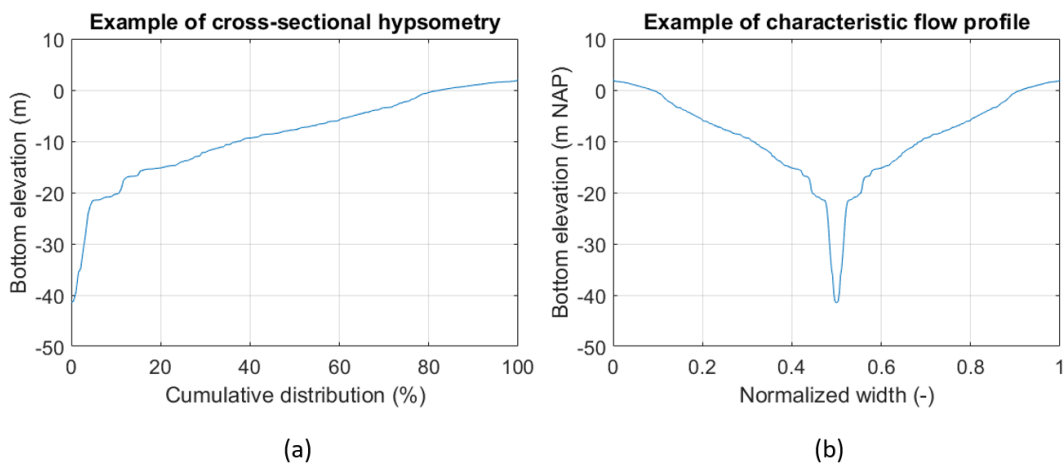


FIGURE 2.7: Example of channel-shoal schematization. Panel (a) shows the hypsometry of a single cross-section, panel (b) shows the vertically mirrored hypsometry to obtain depth profile with a channel centered at the middle and with shoals to the side.

1. Determine the hypsometry of each cross-sectional depth profile (Figure 2.7a)
2. Take average of all hypsometries to obtain a cumulative depth profile
3. Mirror the profile along the vertical axis and fit to normalized width (Figure 2.7b)

This procedure is performed for both the 1955 and 2005 bathymetries of the Western Scheldt.

2.3 Model description

This study will design and use a hydrological model to simulate water movement in an idealized tidal basin. For the description of the general motion of water, the Navier-Stokes equations are used which have been derived from the conservation laws of mass and linear momentum. The Navier-Stokes equations take into account inertia of the fluid, convection and diffusion processes, stresses within the fluid and the external forces that act on the fluid and the conservation of mass within the control volume. However, an important assumption is made, namely that water is an incompressible fluid. This implies there are no changes in density due to pressure differences, however this does not mean the density is constant. Sea water near and in estuaries experience strong gradients in salt concentration which affects the density of the fluid.

To describe the tidal dynamics in open oceans and coastal waters, the shallow water equations (SWE) have been derived from the incompressible Navier-Stokes equations. For this study it is important to model the hydrodynamics in two spatial dimensions with a depth averaged velocity (2DH). Due to the complexity of the intended interventions, it is not possible to use the analytical solution by [Savenije \(2001\)](#) to determine tidal amplification in the model domain. Therefore a numerical model has to be set-up. The choice has been made to implement a numerical hydrological model using Delft3D software, because it solves the unsteady shallow-water equations in both two (depth-averaged) and three dimensions ([Lesser et al., 2004](#)). The system of equations consists of the horizontal momentum equations, the continuity equation, the sediment transport equation and a turbulence closure model. Because it is assumed that vertical accelerations are small ($kh \ll 1$), the vertical momentum equation reduces to hydrostatic pressure. For a more detailed explanation of the model equations see [Lesser et al. \(2004\)](#).

The module that lies at the heart of Delft3D is the FLOW-module. This module solves the following computations simultaneously ("online"):

- Hydrodynamic computations
- Transport of salinity and heat computations
- Sediment transport computations
- Morphological changes

The module includes many processes such as, wind shear, wave forces, tidal forces, density-driven flows, stratification due to salinity and temperature differences, atmospheric pressure changes, drying and flooding of intertidal flats ([Lesser et al., 2004](#)). For this study, the focus lies on the interaction between the planimetry and altimetry of the tidal basin and the tidal forcing. To isolate the processes related to tidal amplification, many processes are neglected for this model study. The hydrodynamics are calculated without the effects of salinity and temperature differences. Effects of

wind waves are not considered and sediment transport processes and morphological evolution are not modeled for this study.

The model employs a staggered numerical grid to solve the model equations. This grid can both be a structured (rectangular) grid or be solved using a curvilinear grid. A curvilinear grid can follow more complex planimetric shapes which allows for a more accurate spatial discretization of the tidal basin.

2.4 Model set-up

For the design of the idealized tidal basin, the Scheldt estuary has been used as a case study (Section 2.1). In reality, the Scheldt estuary has many complex bends, channels, shoals, irregular boundaries and several tributary channels along its banks. In the idealized basin, these characteristics have been simplified to a funnel-shaped geometry with a closed landward boundary according to the exponential decreasing profile described in section 1.2.5 (Figure 2.8). The following choices for simplifications have been made:

Closed landward boundary The Scheldt estuary receives water from the Scheldt river with a discharge of approximately $120 \text{ m}^3/\text{s}$ on average. Studies by [Van Rijn \(2010\)](#), [Hibma, Vriend, and Stive \(2003\)](#) and [Bolle et al. \(2010\)](#) have shown that this discharge has no significant influence on the water levels in the estuary. Additionally, the Scheldt estuary is abruptly blocked by sluices at Gent. Therefore, the decision has been made to neglect river discharge in the model and put an artificial 'wall' at the end of the spatial domain.

No tributaries Several artificial channels flow into the Scheldt estuary along its banks. Similar to the river discharge is that their effect on water levels are negligible. They might have an effect on the dilution of salty seawater, but salinity is not considered in the model. Therefore, no fresh water sources are implemented in the model.

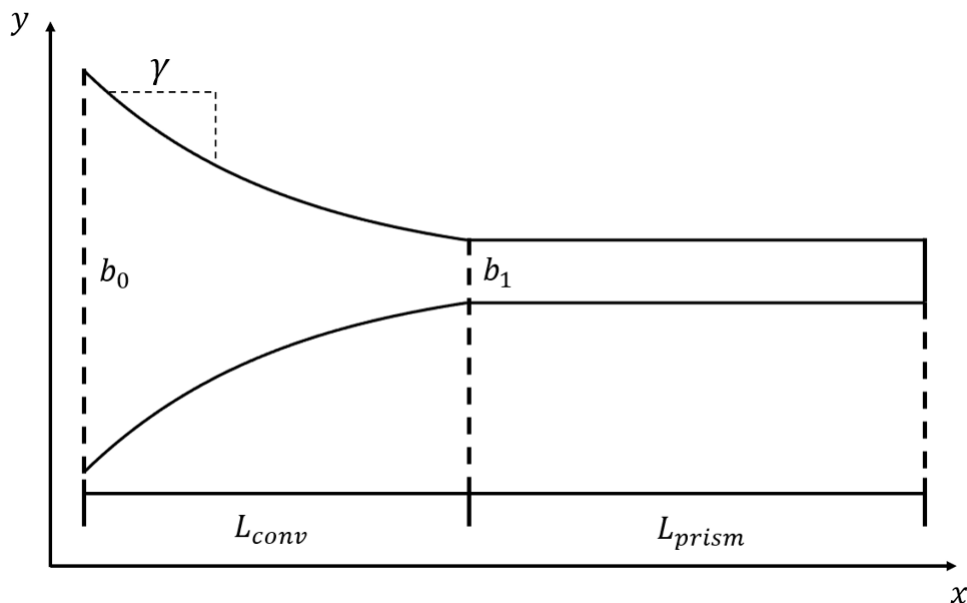


FIGURE 2.8: Geometry of the idealized tidal basin used in the hydrological model

Monochromatic boundary condition The tidal forcing of the model is described by the tidal signal at the seaward boundary. This tidal signal can consist of many tidal constituents and can contain asymmetries which affect the water levels in the estuary (Section 1.2.4). To be able to isolate the effects of planimetry and altimetry on water levels in the estuary, the effects of tidal asymmetries are removed from the model. This is done by imposing a simple harmonic tidal signal according to the S_2 tidal constituent.

No Coriolis forcing Coriolis forces have been neglected in the model by putting the model at a latitude of 0° with an orientation along the equator. Because the width of the tidal basin is small, it is expected that there is no significant influence from the Coriolis forces on the hydrodynamics in the model (Van Rijn, 2010).

2.4.1 Model parameters

A schematic of the model geometry is shown in figure 2.8. The model geometry consists of a converging section and a prismatic section, which represent the estuarine basin and river geometry respectively. Several parameters are used to describe the shape of this geometry as shown in table 2.3.

Parameter	Symbol	Unit
Basin length	L_{conv}	[m]
River length	L_{prism}	[m]
Mouth width	b_0	[m]
River width	b_1	[m]
Converging e-folding length scale	γ	[m]

TABLE 2.3: Model geometry parameters

In this study the tidal forcing will be simplified to a S_2 tidal signal. This means that the seaward boundary condition can be defined as a harmonic water level series given by:

$$\zeta_0(t) = H_0 \cos(\sigma_0 t) \quad (2.4)$$

Where $\zeta_0(t)$ is the water level [m] at time t at the mouth of the estuary, H_0 the amplitude of the harmonic signal [m] and σ_0 the angular frequency [rad/s]. Table 2.4 shows an overview of the parameters used in Delft3D-FLOW.

Parameters	Symbol	Unit
Tidal amplitude	H_0	[m]
Tidal frequency	σ_0	[deg/h]

TABLE 2.4: Parameters related to the model boundary conditions

The spatial domain is discretized using a curvilinear grid. The size of grid cells varies throughout the grid with large cells at the mouth and smaller cells towards the land boundary. The size of the cells follows an exponential decreasing profile similar to the width of tidal basin. Table 2.5 shows the parameters that define the computational grid of the model.

The model also has a temporal dimension. Using a start and end date a simulation period is defined. This period is then discretized using time steps. The size of time

step in conjunction with grid cell size plays an important role in the stability of the numerical model. This is related to the Courant-number in computational fluid dynamics and stems from the numerical discretization of space and time dimensions.

The bathymetry of the model is implemented is designed in Matlab. The bathymetry is defined by a spatial function which is interpolated, using Matlab's `griddedInterpolant` function, to points corresponding to cells of the computational grid. The bottom elevation is defined for each cell in the computational grid and is defined at the center of each grid cell relative to a datum (m NAP).

Certain physical parameters are required to be able to solve the shallow equations used by the FLOW module of Delft3D. Without salinity and sediment transport processes the following parameters are relevant to the hydrological model:

The wall roughness is neglected in this model as the width of the estuary is much larger than the depth of the estuary and flow speeds close to the estuarine wall are comparable to those further away from the boundaries. This means that the wall roughness assumes a free slip-condition.

2.4.2 Numerical grid design

For multiple steps in the study the grid of the model had to be revised to fit new geometric shapes. The model can use either a rectangular grid or a curvilinear grid (see figures 2.9 and 2.10). These grids are used to solve the shallow water equations. The quality of the computation with the grid is to a large extent determined by its orthogonality and the rate with which certain characteristics change over the modeled area:

Grid resolution and time step Instability of the numerical model can occur if the time step is too large compared to the size of the grid resolution. In the hydrodynamic model this instability is purely based on the water movement through the grid. Delft3D allows for the option to dynamically adjust the time step size during model simulation, however this has the risk that the model assumes such small time steps that the simulation comes to a halt. Therefore, a constant time step size is chosen based on estimates of the maximum flow speeds and grid cell size.

Orthogonality The orthogonality of a grid cell is the angle of the gridlines in M- and N-direction. In this study a max orthogonality value of 0.05 is adhered for all computational grids.

Aspect ratio The aspect ratio is the ratio of grid cell dimensions in M- and N-direction. Usually, this value must be in the range of 1 to 2. However, the flow in these models is predominantly in the direction of the M grid lines so a larger

Parameter	Symbol	Unit
x-resolution at mouth	res_x	[m]
y-resolution at mouth	res_y	[m]
Convergence of x-res	γ_x	[m]
Convergence of y-res	γ_y	[m]
Grid orientation		[°]
Number of layers		[—]

TABLE 2.5: Parameters related to computational grid

Parameters	Symbol	Unit
Start date		[dd mm yyyy hh mm ss]
End date		[dd mm yyyy hh mm ss]
Time step	Δt	[min]

TABLE 2.6: Temporal model parameters

Parameter	Symbol	Unit
Latitude		[°]
Gravitational acceleration	g	[m/s ²]
Water density	ρ_w	[kg/m ³]
Bottom roughness (Chézy)	C	[m ^{1/2} /s]
Wall roughness		
Horizontal eddy viscosity	ν	[-]

TABLE 2.7: Physical parameters used in Delft3D

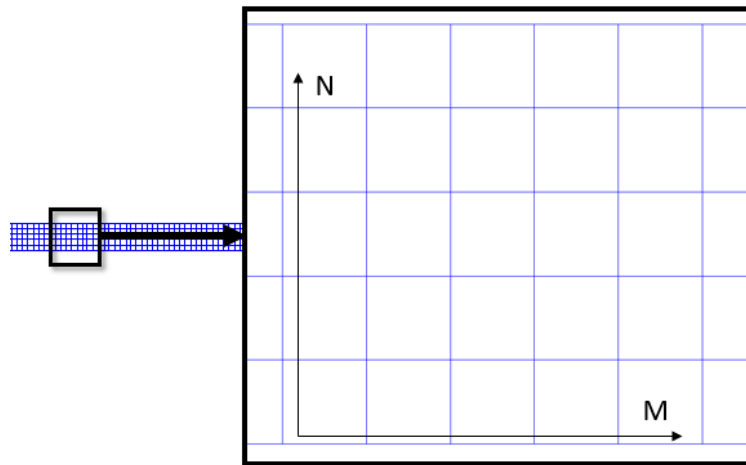


FIGURE 2.9: Example of a rectangular numerical grid used in Delft3D-FLOW for hydrodynamic modeling

aspect ratio does not significantly affect the model results. To keep run times reasonable, the max aspect ratio in the grid has been limited to 4.

Ratio neighbouring cells The size of neighboring cells must be in the same order of magnitude. For cells close to each other a ratio of 1.2 is adhered while cells far away should not have a ratio larger than 1.4.

A rectangular grid consists of perfectly square grid cells of equal size creating a grid with perfect quality for the numerical computation. In case of the simple prismatic basins, this type of grid is best suited to discretize the spatial domain. When more complex geometries are introduced, such as convergence of the lateral boundaries, a rectangular grid isn't always the best solution. As lateral boundaries converge the grid gets narrower in a specified direction. In a rectangular grid this is realized by removing the outer grid cells one by one until the preferred basin width is reached. Locally, this creates a sharp decrease in width of the model domain with walls almost perpendicular to the flow direction (see figure 2.11), possibly creating a strong sudden reflection of incoming waves. In situations where grid cell size is much smaller than the total grid width this is fine as the narrowing does not have a significant influence

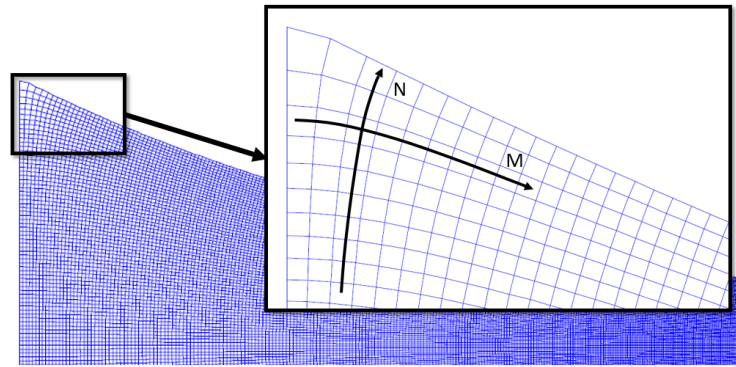


FIGURE 2.10: Example of a curvilinear numerical grid used in Delft3D-FLOW

on the hydrodynamics. But as the narrowing of the lateral boundaries continues this starts to become a problem in upper regions of the modeled grid.

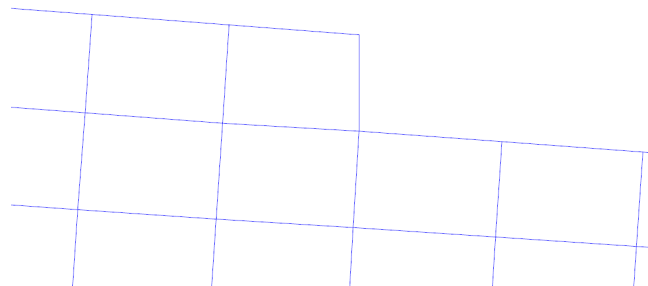


FIGURE 2.11: Jump in lateral boundary caused by computational grid not fitting to the actual lateral boundaries

The solution is to create a curvilinear grid that follows the lateral boundaries of the spatial domain, while taking into account the aforementioned characteristics of grid quality. The following steps have been used to create a numerical grid for the converging geometries:

1. Create curvilinear grid that completely follows the converging lateral boundaries ($\gamma_y = \gamma$) using Matlab.
2. Increase the γ_y parameter until river section contains ~ 15 cells in N-direction.
3. Adjust γ_x parameter to decrease length of cells in M-direction to obtain aspect ratios smaller than 4.
4. Import grid in Delft3D-RGFGRID and use automatic orthogonalization of the grid and use additional manual adjustments to get the maximum orthogonality value below 0.05.

2.4.3 Model output

Delft3D-FLOW has the option to generate enormous amounts of output data. For the hydrodynamic model used in this study, only two variables are relevant for the analysis of the model, namely water levels and flow speeds. The model has two options for the format of these variables:

History files By defining observation points in the model domain time series can be created of the water levels and flow speeds for all layers of the water column. This allows the option to define transects along which data can be gathered. The interval with which this output is generated can only be a multiple of the simulation time step.

Map files Output of all grid cells can be saved in a map file for several time steps. This option requires a lot of space as the output files generated easily reach multiple GB's. These map files allow for the detailed analysis 2D analysis of water level in flow speed data. This is useful in situation where lateral flows become a significant process, such as in basins with a channel-shoal system.

The model output is given in the NEFIS format used by Delft3D. Using OpenEarthTools and Matlab the data is read and parsed for usage in calibration, validation and analysis. Using the water level data and flow speed data the following characteristics have been extracted:

LW and HW For every point x-location in the model the LW and HW statistics are obtained from the water level data. This is done by selecting the last two days of the simulation period (4 tidal cycles) and calculating the minimum and maximum water levels for every location.

Mean WL The mean water level is obtained by averaging the water levels of the last two days of the simulation period for every x-location along the estuary.

Tidal range The tidal range is obtained by subtracting the LW from HW at every x location along the estuary. By dividing this by the tidal range at the mouth the relative tidal amplification in the estuary is obtained.

Phase lag The phase difference between HW and HW slack is determined by taking a single tidal cycle and calculating the peak of the vertical tide and determine the zero-crossing of the velocity profile (time of flow reversal). This is visualized in figure 2.12. The time difference is divided by the wave period and converted to degrees.

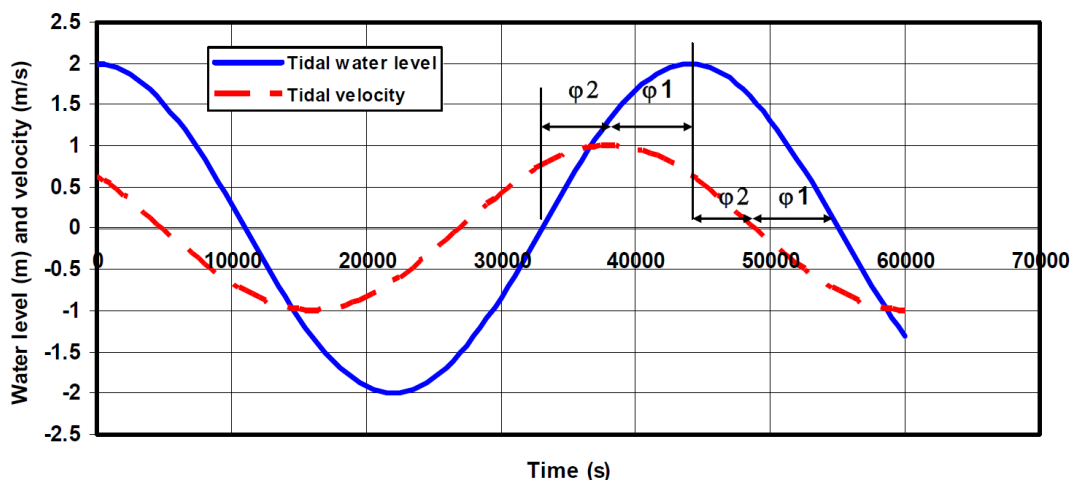


FIGURE 2.12: Phase lag φ_1 between horizontal and vertical tide. $\varphi_1 = 0^\circ$ is a progressive wave, $\varphi_1 = 90^\circ$ is a standing wave. (Van Rijn, 2010, p. 18)

2.4.4 Calibration and validation of model

Calibration of the model is done based on data gathered from literature and data analysis. For the first step of the model set-up, the Van Rijn models have been replicated. The model performance has been tested using visual inspection of the amplification profiles produced by Van Rijn and those produced by the models in Delft3D. Additionally, the data on flow speeds, phase lag and discharge at the mouth of the models is compared.

Further calibration of the model after initial set-up is done by calculating and comparing several indicators of the modeled tidal range curve and the observed tidal range curve:

Peak amplitude value Determined by calculating the maximum amplitude

Peak amplitude location Location of the maximum value of amplitude

Amplitude Antwerp Amplitude at location of Antwerp (82km from Vlissingen)

Root mean square error RMSE of two profiles calculated with equation 2.5

$$RMSE = \sqrt{\sum_{i=1}^N (H_{rel,m,i} - H_{rel,o,i})^2} \quad (2.5)$$

Where $RMSE$ is the root mean square error of the relative tidal range $[-]$, $H_{rel,m,i}$ the modeled relative tidal range at location i $[-]$, $H_{rel,o,i}$ the observed relative tidal range at location i $[-]$ and N the number of data points in the dataset. A small $RMSE$ value means that the modeled results match observed values closely, where $RMSE = 0$ means a perfect fit. All of the four above mentioned indicators will be used to determine the performance of the model.

For the calibration and validation during the systematic analysis the tidal ranges have been normalized using the tidal range at Vlissingen as reference. For validation of the model results, additional analysis is performed. To this end the tidal curves at four locations in the estuary ($x = 0$, $x = 0.25L$, $x = 0.5L$ and $x = 0.75L$) are determined and compared. From this data the following wave characteristics can be determined:

Wave celerity Calculated by determining the propagation speed of the peak of the tidal wave through the basin.

Deformation of tidal wave The deformation of the wave is determined by the increase in amplitude, the change in ebb and flood duration and additional visual inspection of asymmetries in the wave tidal curve at multiple locations in along the modeled domain.

Phase lag Phase lag between horizontal and vertical tide is calculated along the length of the estuary, as described in section 2.4.3 and figure 2.12. This is compared to known values of the phase lag in the Scheldt estuary.

2.4.5 First set-up with Van Rijn's model

The model has been set-up based on the depth-averaged Delft3D model used by Van Rijn (2010). Similar to this study, Van Rijn (2010) implemented a strongly simplified tidal basin of the Scheldt estuary. A comparison between the numerical model

results and analytical solutions was made to verify the processes and hydrodynamic behavior shown in the numerical models. The results from the study showed that the numerical results could match the analytical results adequately for cases without complete reflection at the landward end.

Van Rijn modeled several cases with varying geometry and depth, starting with a simple prismatic basin to more complex converging geometries. As a starting point for the model set-up, the results of Van Rijn's model cases have been reproduced in Delft3D. The different prismatic and converging cases are shown in tables 2.8 and 2.9.

	Length [m]	Width [m]	Depth [m]	Bed roughness [$m^{1/2}/s$]
CASE1	60000	1000	10	60
CASE2	180000	1000	10	60
CASE3	60000	1000	5	60
CASE4	180000	1000	5	60

TABLE 2.8: Prismatic tidal basins by Van Rijn

	Length basin [m]	Length river [m]	Mouth width [m]	Conv. length scale [m]	Depth [m]	Roughness [$m^{1/2}/s$]
CASE1	60000	0	25000	25000	10	60
CASE2	60000	120000	25000	25000	10	60
CASE3	60000	0	25000	25000	5	60
CASE4	60000	120000	25000	25000	5	60
CASE5	180000	0	25000	25000	10	60
CASE6	180000	0	25000	25000	5	60

TABLE 2.9: Converging tidal basins by Van Rijn

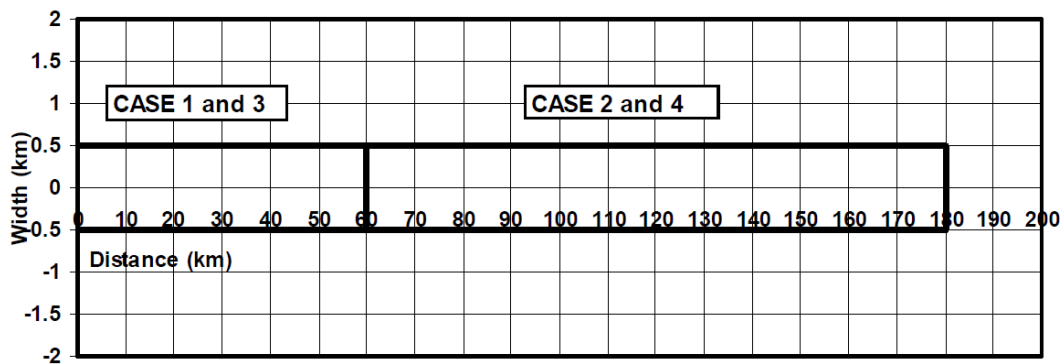


FIGURE 2.13: Prismatic basins used in the model cases by Van Rijn (2010, p.A-1)

Van Rijn assumed the mouth of the Scheldt estuary at Westkappelle 12km west of Vlissingen. For all of the converging numerical models, a mouth width b_0 of 25km was used. Furthermore, the water depth and tidal water levels are defined relative to mean sea level (MSL). For the boundary conditions of his model Van Rijn used the following settings:

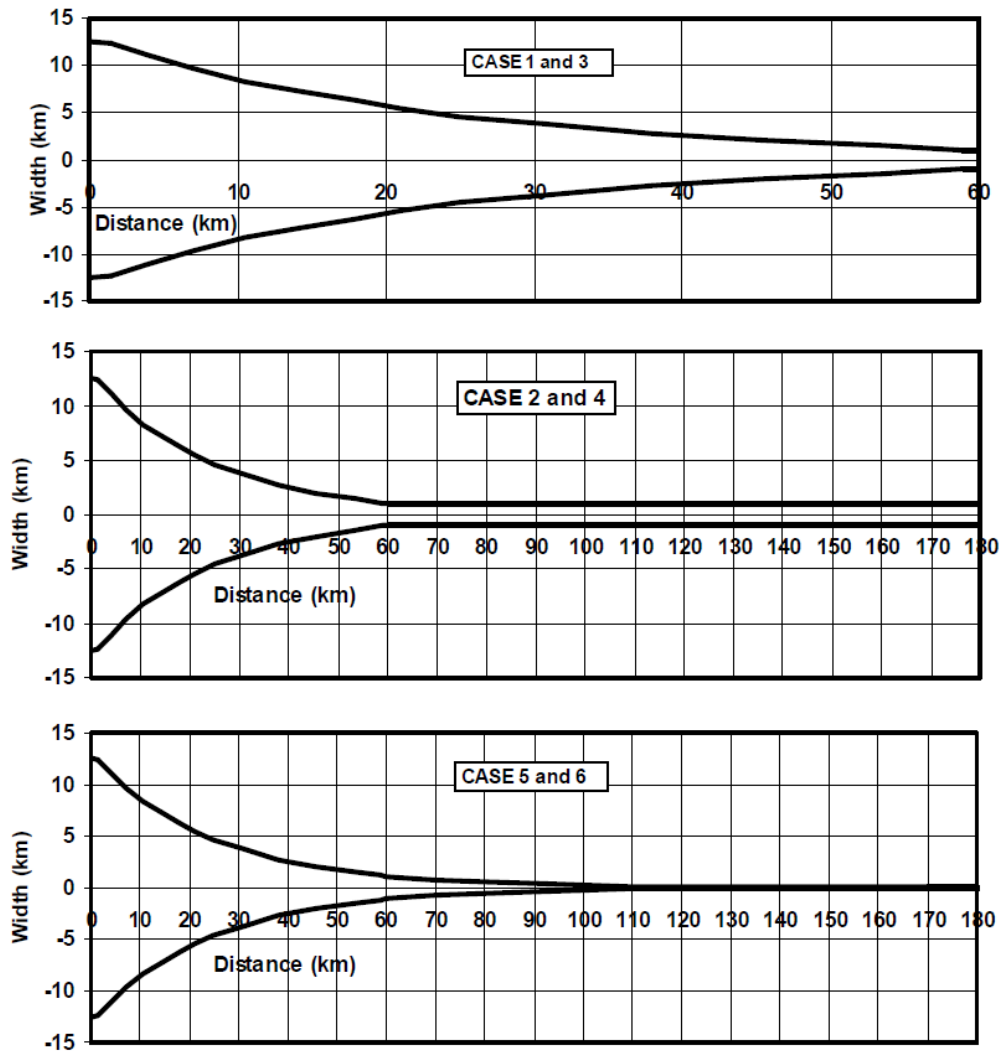


FIGURE 2.14: Converging basins used in the model cases by [Van Rijn \(2010, p.38\)](#)

Sea boundary ($x=0$) Harmonic water level condition: $\zeta_0 = H_0 \cos(\sigma t)$ with $\zeta_0 = 2.1m$ and $\sigma_0 = 2\pi/T$ with $T = 12$ hours

Closed boundary ($x=L$) No river discharge is assumed: $Q = 0m^3/s$

Unfortunately, not all relevant parameters used in Delft3D had been described in the report by [Van Rijn \(2010\)](#). Based on model studies by [Bolle et al. \(2010\)](#), [Hibma, Vriend, and Stive \(2003\)](#) and [Van der Wegen, Wang, et al. \(2008\)](#), remaining unknown parameters have been determined. Several parameter sets have been tested and the model results were compared with the results of [Van Rijn \(2010\)](#). Appendix C shows the detailed result comparison based on the tidal range, flow velocities and phase lag at the mouth.

From the cases of [Van Rijn \(2010\)](#), converging CASE2 has the best fit with the Scheldt estuary based geometry and tidal range output. Figure 2.15 shows the tidal range profile compared to the observed tidal range in the Scheldt estuary. This is the only case that shows the process amplification in the lower regions and damping in the upper regions. Therefore, this case has been chosen as a starting point for the

systematic analysis described in section 2.5. The total parameter set of this so-called 'reference-case' is shown in table 2.10.

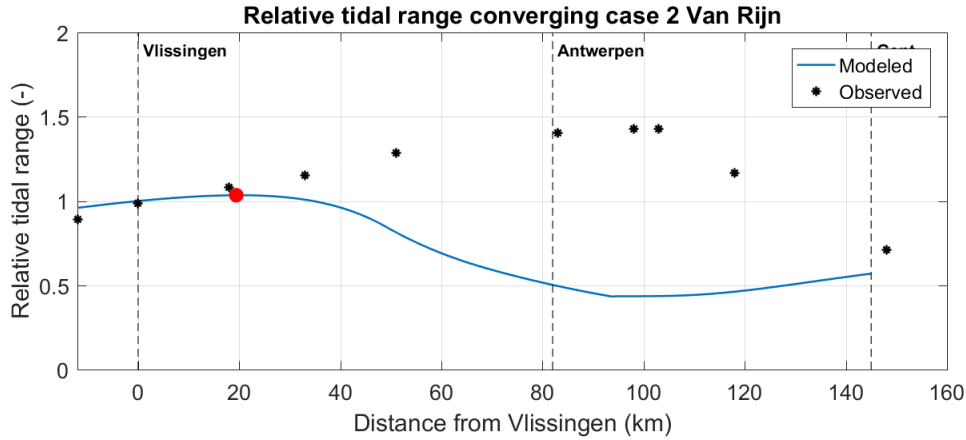


FIGURE 2.15: Tidal range profile of reference model based on converging case 2 of the models by Van Rijn (2010)

Parameters	Values	Parameters	Values
L_{conv}	60000 m	grid orientation	0°
L_{prism}	120000 m	# of layers	1
b_0	25000 m	Start date	03 10 2017
b_1	2274 m	End date	08 10 2017
γ	25000 m	Δt	1 min
H_0	2.1 m	Latitude	0°
σ_0	30 deg/h	g	9.81 m/s ²
res_x	200 m	ρ_w	1000 kg/m ³
res_y	200 m	C	60 m ^{1/2} /s
γ_x	25000 m	Wall roughness	Free slip
γ_y	50000 m	ν	1 m ² /s

TABLE 2.10: Parameters of reference model used for the systematic analysis based on the set-up with the models by Van Rijn (2010)

2.5 Systematic model analysis

In order to determine dominant processes, the effects of several model parameters on the tidal range will be analyzed. The aim of the analysis is to determine the effects of the following estuarine characteristics on tidal amplification:

- A) Planimetry of lateral boundaries
- B) Changes in uniform depth
- C) Longitudinal bed slopes
- D) Channel-shoal system
- E) Local depth changes

This section will explain the parameters relevant in each step of the analysis and the range of values that is tested. An overview of the systematic analysis is shown in figure 2.16.

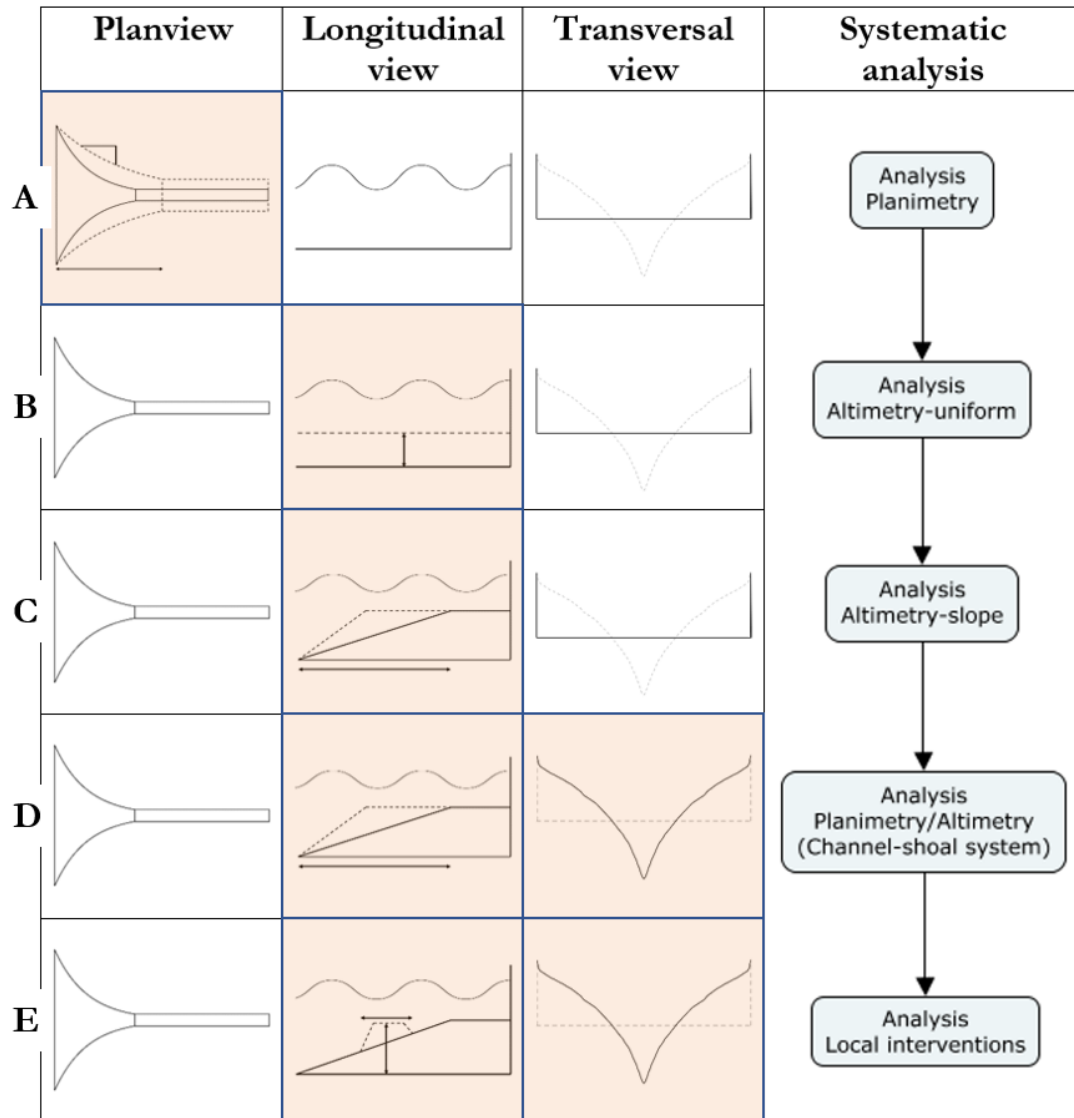


FIGURE 2.16: Overview of the 5 steps in the systematic analysis. Each line is a individual step within the analysis. The columns describe the planimetric and altimetric properties of the model. The orange blocks highlight in what area the parameters will be altered during that step. The individual steps and their parameters are explained in the sections below.

It is not feasible to test every combination of parameters due to long run times of the model and the amount of variables. Therefore a stepwise systematic analysis will be performed. The systematic analysis will use the simple reference model obtained from model set-up (Section 2.4.5). Each step of the analysis will increase the complexity of the model by adding a new variable to the system. Within each step a small sensitivity analysis is performed to see how the model reacts to changes of the variable. Based on validation of the model results (Section 2.4.4) a choice is made for the best performing parameter set within the current step of the analysis. This model is then used as the base case for the next step in the analysis.

The list shown above shows the order in which the different characteristics of the estuary are added to the model. The order of this list is based on results from previous studies on the individual aspects and their effects on water levels in estuaries.

The choice has been made to start with the sensitivity and calibration of the lateral boundaries, because the uniform depth profile used on the model set-up is already based on the actual water depth in the Scheldt estuary. Additionally, studies by [Van Rijn \(2010\)](#), [Savenije \(2001\)](#) and [Vandenbruwaene et al. \(2013\)](#) have shown that the tidal range profile is relatively sensitive to the rate of convergence γ and convergence length L_{conv} compared to realistic values of the uniform depth. The uniform depth is then analyzed before adding more complex width-averaged altimetric profiles by introducing slopes to the system. The step of adding shoals is the final step in which the model will be calibrated and adds the final step of complexity to the idealized model. Finally, the effects of local changes in bathymetry are tested by looking at several different intervention cases.

2.5.1 Step A: Lateral boundaries

This step analyzes the effects of shape of an estuary on the tidal amplification in the idealized tidal basin. The idealized geometry of the tidal basin can be described by the five parameters as shown in table 2.3 (Section 2.4.1). Here only two of these parameters are varied:

1. Converging e-folding length scale, γ
2. Length of converging basin, L_{conv}

The other parameters, defined during model setup (Table 2.10), are kept at a constant value, except for b_1 , which immediately follows from L_{conv} and γ according to:

$$b_1 = b_0 \exp(-L_{conv}/k) \quad (2.6)$$

According to Van Rijn the rate of convergence, γ , is approximately 25 km. Data analysis of the bathymetry and geometry has shown value ranging from 23 km to 27 km. The length of convergence is chosen according to the geometry of the Scheldt estuary and a value chosen by [Van Rijn \(2010\)](#). Combinations of the two parameters are tested for a total of 17 model cases as shown in table 2.11. The models are

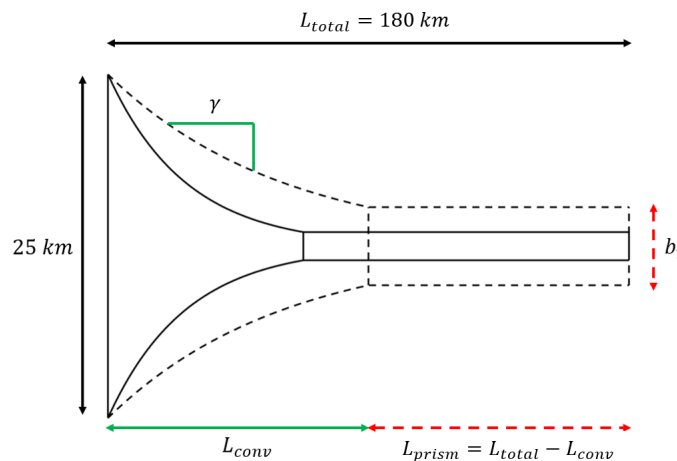


FIGURE 2.17: Parameters and variables used for step A of the systematic analysis. The green arrows denote the variables varied in the analysis. The dashed red arrows are parameters that change depending on the variables. The black arrows are parameters with a constant value throughout the analysis.

numbered using an identifier as a prefix and the row and column number from the table (e.g. A14 or A51). Based on the results of these 17 models, a choice is made for the best performing model to be adopted in steps B to E.

		L_{conv}			
		60 km	80 km	100 km	120 km
γ	23000 m	x	x	x	x
	24000 m	x	x	x	
	25000 m	x	x	x	
	26000 m	x	x	x	
	27000 m	x	x	x	x

TABLE 2.11: Combination of parameter values used in step A. Marked cells are models that have been created and unmarked cells are combinations that have been omitted

2.5.2 Step B: Uniform depth

This step will analyze the effects of a deeper and shallow uniform bed profile on the tidal amplification. All bottom depths are defined relative to MSL. Figure 2.18 shows the longitudinal view of the system and how the bottom profile is varied. The range of variation of the uniform depth, $d_{uniform}$, has been determined based on data analysis and values from literature. Savenije (2001) and research by Vandenbruwaene et al. (2013) suggests there is a threshold depth for which damping through bottom friction becomes a significant aspect for the tidal range in an estuary. Based on measurements of several estuaries and the analytical method by Savenije (2001), Vandenbruwaene et al. (2013) found that this threshold lies somewhere between 5 m to 7 m deep (width averaged) for typical funnel-shaped alluvial estuaries.

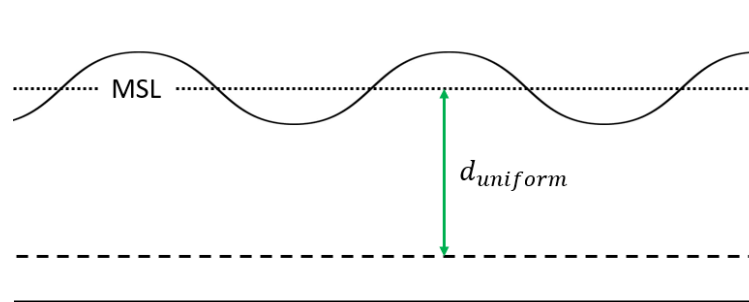


FIGURE 2.18: Parameters and variables used for step B of the systematic analysis. The green arrows denote the variables varied in the analysis.

Bathymetric data of the Scheldt estuary and from literature shows that the actual width-averaged depth can reach 15 m NAP, while the width-averaged depth at the alluvial plain is approximately 10 m NAP. Therefore, a range of 15 m to 5 m deep is chosen for this step of the systematic analysis. The depth is incremented with steps of 1 m. The uniform depth profile is discarded in the subsequent steps of the analysis, but this analysis provides insight in the effects of depth on the tidal range without interfering processes such as shoaling caused by longitudinal and lateral bottom gradients.

2.5.3 Step C: Longitudinal slope

The effects of the slope on tidal amplification is analyzed by taking the best performing model from step A and implementing several different slope longitudinal slope profiles. Based on data analysis, the results from step B and values from literature (Coen and Plancke, 2015; Jeuken and Wang, 2010) it was determined that the width-averaged depth in the upper regions of the estuary is approximately 5 m, as will be explained in section 3.2. The slope is then defined by two variables (Figure 2.19):

1. Depth at mouth, d_{mouth}
2. Slope length, L_{slope}

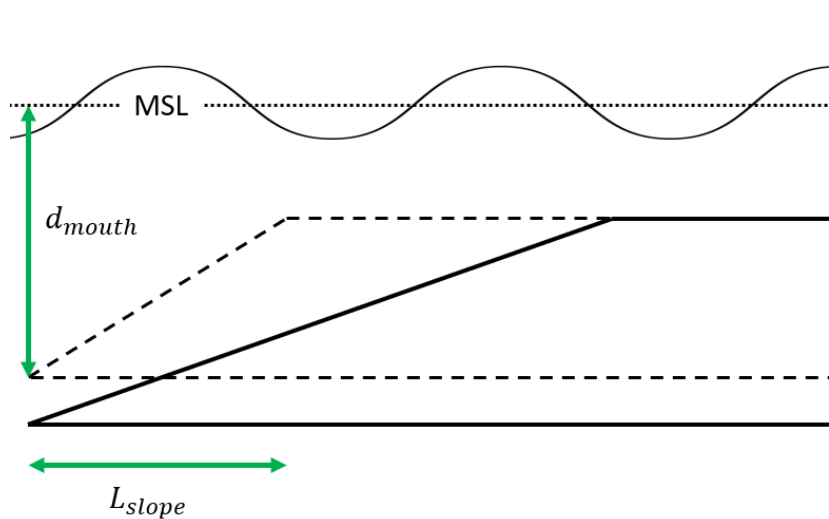


FIGURE 2.19: Parameters and variables used for step C of the systematic analysis. The green arrows denote the variables varied in the analysis.

For the depth at the mouth of the model, two values have been chosen based on literature and data analysis, namely 10 m and 15 m. In combination with this depth, two slope lengths have been studied of 120 km and 180 km respectively. An overview of the four altimetric profiles is given in table 2.12.

Case	d_{mouth}	L_{slope}
C1	10m	120km
C2	15m	120km
C3	10m	180km
C4	15m	180km

TABLE 2.12: Slope cases and their parameters

Based on validation results a choice is made for the best performing slope parameters, which is used both in step D and step E of the systematic analysis.

2.5.4 Step D: Channel-shoal system

The effects of the channel-shoal system has on tidal amplification has been analyzed using the scenario shown in table 2.13. The channel-shoal system is implemented in both the uniform bed profile (Section 2.5.2) and in one with a sloping profile (Section

2.5.3). The channel-shoal system has been obtained from data analysis for both 1955 and 2005 as described in section 2.2.2.

For all cases the 2005 channel-shoal profile has been implemented by rescaling the profile such that the average depth of the channel-shoal profile corresponds to the width-averaged depth longitudinal profile. The rescaling is done based on the average depth of the cross-sectional bottom profile.

(2.7)

By rescaling the channel-shoal profile in such a way there are two parameters altered simultaneously, namely surface area of shoals and the width and depth of the main channel. Through comparison of the validation results the scenarios are compared in their accuracy to model observed tidal range profile. The best performing channel-shoal case is chosen to be used in the following step.

Case	Channel-shoal profile	Longitudinal profile
D1	Normalized channel profile 2005	Constant avg. depth 10m
D2	Normalized channel profile 2005	Constant avg. depth 8.62m
D3	Normalized channel profile 2005	Slope 180km: 15m to 5m
D4	Normalized channel profile 2005	Slope 120km: 15m to 5m

TABLE 2.13: Channel Cases implemented for sensitivity analysis

2.5.5 Step E: Interventions

The historical interventions in the Western Scheldt can be represented by the evolution of the bathymetry between 1955 and 2005. To this end the smoothed longitudinal profiles of 1955 and 2005 are implemented in the model with a channel-shoal system. The smoothed profiles are used to determine the effects of gradual changes of the slope in the Western Scheldt caused by human interventions.

To determine the effects of local changes in bathymetry several width averaged bumps are implemented in the longitudinal bathymetric profile obtained from step D. The location of interest for this study lies between Hansweert and the Dutch-Belgium border, therefore the 'bumps' are implemented in this area. Both the height and length of the interventions has been studied as shown in table 2.14. Additionally, the interventions are implemented in a width averaged longitudinal profile obtained

Case	Intervention depth	Intervention length
	[m]	[km]
E1	7	20
E2	6	20
E3	5	20
E4	4	20
E5	7	10
E6	6	10
E7	5	10
E8	4	10
E9 (Incl. Channel)	4	20
E10 (Incl. Channel)	4	10

TABLE 2.14: Intervention scenarios

from step C of the systematic analysis (Section 2.5.3) and using the channel-shoal case obtained from step D (Section 2.5.4).

3 Results: Data Analysis

3.1 Water level analysis

3.1.1 Tidal range profile

Analysis of the tidal range data from the three sources shows that the historic data of the periods around 1900 and 1950 are in good agreement between the studies of [Pieters \(2002\)](#) and [Taal, Meersschaut, and Liek \(2015\)](#) (Table 3.1). For these periods the largest difference is noticed in the amplification taking place in the section between Westkapelle and Vlissingen as can be seen in figures 3.1 and 3.2. Data by [Pieters \(2002\)](#) suggests that the tidal range stays relatively constant in this section, showing an increase of the tidal range of approximately 1%. However, [Taal, Meersschaut, and Liek \(2015\)](#) show an increase of the tidal range of 15% between Westkapelle and Vlissingen.

More inconsistencies in the data are noticed in the period around 2000. As can be seen in table 3.1, both the maximum value of relative tidal range and the location of the peak are significantly different for each dataset. Similarly to the data of the historic periods, a large difference in tidal amplification is seen in the section between Westkapelle and Vlissingen.

Of the three datasets a choice has been made to use the tidal range profile of [Taal, Meersschaut, and Liek \(2015\)](#) for calibration and validation of the model. The reason for this is that this dataset has more recent data than the dataset by [Pieters \(2002\)](#). The data from these datasets in the period of 1951-1960 are also very similar (see figure 3.2) supporting the fact that the data is at least supported by two different sources.

Looking at the data by [Taal, Meersschaut, and Liek \(2015\)](#), it can be seen that in the period of 1900 to 2000 an amplification of the tide has taken place of approximately 18%, going from a maximum relative tidal range of 1.21 to a maximum relative range of 1.44. The location of the peak seems to have shifted in landward direction by 25km as well. The shift of the peak of the maximum tidal range has occurred in

Tidal curve		Peak		
Period	Source	Loc. [km]	Amp. [-]	Amp. Antwerp [-]
1888-1895	Pieters	61	1.21	1.16
1901-1910	Taal	77	1.21	1.20
1951-1960	Pieters	88	1.29	1.28
1951-1960	Taal	78	1.28	1.27
1981-1990	Pieters	88	1.40	1.38
2001-2010	Taal	102	1.44	1.42
2001-2010	Van Rijn	98	1.32	1.30

TABLE 3.1: Tidal range profile characteristics Scheldt estuary

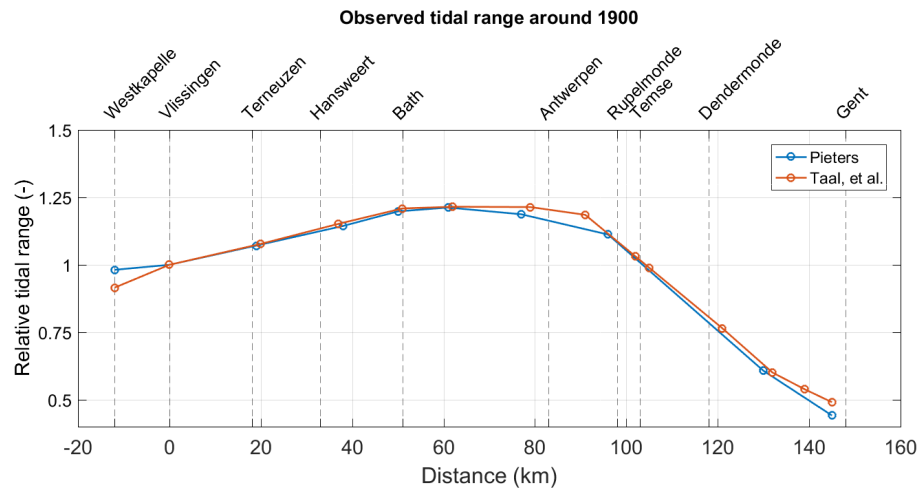


FIGURE 3.1: Tidal range profile in the Scheldt estuary around 1900

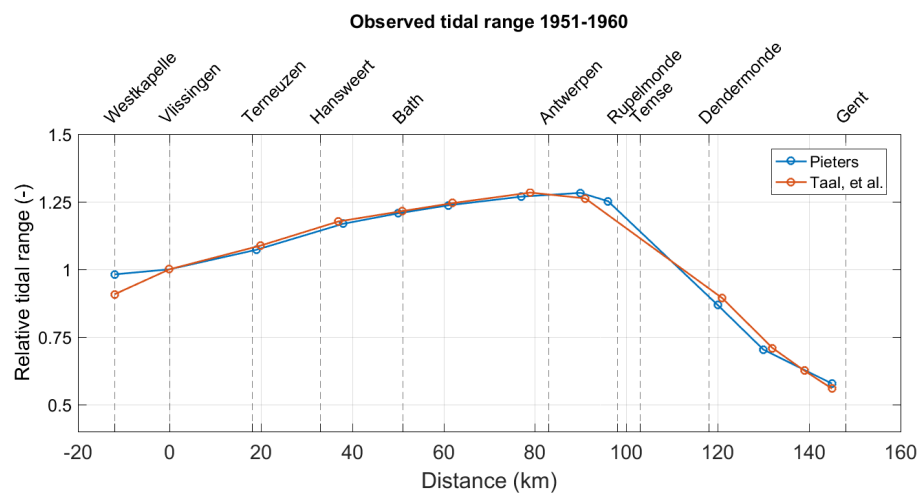


FIGURE 3.2: Tidal range profile in the Scheldt estuary for the period of 1951-1960

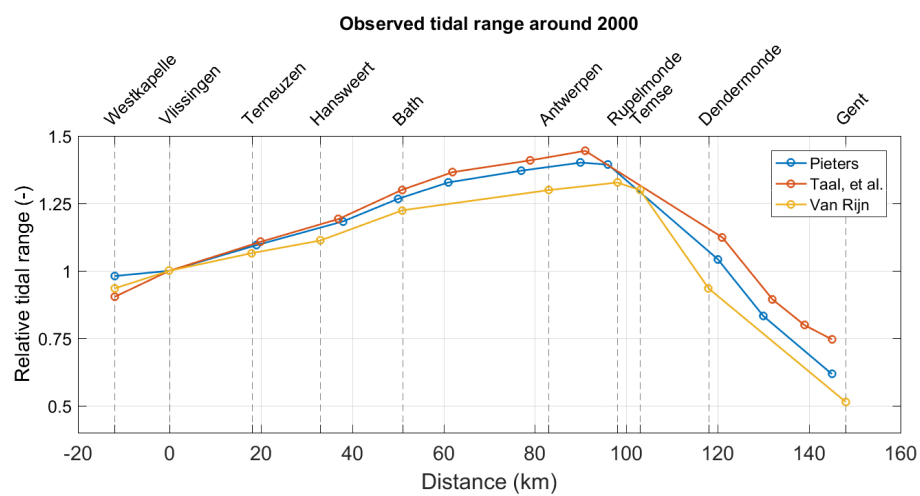


FIGURE 3.3: Tidal range profile in the Scheldt estuary around 2000

the last 50 years as the peak location has remained constant in the period of 1900 to 1950.

3.1.2 Tidal deformation

The tidal curves along the Scheldt estuary for neap and spring tide are shown in figures 3.5 and 3.4. The duration of the flood and ebb phases has been calculated and are shown in table 3.2. The flood and ebb-durations at Westkapelle are nearly identical suggesting a nearly symmetrical tide for both the spring and neap tide conditions. This is supported by the tidal analysis of Pieters (2002) and Bolle et al. (2010). For neap-tide conditions this situation remains fairly constant throughout the estuary, showing only slight increases in ebb-duration at Antwerp. For spring tide however, there is a significant increase of the ebb-duration and decrease of the flood-duration. This means that in spring tide conditions the estuary becomes more and more flood-dominant as the tidal wave progresses in upstream direction.

Based on the peaks of the tidal curves it can be seen that the wave celerity in the estuary ranges between 10 to 15 m/s. This is supported by the tidal analysis of Pieters (2002) who found a wave celerity of 12 m/s throughout the estuary.

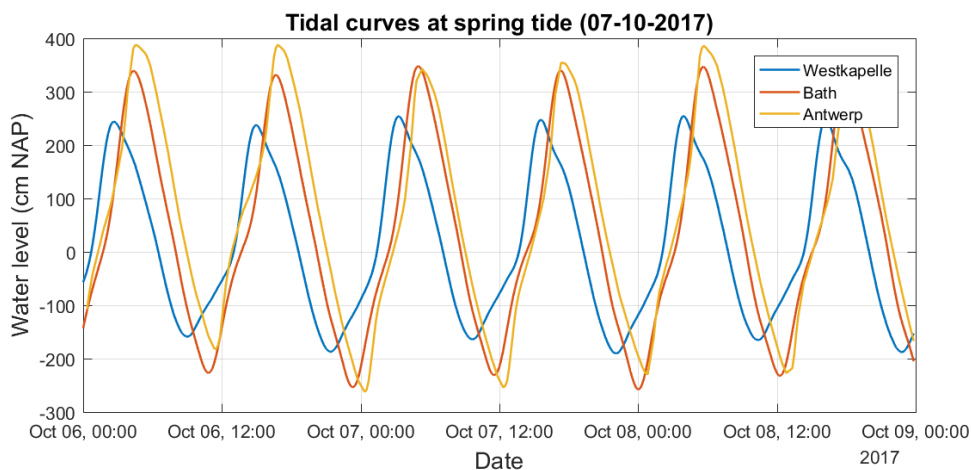


FIGURE 3.4: Tidal curves in Scheldt estuary at spring tide for three locations (Source: (RWS) (2017))

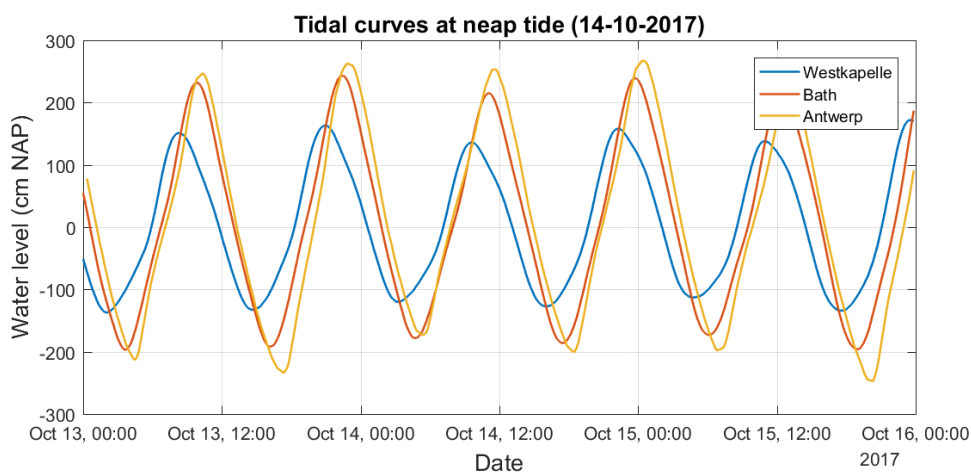


FIGURE 3.5: Tidal curves in Scheldt estuary at neap tide for three locations (Source: (RWS) (2017))

	Spring		Neap	
	Flood [hours]	Ebb [hours]	Flood [hours]	Ebb [hours]
Westkapelle	6.00	6.33	6.33	6.33
Bath	5.66	6.5	6.33	6.33
Antwerp	5.00	7.00	6.17	6.83

TABLE 3.2: Ebb and flood phase duration in hours during spring and neap tide in the Scheldt estuary at three measurement stations

3.2 Bathymetry analysis

The bathymetry of the Scheldt for 1955 and 2005 can be seen in figure 3.6 and 3.7. In general it can be said there are two clear channels in lower region of the Western Scheldt. About 50 km upstream of Vlissingen the multichannel system changes to a single meandering channel.

There are multiple significant differences between the 1955 and 2005 bathymetries. The Western Scheldt has become $\sim 0.6\text{m}$ deeper over the whole domain from 8.73m to 9.33m . This deepening can be translated to a total volume difference of approximately

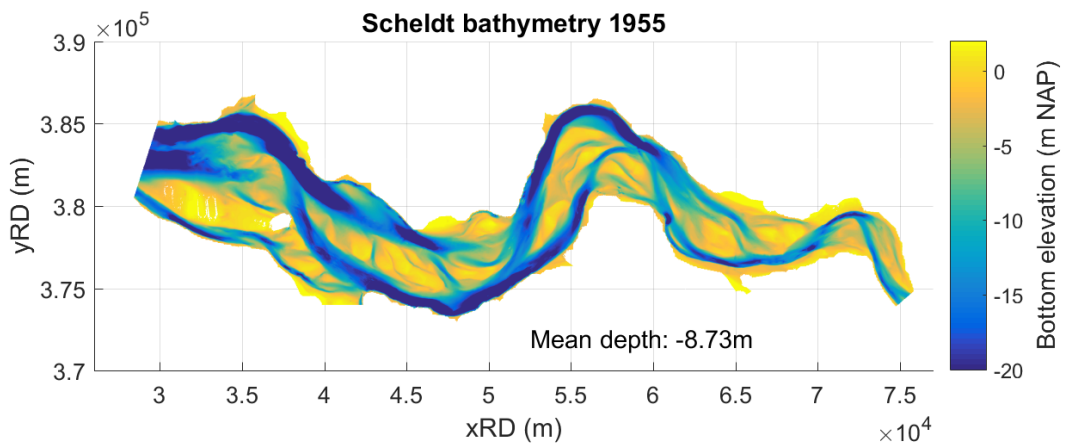


FIGURE 3.6: Bathymetry of Western Scheldt estuary in 1955

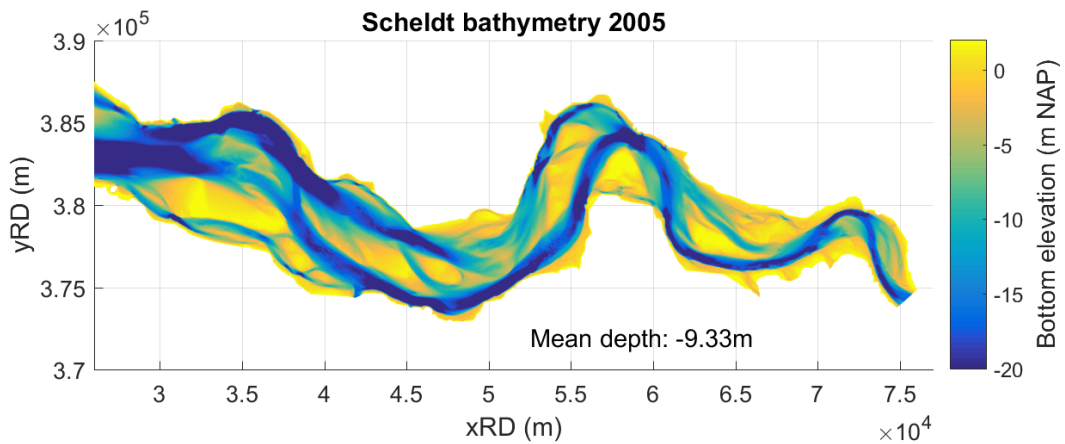


FIGURE 3.7: Bathymetry of Western Scheldt estuary in 2005

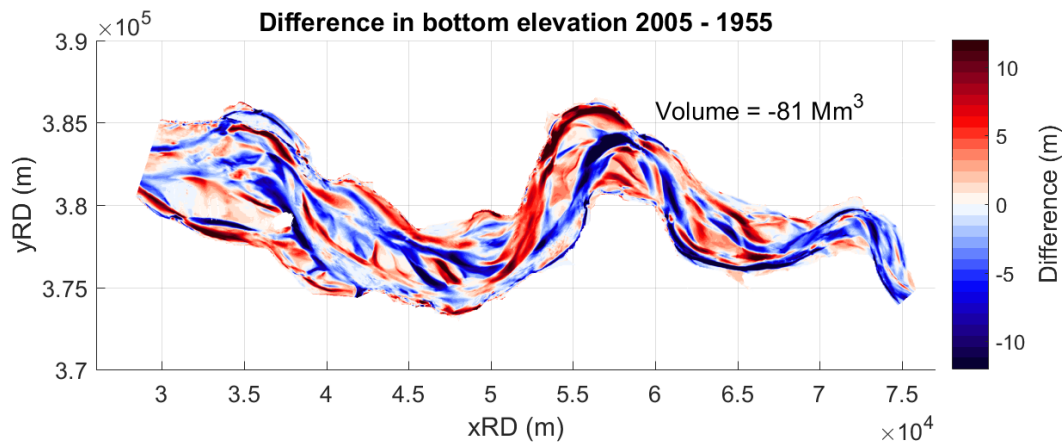


FIGURE 3.8: Evolution of bathymetry in Western Scheldt

81 Mm^3 (Figure 3.8). The loss of this volume is likely caused by sand extraction in the estuary. On average the estuary lost $\sim 1.6 \text{ Mm}^3$ annually, which is in the same order of magnitude of the figures of sand extraction by Coen and Plancke (2015) of $2 \text{ Mm}^3/\text{year}$. Figure 3.8 shows that both sedimentation and erosion have taken place in the estuary. Most significant is the shift of the main channels at several locations. This is most visible in the section near Hansweert. In 1955 the main channel was located at the northern bank, but in 2005 the new channel lies more to the south in the middle of the estuary. For a more detailed map of the locations of shallowing and deepening in the Western Scheldt see Appendix D.

Using a hypsometric curve a noticeable difference is observed for three categories of depths (Figure 3.9). The occurrence of elevations between 30 m NAP and 20 m NAP have decreased in 2005 compared to 1955. These elevations are found at certain locations along the main channels. However, the occurrence of elevations between 20 m NAP and 3 m NAP has increased significantly. Although the deepest points in the main channels have become more shallow, the main channels with a depth of 20 m NAP to 10 m NAP have become more prevalent. Lastly, the range of elevations

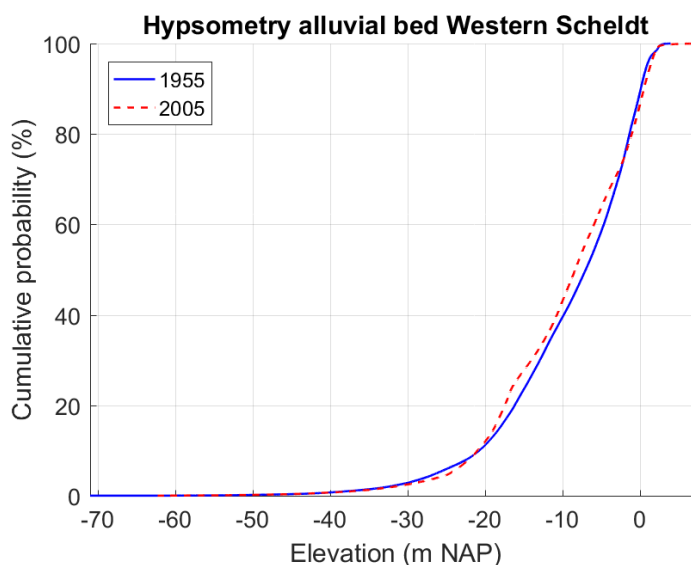


FIGURE 3.9: Hypsometric curves of Western Scheldt in 1955 and 2005

between 3 m to -1 m NAP shows a decrease of occurrence in 2005 compared to 1955. This range describes the intertidal areas in the alluvial plain of the estuary. In summary this curve implies that a widening of the main channels has taken place, partly due to a decrease in very deep areas, but also at the expense of intertidal areas.

3.2.1 Longitudinal profile

Figure 3.10 shows the defined cross-sections defined in the Western Scheldt area. Appendix E gives an overview of the characteristics of all cross-sections. The longitudinal profiles shown in figure 3.11 have been extracted from the cross-section data. The average depth along the estuary varies greatly depending on the cross-section. The depth of the estuary is defined relative to NAP. This is because some parts of the alluvial plain are narrower and contain less intertidal area relative to the width of the main channels. However, a trend can be recognized where the average bottom depth decreases in upstream direction. The cross-sections start close to Vlissingen, but data on the bathymetric profile of the mouth near Westkapelle are missing for the year 1955. Even though it can be seen that the average depth coming from the mouth is significantly deeper than in the tidal basin. The width average depth stays

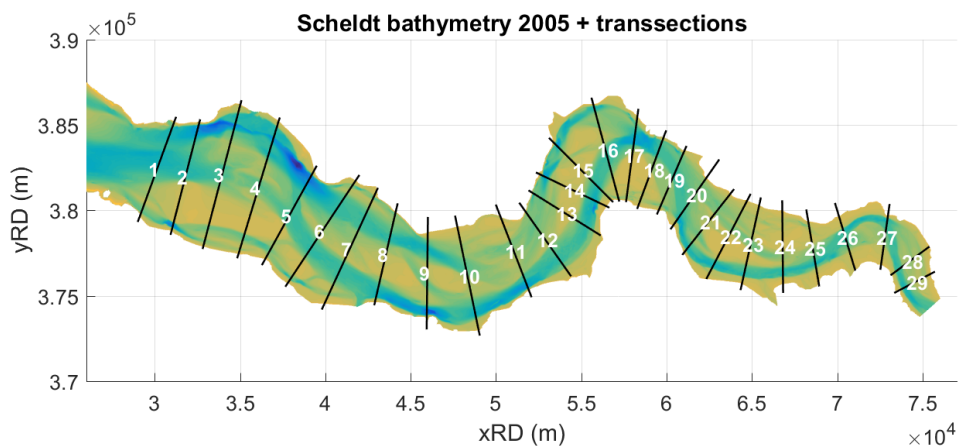


FIGURE 3.10: Overview of defined cross-sections in the Western Scheldt estuary

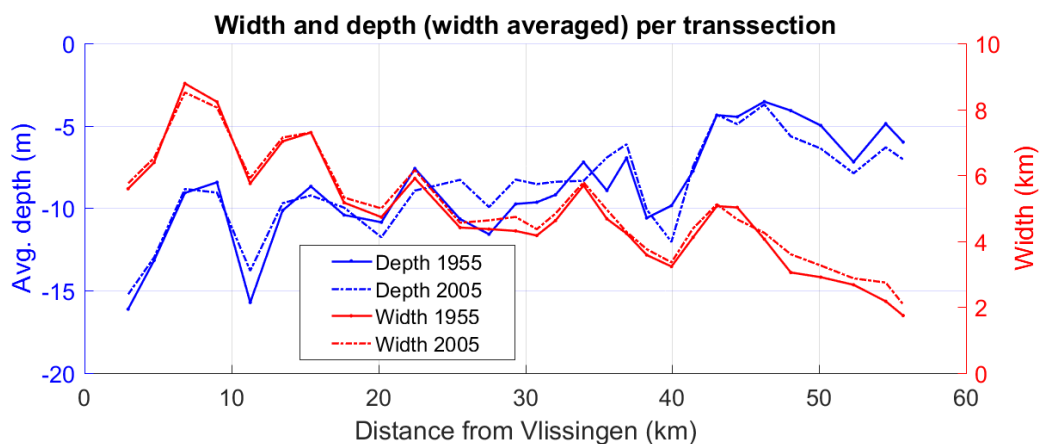


FIGURE 3.11: Longitudinal depth and width Western Scheldt in 1955 and 2005

around 10 m NAP between 10 km and 40km. Then a rise in average bed level happens in the upper parts of the estuary to approximately a depth of 5 m. This shows similarities with the longitudinal profiles described by [Savenije \(2001\)](#) and [Van Rijn \(2010\)](#) typical for alluvial estuaries.

The width of the estuary also shows a decreasing trend in upstream direction in figure 3.11. The data is not sufficient to determine whether the width shows an exponential decrease as described in section 1.2.5. Figure 3.12 shows hints of steady exponential decrease with an average converging length scale k of ~ 23 km. However, there are significant irregularities in some location where there is no convergence or even divergence of the lateral boundaries.

The cross-sectional flow area based on the width and average depth of each cross section is shown in figure 3.13. The largest difference between 1955 and 2005 can be seen in the region near Hansweert and upstream from Bath. The depths near Hans have decreased on average while a deepening has taken place in the region between Bath and Antwerp.

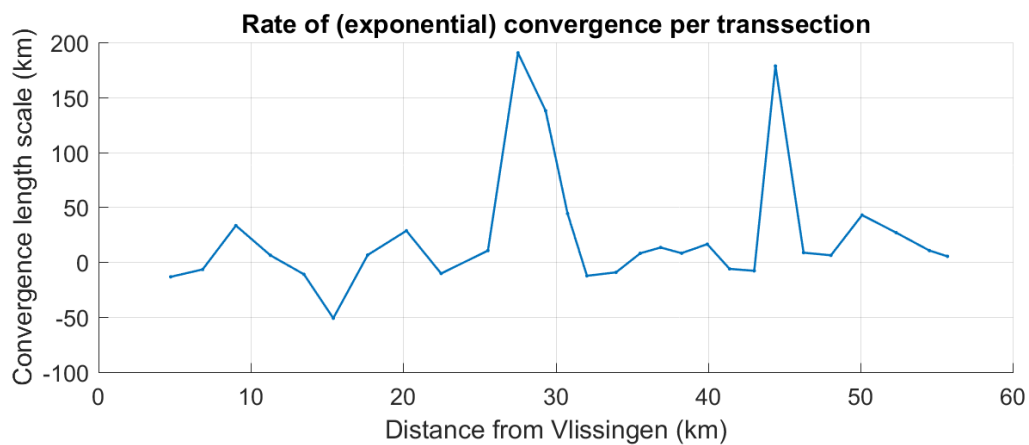


FIGURE 3.12: Exponential rate of convergence of the geometry of the Western Scheldt

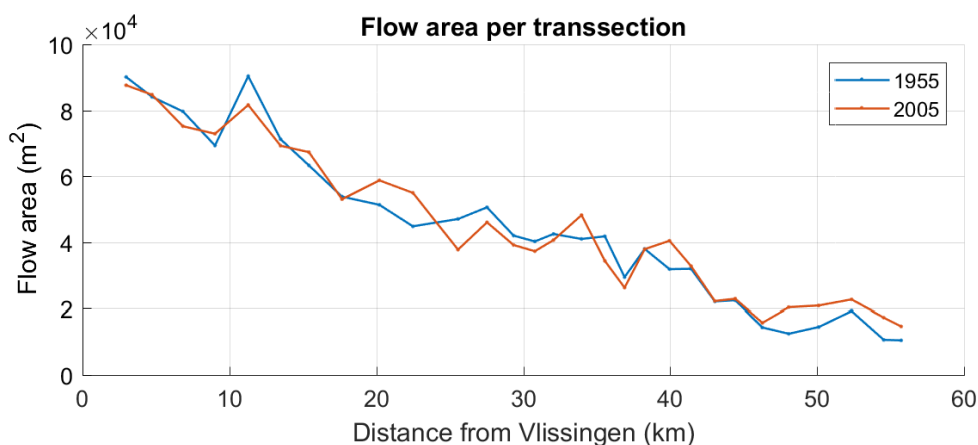


FIGURE 3.13: Longitudinal cross-sectional flow area Western Scheldt in 1955 and 2005

3.2.2 Cross-sectional hypsometry

Figures 3.14, 3.15 and 3.16 show the cross-sectional depth of the multi-channel system down stream and the single channel upstream near Antwerp. The cross-sectional depth of all transects is visualized in Appendix F. Cross-sections 7 and 28 show that the in many cases the main channels have become deeper and wider in 2005 compared to 1955. However, in some cases the intertidal areas have become higher as can be

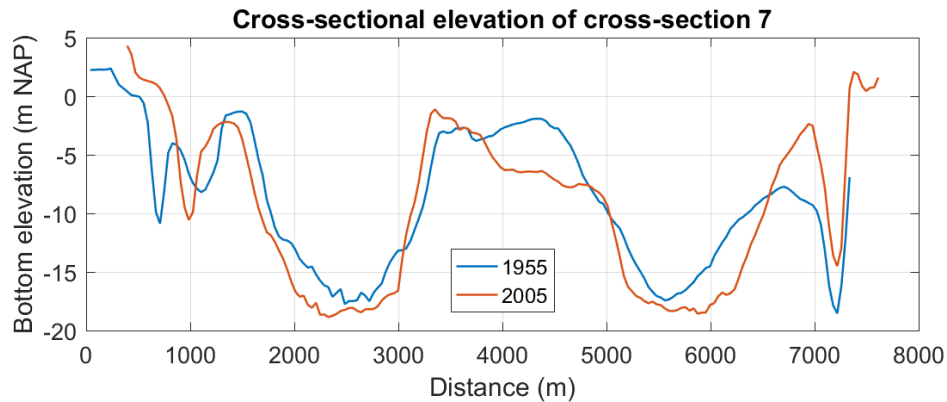


FIGURE 3.14: Depth profile cross-section 7 showing the downstream multi-channel system

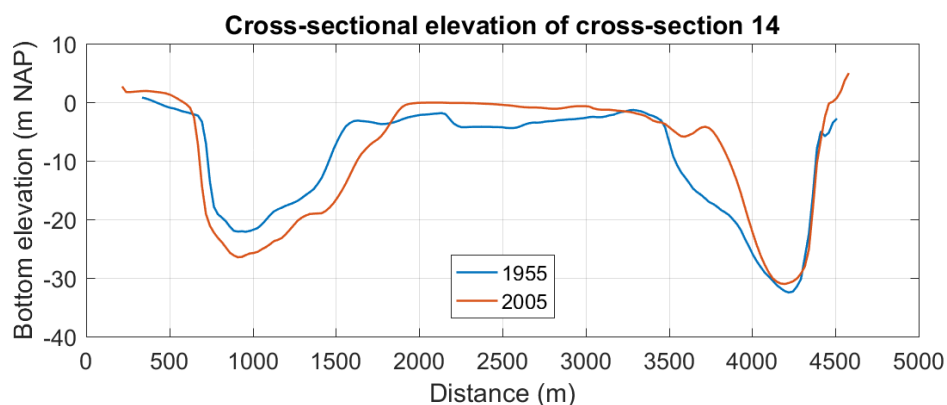


FIGURE 3.15: Depth profile cross-section 14 showing the multi-channel system in the middle of the Western Scheldt near Terneuzen

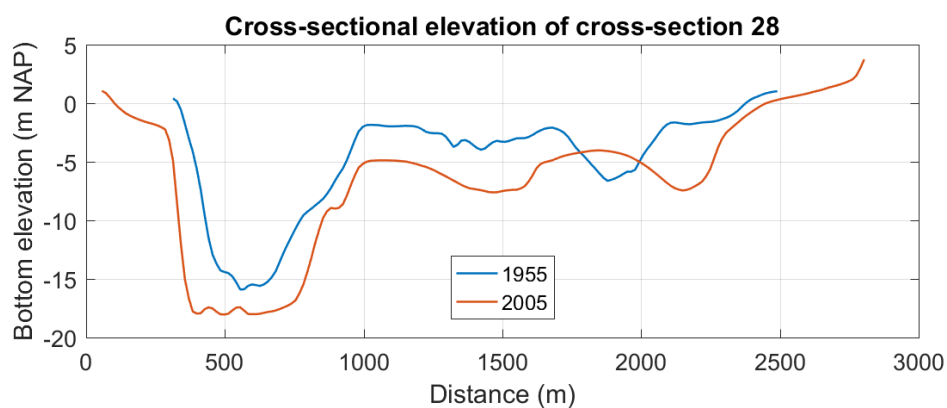


FIGURE 3.16: Depth profile cross-section 28 showing the upstream single channel system toward Antwerp

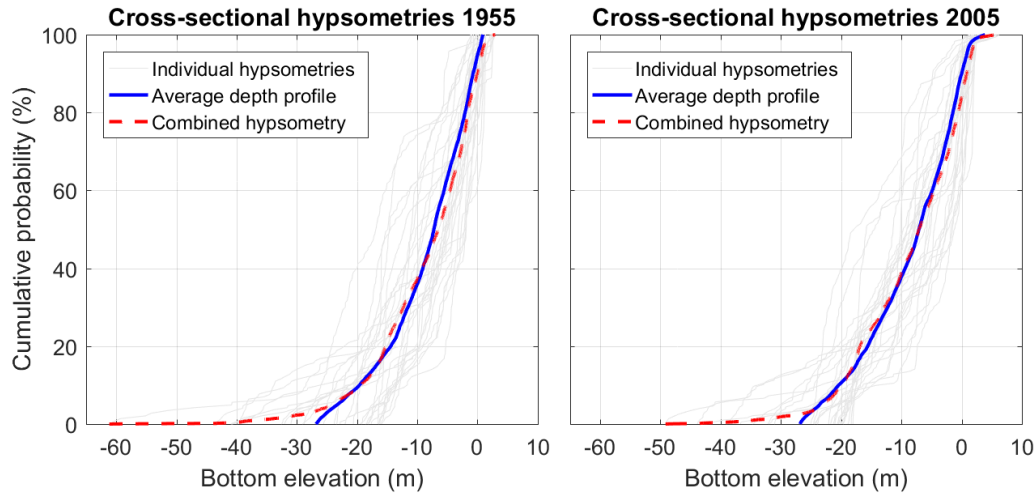


FIGURE 3.17: Cross-sectional hypsometries for 1955 and 2005 of the Western Scheldt

seen in the depth profile of cross-section 14. Figure 3.17 shows an overview of all cross-sectional hypsometries and how the average depth profile compares to this.

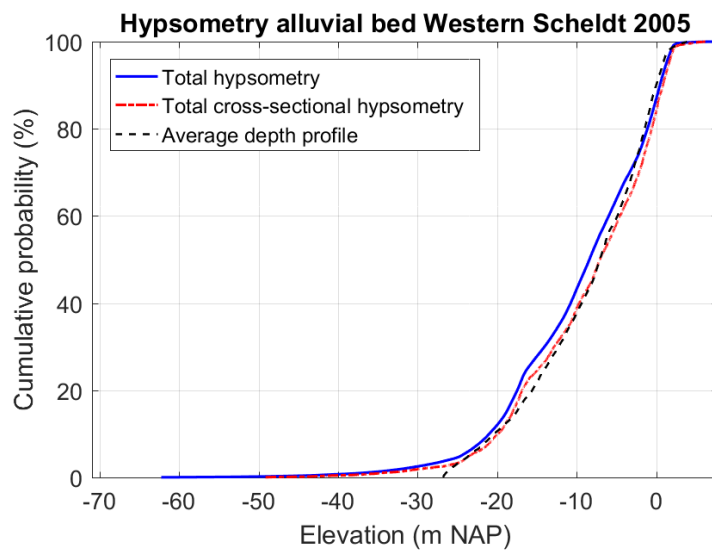


FIGURE 3.18: Comparison total hypsometry against cross-sectional hypsometry

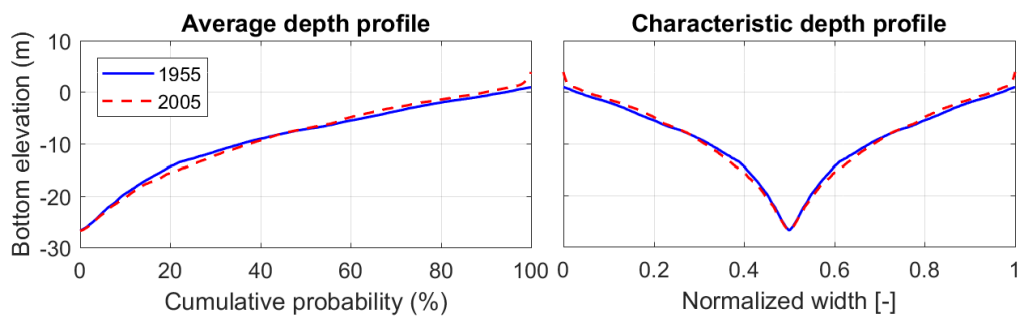


FIGURE 3.19: Characteristic cross-sectional depth profile

The hypsometric profiles of the cross-sections show that there is a significant deviation for per cross-section from the system wide hypsometry. Although, there is a limited amount of cross-sections, the total hypsometry based on this resembles the overall hypsometric curve (Figure 3.18). However, the cross-sectional hypsometry shows a profile that is slightly more shallow than then total hypsometry. The average depth profile based on the cross-sectional hypsometries, also follows the hypsometric curve quite well. It does however eliminate the extreme values, observed at the end of the curve, making it more suitable for characterizing the average cross-sectional flow area of the estuary.

Based on the average depth profile the characteristic channel-profile has been defined as shown in figure 3.19.

4 Results: Systematic Model Analysis

4.1 Step A: Lateral boundaries

This section will investigate the effect of two planimetric parameters, the convergence length (L_{conv}) and the converging length scale (k), on the amplification of the tidal range. Seventeen parameter combinations (Table 2.11) have been tested using the 2DH process-based model described in sections 2.3 and 2.4.

Figure 4.1a shows the relative tidal range (H_{rel}) profiles along a 180 km long

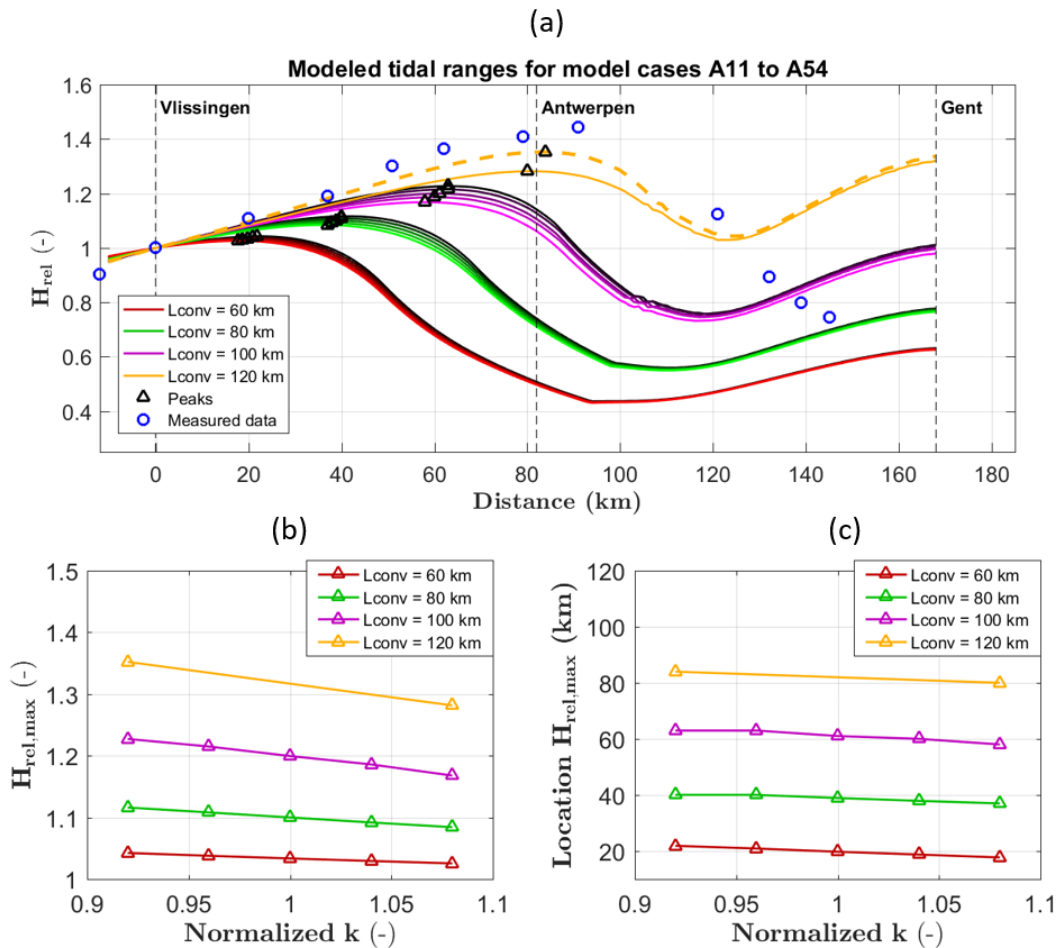


FIGURE 4.1: Comparison of the relative tidal range output of models A11 to A54. Figure (a) shows the tidal range profile along longitudinal axis of the estuary, where the dashed line highlights model case A14. Figure (b) and (c) show the sensitivities of the tidal range peak value and location to relative changes of the converging length scale (k).

idealized funnel-shaped basin. For all modeled cases, the tidal range shows three stages: 1) amplification downstream; 2) damping in middle section; 3) amplification toward landward boundary. The model results show four distinct groups of models, characterized by the convergence length. The bandwidth of each group is caused by the different values for the converging length scale ranging from 23 km to 27 km.

Figures 4.1b and 4.1c show that an increasing convergence length results in an increase of the maximum tidal range ($H_{rel,max}$) and a shift of the location of the peak in landward direction. The landward shift of the peak is linearly correlated to the increase of the convergence length, showing a peak that is always approximately 30 km downstream of the location where the prismatic section of the estuary starts.

Tables 4.2 and 4.2 show the data corresponding to figures 4.1b and 4.1c. These results show that the location of the peak is not significantly influenced by changes in the value of the converging length scale (k), and is mainly dependent on the value of the convergence length (L_{conv}). The maximum relative tidal range $H_{rel,max}$ is also strongly influenced by value of the convergence length. In case of a small convergence length ($L_{conv} = 60$ km), a 17% decrease of the converging length scale causes an increase of the maximum tidal range of 2%, which is small compared to the relative effects of the convergence length. For higher values of the convergence length ($L_{conv} \geq 100$ km), the effects of the converging length scale increases to 5%, which is comparable to the effects of the convergence length on the maximum relative tidal range.

The model performance is assessed using three validation criteria based on the

		L_{conv}			
		60 km	80 km	100 km	120 km
k	23 km	1.042	1.116	1.227	1.352
	24 km	1.038	1.108	1.215	-
	25 km	1.034	1.100	1.199	-
	26 km	1.029	1.092	1.186	-
	27 km	1.025	1.084	1.168	1.282

TABLE 4.1: Maximum relative tidal range values for all models A11 to A54 in analyzed during step A

		L_{conv}			
		60 km	80 km	100 km	120 km
k	23 km	21.9	40.0	63.0	84.0
	24 km	21.0	40.0	63.0	-
	25 km	19.8	38.9	61.0	-
	26 km	18.8	37.9	60.0	-
	27 km	17.7	37.0	58.0	80.0

TABLE 4.2: Relative tidal range peak locations [km] for all models analyzed in step A

Model	RMSE	Peak height ratio	Peak location ratio
A14	0.127	0.936	0.923
A54	0.149	0.887	0.879

TABLE 4.3: Validation parameters of two best performing spatial geometries

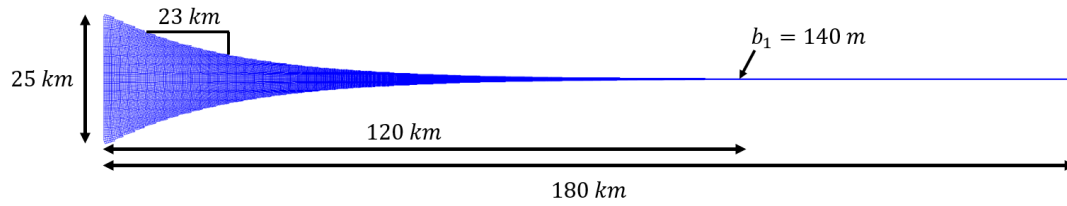


FIGURE 4.2: Computational grid of model case A14

relative tidal range profile: 1) RMSE; 2) Relative value of peak value compared to measured data; 3) Relative value of peak location compared to measured data (Section 2.4.4 and appendix G). Table 4.3 shows that the best performing model is case A14, with convergence length $L_{conv} = 120$ km and converging length scale $k = 23$ km (Figure 4.2). The model results slightly underestimate the value and location of relative tidal range peak and show more damping after the peak than observed in reality. The relative tidal range near the landward boundary shows strong amplification of the tidal range after damping, whereas measured data shows continuous damping in landward direction.

4.2 Step B: Uniform depth

This section analyzes the effect of changes in uniform depth on the amplification of the tidal range. The planimetric layout of model case A14 (Figure 4.2) has been used to test several uniform depth profiles ranging from 15 m to 5 m deep.

Figure 4.3a shows the relative tidal range profiles per model case, and figure 4.3b the change of the relative tidal range at specific locations across all model cases. From the relative tidal range profiles it can be seen that changes in uniform depth have a significant impact on the tidal range. The results show a difference in behavior of the tidal range in the converging section and the prismatic section. The amplification in the converging section is induced by convergence of the lateral boundaries and shows a linear trend. As the depth increases, the amount of amplification does not exceed a certain value and even decreases slightly for increasing depths (Figure 4.3b). The depths for which bottom changes significantly affect the relative tidal range lies at $d \leq 8$ m. This is close to the threshold depth as observed in the Scheldt estuary of approximately 7 m (Vandenbruwaene et al., 2013).

In the prismatic section of the basin amplification of the tidal range is caused by

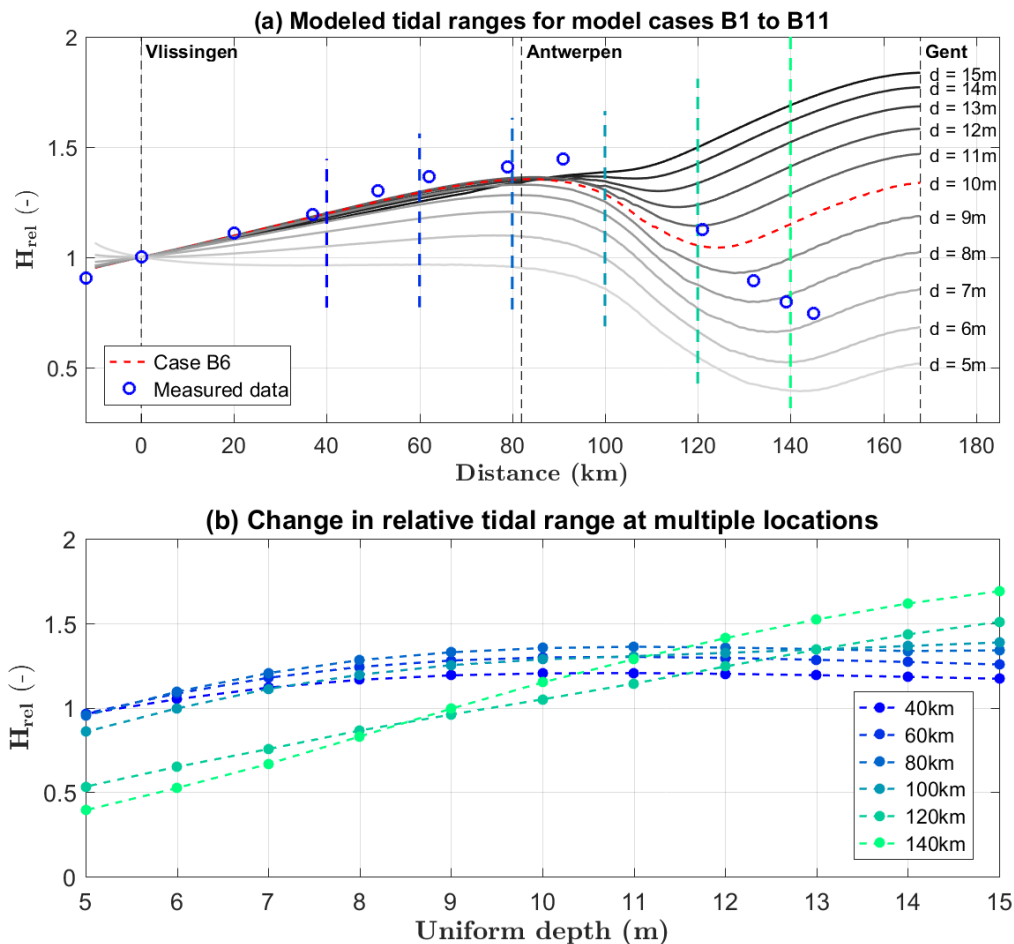


FIGURE 4.3: Comparison of relative tidal range output of models B1 to B11. Figure (a) shows the relative tidal range profiles along the longitudinal axis of the estuary. The red dashed line highlights model case B6. Figure (b) shows the effect of changing depths on the tidal range at different locations in the estuary.

Model case	$H_{Vlissingen}$ [m]	$H_{rel,max}$ [-]	$H_{rel,max}$ location [km]	RMSE [-]	Peak value ratio [-]	Peak loc. ratio [-]
B1	4.40	1.785	153.0	0.304	1.236	1.681
B2	4.41	1.715	153.0	0.273	1.187	1.681
B3	4.42	1.624	153.0	0.236	1.124	1.681
B4	4.43	1.519	153.0	0.196	1.051	1.681
B5	4.44	1.398	153.0	0.157	0.968	1.681
B6	4.44	1.354	83.98	0.127	0.937	0.923
B7	4.43	1.329	82.00	0.119	0.92	0.901
B8	4.39	1.282	79.98	0.150	0.887	0.879
B9	4.30	1.206	79.98	0.214	0.835	0.879
B10	4.14	1.099	76.03	0.301	0.760	0.835
B11	3.88	1.064	-9.98	0.405	0.737	-0.110

TABLE 4.4: Tidal range profile characteristics and validation of model output for cases with a uniform bottom profile

reflection. From figure 4.3b it can be seen that the sensitivity of the tidal range shows a continuous linear trend for increasing bottom depths, showing no clear threshold depth as is seen in the converging part of the estuary.

Validation of the tidal range profiles for model cases B1 to B11 show that the initial uniform depth of 10 m has the best fit compared to measured data (Table 4.4). Depths below 10 m underestimate the tidal range in the converging section and depths greater than 10 m overestimate the tidal range in the prismatic section. Therefore model case B6 with a uniform depth profile of 10 m is chosen for analysis in the following steps.

4.3 Step C: Longitudinal slope

The effect of bottom slopes on the relative tidal range has been analyzed using four longitudinal slope profiles as shown in figure 4.4 (Section 2.5.3). Two types of slopes have been analyzed: 1) a slope with the same length as the converging section of the basin (C1 and C2); 2) a constant slope along the model domain (C3 and C4). The resulting tidal range profiles are shown in figure 4.5 with a comparison of the tidal range results of model case B6, without any slope.

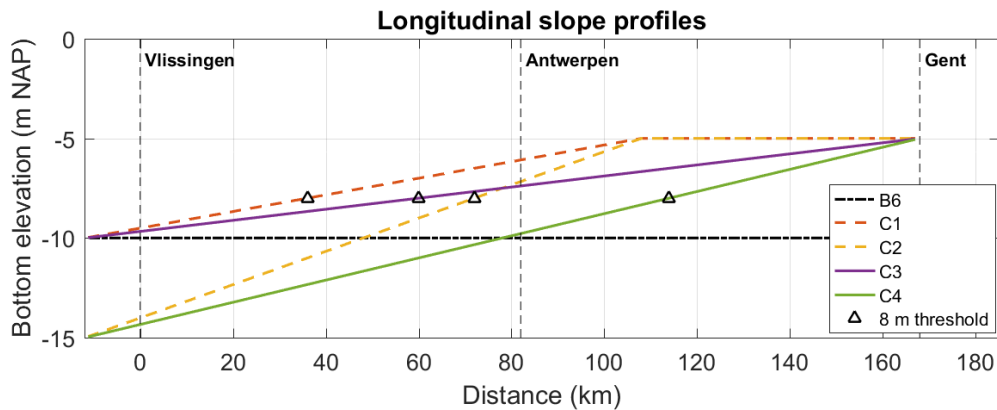


FIGURE 4.4: Comparison of tidal range output from the different longitudinal slope profile described in table 2.12

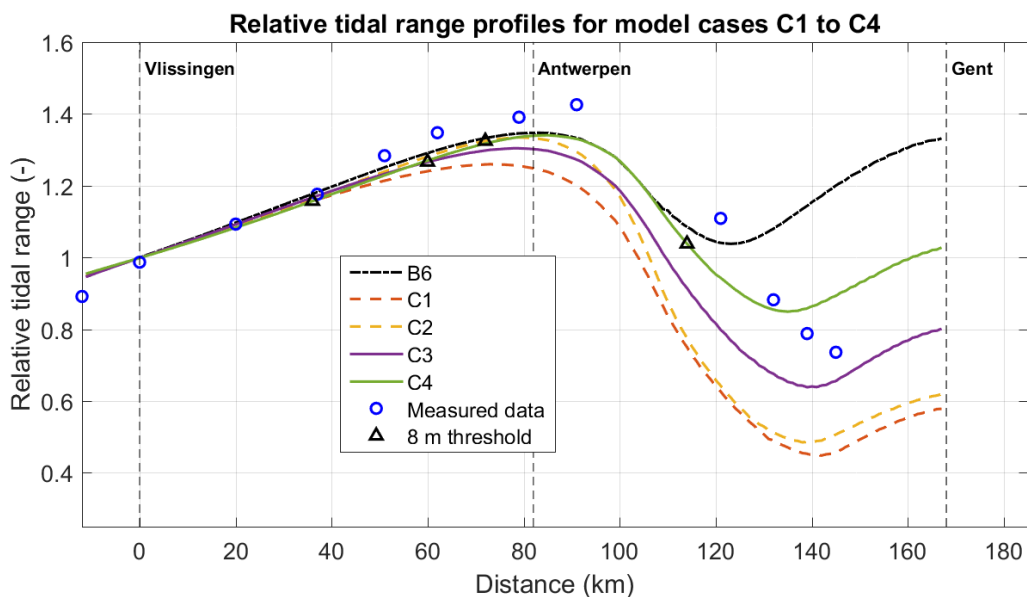


FIGURE 4.5: Comparison of tidal range output from the different longitudinal slope profile described in table 2.12

All profiles show linear amplification of the tide in the converging section, damping in the prismatic section and amplification in the landward boundary through reflection. The results show that the slope of the bottom profile does not have a significant impact on the relative tidal range when the bottom profile is deeper than the 8 m threshold determined in the previous section. At $x = 38$ km, model case C1 becomes more shallow than this threshold. At this location, the relative tidal range decreases compared to the other models that lie deeper than the 8m threshold. The

same difference is noticed in a comparison between model cases C3 and C4. The initial tidal range profiles of both models show no significant differences until $x = 60$ km. Upstream of this location, the tidal range of model case C3 is smaller compared to the tidal range of model case C4. The damping in the upstream prismatic section of the basin increases as the depth becomes smaller. This is apparent from the steeper negative gradients for $100\text{km} > x < 140$ km, for the shallow model cases (C1 and C2) compared to the deeper model cases (C3, C4 and B6).

All model cases underestimate the peak of the tidal range and generally overestimate the tidal range at the landward boundary. Based on validation, model C4 shows the best fit to observed data (Table 4.5). The introduction of a slope has increased the performance of the model compared to a uniform bed.

Model case	$H_{V\text{lissingen}}$ [m]	$H_{\text{rel,max}}$ [-]	$H_{\text{rel,max}}$ location [km]	RMSE [-]	Peak value ratio [-]	Peak loc. ratio [-]
B6	4.44	1.354	83.98	0.127	0.923	0.923
C1	4.46	1.260	73.00	0.259	0.872	0.802
C2	4.42	1.335	78.98	0.229	0.924	0.868
C3	4.46	1.304	77.98	0.168	0.903	0.857
C4	4.42	1.34	85.01	0.106	0.928	0.934

TABLE 4.5: Step C: Slope - Model output and validation results

4.4 Step D: Channel-shoal system

The implementation of the channel-shoal system is shown in figure 4.6 for the model case of D1 ($L_{conv} = 120$ km, $k = 23$ km, uniform width average depth 10m). Although the other models have different width average depths, planimetric parameters remain constant. The channel-shoal profile is defined as a proportion of the basin width. This means the channel-shoal profile has the same converging length scale as the lateral boundaries of the idealized basin. The effect of the channel-shoal system has been analyzed for models without a longitudinal slope (Section 4.2) and with a longitudinal slope (Section 4.3). The results of the channel-shoal models are shown in figures 4.8 and 4.9.

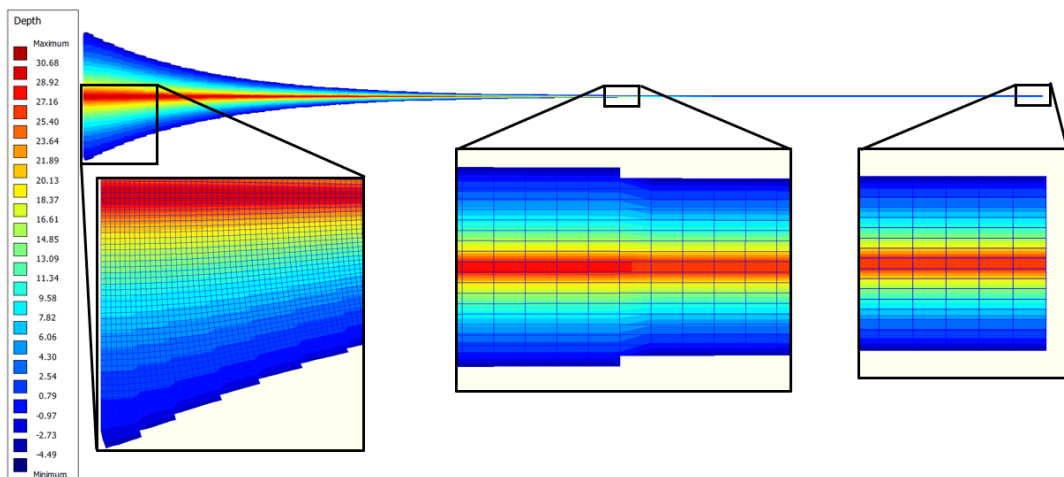


FIGURE 4.6: Top-down view of an example of channel-shoal bathymetry

4.4.1 Without longitudinal slope

The cross-sectional depth profiles of model cases D1, D2 and B6 are shown in figure 4.7. The tidal ranges resulting from these model cases without a longitudinal slope along the length of the estuary, are shown in figure 4.8. The two models with a channel-shoal pattern (D1 and D2) are compared with a situation without a channel-shoal pattern (B6). Model cases B6 and D1 both have the same width-average depths,

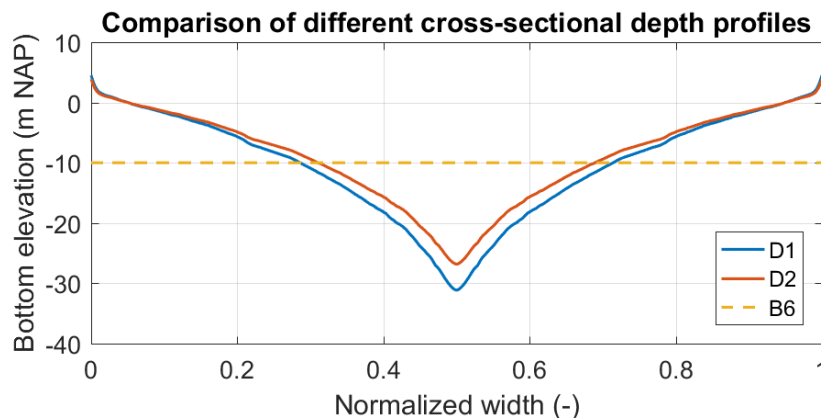


FIGURE 4.7: Cross-sectional profiles model cases D1, D2 and B6

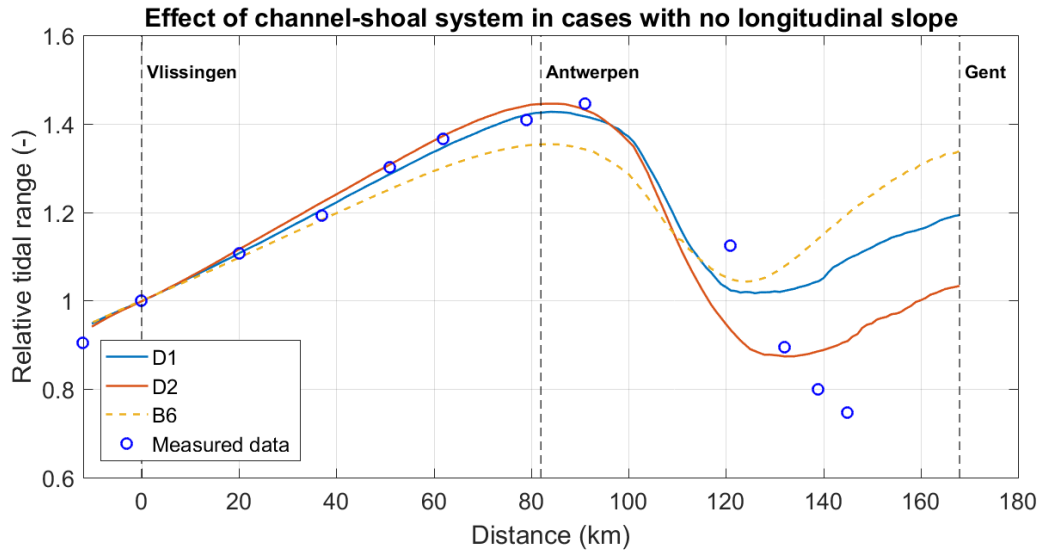


FIGURE 4.8: Comparison of tidal range profiles of models with and without a channel-shoal system

however there is a clear difference in the tidal range profiles. The model with a channel-shoal profile has a higher relative tidal range in the converging section of the basin compared to the model a uniform bed profile. The channel-shoal profile also causes increased damping in the prismatic section of the basin.

Comparison of the two models with a channel-shoal profile shows that an average depth decrease from 10 m to 8.62 m causes a slight increase of the relative tidal amplitude in the converging section and significantly increases damping in the prismatic section. The effect of the average width decrease in of the channel-shoal profile has the same characteristics as shown for a decrease of the uniform bed from 10 m to 8 m, shown in step B of the analysis (Section 4.2). A decrease in depth below the 8 m threshold causes a slight increase of the relative tidal range in the converging section and a strong decrease in the prismatic section. The profile with a width average depth of 8.62 m has a relatively larger and shallower shoal area than the profile a width average depth of 10 m. 49% of the bottom elevation lies above the threshold of -8 m NAP for the profile with a width average depth of 10 m. For the width average depth of 8.62 m this is 55%. The analysis in step B suggests that this decreases the relative tidal range in the converging section of the estuary. This is not observed in the results in figure 4.8.

Table 4.6 shows the characteristics of the tidal range profiles and the results of the validation. Model case D1 and D2 both fit the observed data adequately. For a

Model case	$H_{Vlissingen}$ [m]	$H_{rel,max}$ [-]	$H_{rel,max}$ location [km]	RMSE [-]	Peak value ratio [-]	Peak loc. ratio [-]
D1	4.45	1.427	83.98	0.091	0.988	0.923
D2	4.49	1.445	85.01	0.083	1.000	0.934
B6	4.44	1.354	83.98	0.127	0.937	0.923

TABLE 4.6: Tidal range characteristics and validation results of model cases with no longitudinal slope and a channel-shoal profile

constant average depth of 10m the amplification in the converging section is slightly better modeled. However, the damping at the upstream end of the system is better modeled in the case of a constant average depth of 8.62m.

4.4.2 With longitudinal slope

The channel-shoal profile applied to a sloping bed gives the tidal range profiles shown in figure 4.9. A comparison is made between the effects of the channel-shoal profile for a combination of a 120 km slope and 60 km uniform bed (D2) and a constant sloping bed profile (D4).

The results show that the channel-shoal profile increases amplification in the converging section and increases damping in the prismatic section for a sloped profile. This is similar to what is observed for the model cases without a slope (D1 and D2) in the previous section. A notable difference is that the increased amplification caused by the channel-shoal profile is smaller and happens further upstream for models with a slope compared to models without a slope.

Analysis in step C showed that the steepness of the slope had little effect on amplification of the tidal range. By comparing model cases D3 and D4, it can be seen that the amplification in the converging section of the basin is significantly increased for a steeper slope and the presence of a channel-shoal profile.

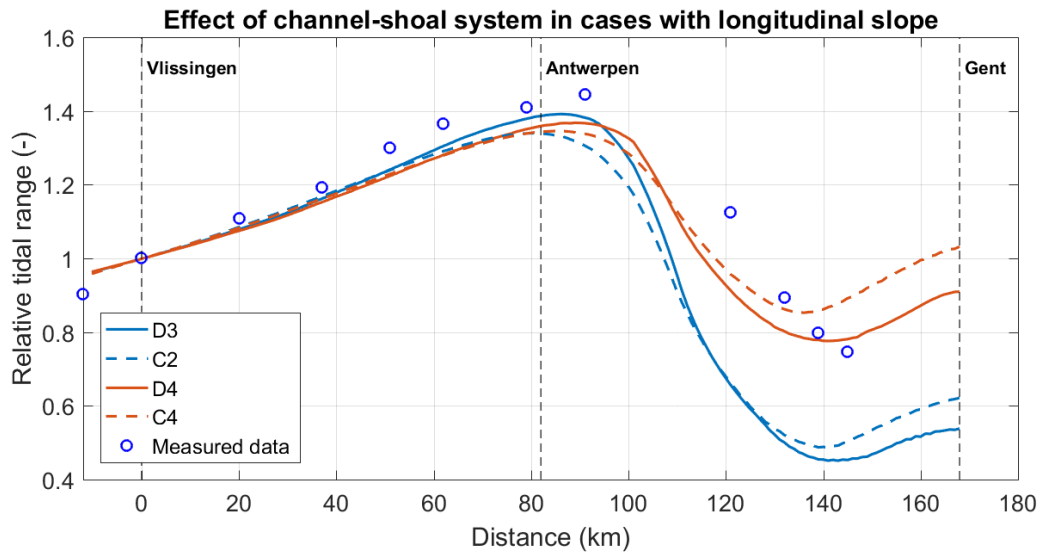


FIGURE 4.9: Tidal range output for models D3 and D4, compared with models C5 and C3

Model case	$H_{Vlissingen}$ [m]	$H_{rel,max}$ [-]	$H_{rel,max}$ location [km]	RMSE [-]	Peak value ratio [-]	Peak loc. ratio [-]
C2	4.42	1.335	78.98	0.229	0.924	0.868
D3	4.38	1.392	86.01	0.211	0.963	0.945
C4	4.42	1.341	85.01	0.106	0.928	0.934
D4	4.37	1.368	88.99	0.102	0.947	0.978

TABLE 4.7: Step D: Channel-shoal - Model output and validation results of model cases with a longitudinal slope

The model validation results shown in table 4.7 show that model case D3 has the best fit to the observed data when looking at the RMSE. However, as can be seen from the peak values and visual inspection, model case D4 performs better in the converging downstream section of the model.

Validation of the model results shows that a constant sloping profile has a better fit to measured data than a slope of 120 km and a uniform bed upstream. The model results of the sloped models, however, perform worse compared to model case D2, with a constant width average depth of 8.62 m (See tables 4.6 and 4.7).

4.5 Step E: Interventions

The effects of interventions has been analyzed based on the historical evolution of bathymetry in the Scheldt estuary and a scenario analysis of several local changes in bathymetry. The bottom profiles are implemented using the planimetric parameters derived in step A ($L_{conv} = 120$ km, $k = 23$ km) and the results are interpreted based on the results of the previous analyses.

4.5.1 Historical analysis

To analyze the effects of bathymetric changes of the last 50 years, the two longitudinal bottom profiles of 1955 and 2005 have been implemented in the model. The width average depth profiles are shown in figure 4.10 and the tidal range results are shown in figure 4.11. The evolution of the longitudinal bottom profile over the last 50 years, described in section 3.2.1, can be summarized with the following characteristics:

- Increased average depth estuary wide
- Largest deepening around $x = 50$ km
- Shallowing around $x = 30$ km
- Slightly decreased channel depths
- Increased main channel width

The model results show that the relative tidal range has increased from 1955 to 2005. There is a small increase between $x = 30$ km and $x = 50$ km. In 1955 there is a noticeable damping of the tidal range at $x = 50$ km. The slight increase from 30 km onward can be explained by the decreased bottom depth below the threshold depth of 8 m. The deepening at $x = 50$ km happens from -5 m NAP to -7 m NAP. In 1955 the shallow depth of 5 m caused visible damping of the tidal range at $x = 50$ km, but this effect is gone in the tidal range results of 2005, which corresponds with measured values in the Scheldt estuary. The gradients in the tidal range profiles in the prismatic section are very similar, showing that damping in these sections is comparable. From the results it can be seen that the local bathymetric changes at $x = 30$ km and $x = 50$ km, have large effects on the tidal range upstream of their location, but none in the downstream direction.

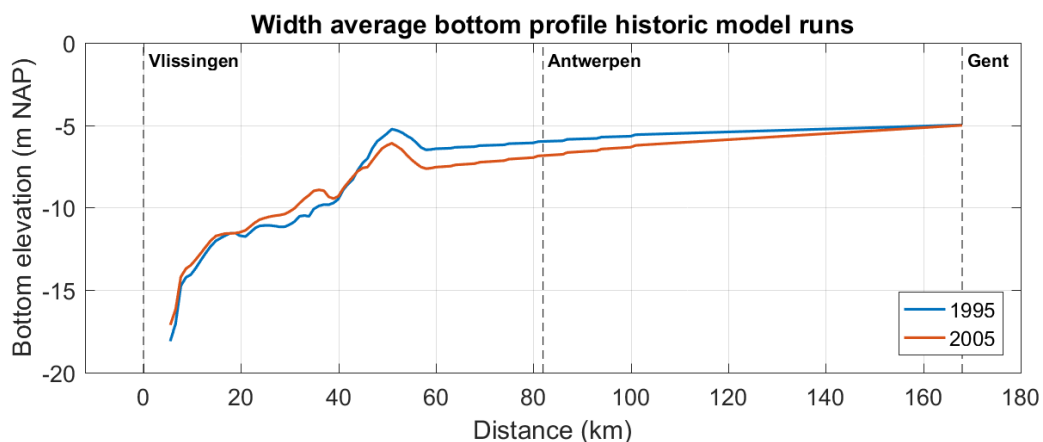


FIGURE 4.10: Longitudinal bottom profiles of Scheldt estuary used in model schematization

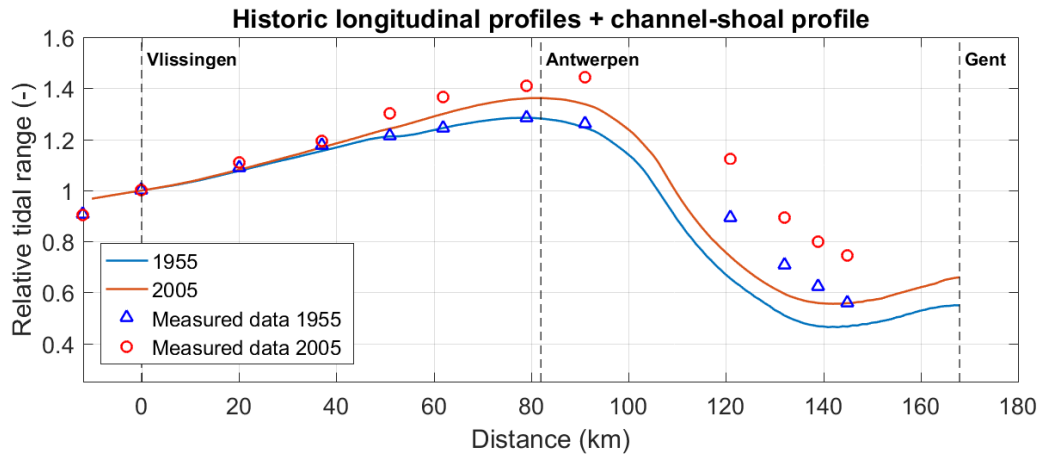


FIGURE 4.11: Comparison of the modeled relative tidal range profiles based on the historic longitudinal bottom profiles, including the 2005 channel-shoal profile obtained from data analysis (Section 3.2)

Table 4.8 shows the tidal range characteristics and the validation results compared to measured data. The 1955 modeled results are compared the 1955 measured data by Taal, Meerschaut, and Liek (2015) (Section 3.1.1) and the 2005 modeled results to the 2005 measured data. This shows that the idealized model with the current geometry accurately models the tidal range amplification in the converging section, but overestimates damping in the upstream section. The model also accurately models the damping caused at $x = 50$ km by a local shallow section of the estuary for the 1955 situation. The performance of the 2005 model is worse than that of the 1955 model. It underestimates the amplification in the converging section of the estuary and strongly overestimates the damping in the upstream section of the estuary.

The overestimation of damping at the end of the system can be attributed to the simplification of the lateral boundaries as prismatic (without any convergence), while in reality there is still a slight convergence of the width in this section. Additionally, the bottom profile in the upstream section is modeled as a nearly uniform bottom based on scarce estimates found in literature. Because the depth lies well above the threshold depth the effect of changes in depth can have significant effects on the damping of the tidal range.

Model case	$H_{Vlissingen}$ [m]	$H_{rel,max}$ [-]	$H_{rel,max}$ location [km]	RMSE [-]	Peak value ratio [-]	Peak loc. ratio [-]
1955	4.36	1.284	78.02	0.107	1.000	0.988
2005	4.36	1.362	82.00	0.178	0.942	0.901

TABLE 4.8: Tidal range characteristics and validation results for historic and present bottom profiles of Scheldt estuary

4.5.2 Intervention scenarios

The 10 intervention cases described in section 2.5.5 have been analyzed. Figure 4.12 and 4.13 show the bottom profiles of the interventions.

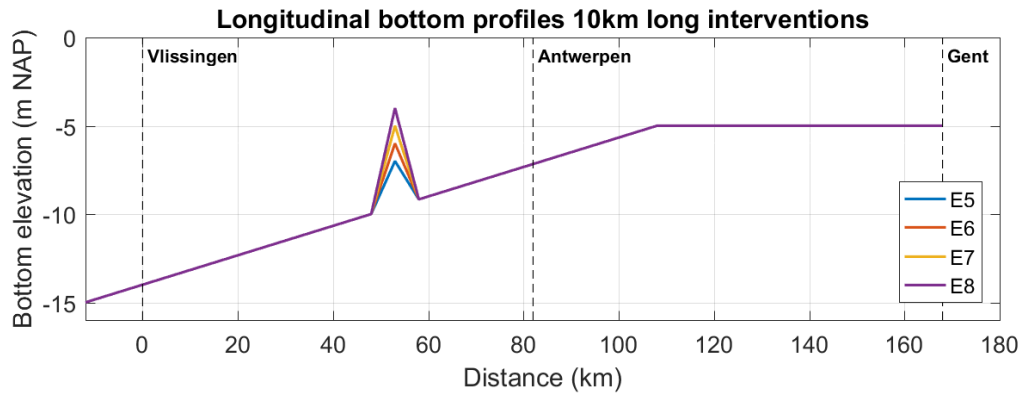


FIGURE 4.12: Altimetric profiles local interventions of 10 km long

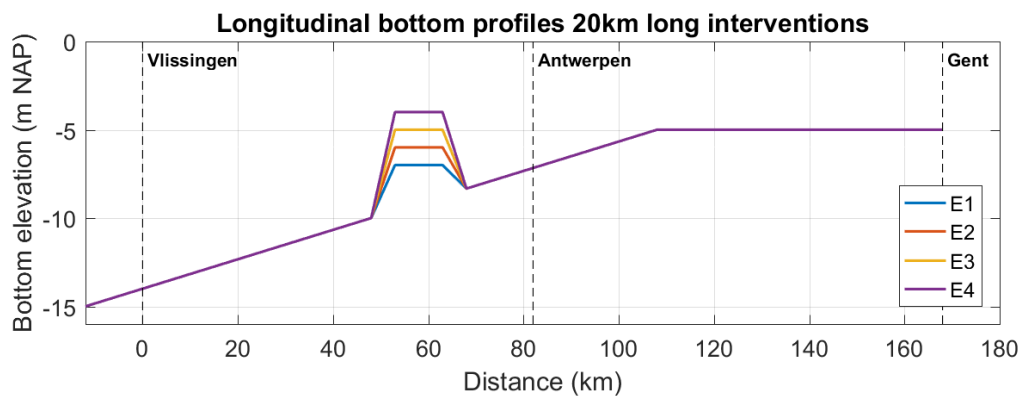


FIGURE 4.13: Altimetric profiles local interventions of 20 km long

Figures 4.14 and 4.15, show the tidal range profiles corresponding to the bathymetric profiles shown above. The results show that the tidal range can be influenced significantly with these local changes in altimetry. The interventions have a damping effect on the tidal range. For the short interventions there is an equal decrease of

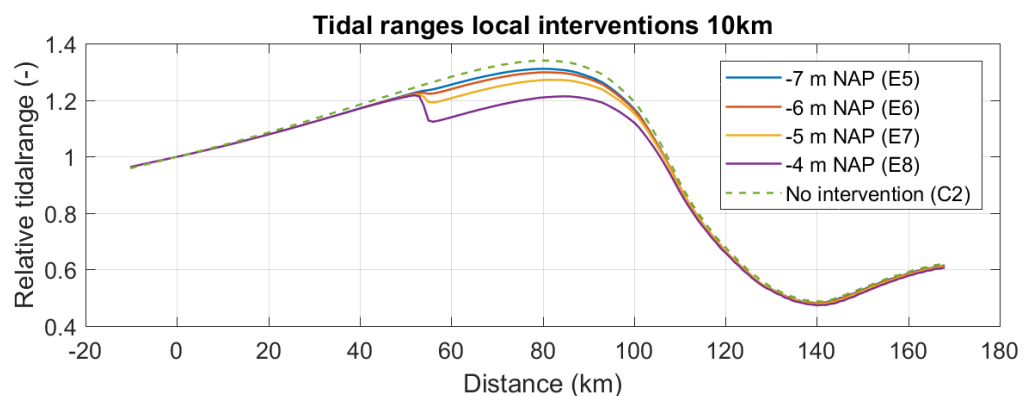


FIGURE 4.14: Tidal ranges of local interventions of 10 km long

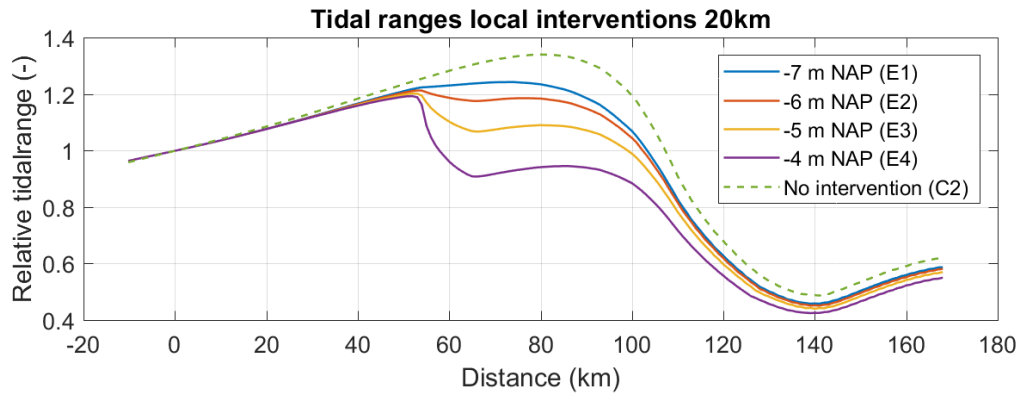


FIGURE 4.15: Tidal ranges of local interventions of 20 km long

the tidal range, downstream of the location of the interventions. Upstream of the intervention the tidal range is decreased more or less depending on the height of the bump. This decrease only affects the tidal range up until $x = 120$ km, showing that there is no significant influence in the prismatic part of the estuary.

The interventions of 20 km long have a larger effect on the tidal range than the short interventions (Figure 4.15). Downstream of the interventions, the tidal range is decreased in the same order of magnitude as for the short interventions. The effects upstream show a more gradual decrease of the tidal range over the length of the intervention of 20 km. The effects are most noticeable in the section just after the intervention. In the prismatic section upstream the tidal range tends back to the original tidal range profile.

Figures 4.16 and 4.17 show the tidal range profiles and water levels for interventions including a channel-shoal profile. The intervention with a channel-shoal profile consist of a shallowing and narrowing of the main channel. The area of the shoals is increased and their depth is slightly decreased. The results show similar behavior of the interventions without a channel-shoal profile. The downstream tidal range is slightly decreased, and the main effect lies in the area directly upstream of the intervention location. The width-averaged depth of models E9 and E10 is equal to that of E4 and E8 (-4 m NAP), but the effect on the tidal range is less in case of the presence of a channel-shoal profile.

Figure 4.17 also shows that the decrease in tidal range is mainly caused by a raise

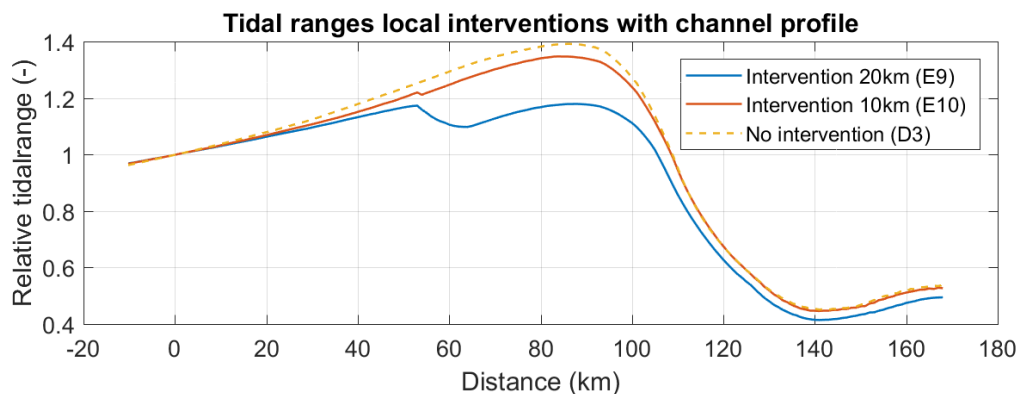


FIGURE 4.16: Tidal ranges of local interventions with a channel-shoal profile

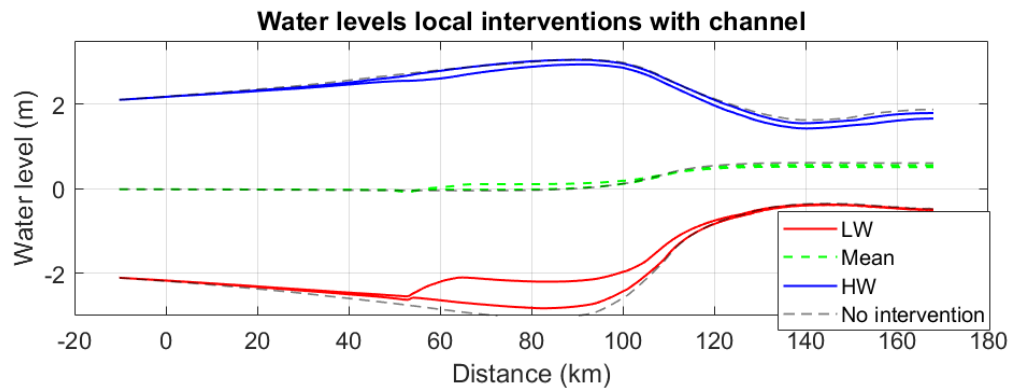


FIGURE 4.17: Water levels of local interventions with a channel-shoal profile

of the lower water levels. The HW levels remain almost the same. The intervention of 10 km long does not alter the HW levels significantly. The 20 km long shows that the decrease of the HW level is happening gradually along the length of the intervention.

4.6 Validation underlying processes

Analysis of the underlying processes has been done based on the wave deformation, wave celerity, flow velocities and phase lag. All model results and validation data are shown in Appendix G. In this section, the validation of model A14 is explained in more detail.

Figure 4.18 and table 4.9 show that the duration of flood phase decreases in upstream direction. This means that the model A14 simulates a flood-dominant system which corresponds to what is observed in the Scheldt estuary. The ratio of flood and ebb duration is overestimated in the model. Measurements at Antwerp (83 km) show that flood and ebb duration are 5 and 7 hours respectively (section 3.1.2), compared to 4.42 and 7.58 hours at 73 km in the model. The shape of the modeled tidal curve shows an increased water level gradient at the start of the flood phase (Figure 4.18) as the wave progresses upstream. This corresponds with observations of the tidal curve at spring tide at Antwerp (Figure 3.4). However, in the model results this gradient increases to unrealistic values in the prismatic section of the basin.

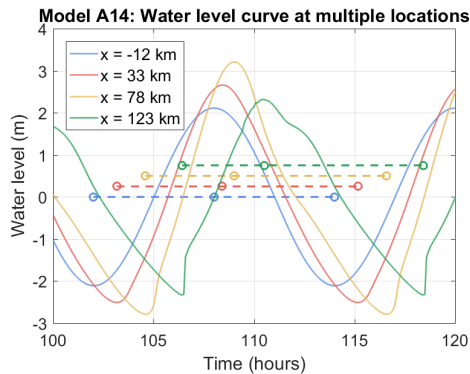


FIGURE 4.18: Water level curves over the duration of one tidal cycle at multiple locations in the modeled tidal basin. The dashed lines highlight the durations of the flood and ebb phases at each location.

Loc. [km]	Flood [hours]	Ebb [hours]	Ratio
-12	6.00	6.00	1.000
33	5.25	6.75	0.778
78	4.42	7.58	0.582
123	4.08	7.92	0.516

TABLE 4.9: Flood and ebb durations within tidal cycle at multiple locations for model case A14

The wave celerity of the modeled tidal wave is significantly higher than the 8-10 m/s observed in the Scheldt estuary. In the downstream section of the idealized basin the wave celerity reaches a values of 30 m/s, with an average along the basin of ~ 20 m/s. This suggests that the model case simulates a more progressive wave than is observed in reality. This is supported by the results on phase lag in the modeled system (Figure 4.19). In reality, phase lag at the mouth in the Scheldt estuary ranges between 22.5° and 30° and according to Savenije (2001), decreases in upstream direction. The model results show that the phase lag at the mouth lies close to observed values, but increases in upstream direction, contrary to observations in most alluvial estuaries. The steps observed in the results of figure 4.19 are caused by increments of 5 minutes with which model output has been generated. Therefore the phase lag can only be determined in increments of 5 minutes. The large jumps at $x = 160$ km, are caused by the fact that the velocity curve becomes increasingly asymmetrical due to complete reflection of the tidal wave at the landward boundary. This results in instabilities in the model results (Figure 4.20).

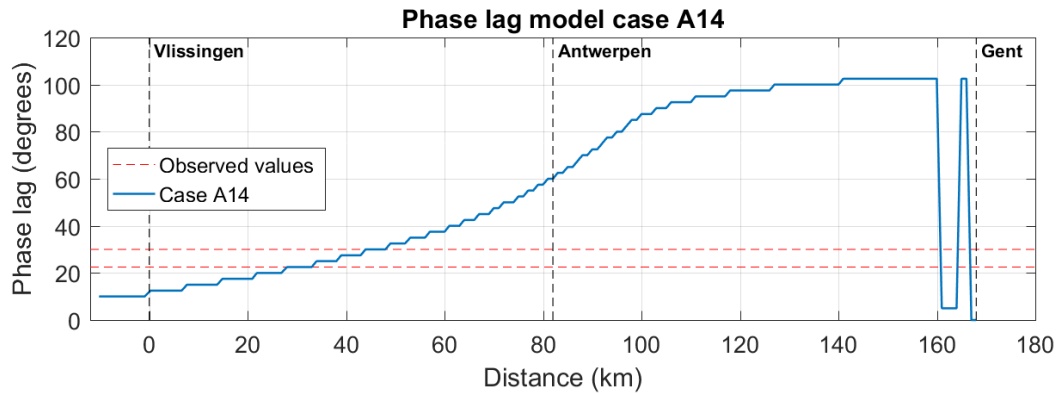


FIGURE 4.19: Phase lag between high water and high water slack along the length of the estuary for model case A14

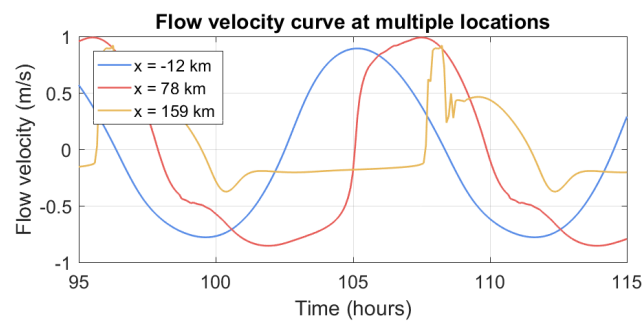


FIGURE 4.20: Flow velocity curve at multiple locations along the tidal basin for model case A14

The flow velocities for model case A14 (Figure 4.21) show that the modeled ebb and flood velocities are in the same order of magnitude as what is observed in the Scheldt estuary. The jumps in maximum flow speeds are the result of sudden narrowing of the computational grid (Section 2.4.2). The jumps are small enough to ensure that the numerical model remains stable, with a run time between 2 to 4 hours.

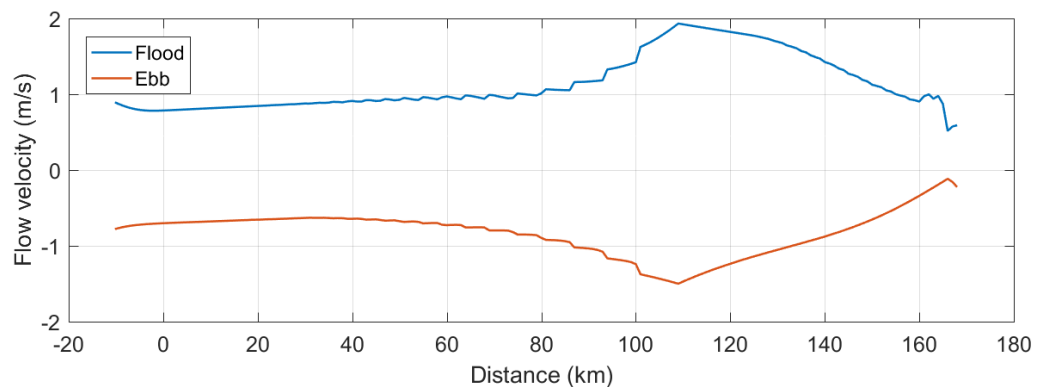


FIGURE 4.21: Maximum flow speeds during flood and ebb along the length of the modeled basin for case A14

5 Discussion

This study has focused on the tidal hydrodynamic processes that occur in estuarine tidal basins and how they are connected to planimetric and altimetric characteristics of the estuary. This chapter will analyze and discuss the results obtained during data analysis and the results obtained from the hydrodynamic model set-up in this study.

5.1 Uncertainty in data

For the historic and current tidal range data, three sources were found by [Pieters \(2002\)](#), [Taal, Meersschaut, and Liek \(2015\)](#) and [Van Rijn \(2010\)](#). The inconsistencies found in the data by [Van Rijn \(2010\)](#) are difficult to explain as the origin and method of how the data was obtained is unknown. The two other sources showed better agreement, apart from the last time period measured by both sources. The deviation between [Pieters \(2002\)](#) and [Taal, Meersschaut, and Liek \(2015\)](#) can be explained by the fact that Pieters' most recent measured data stems from two decades earlier than Taal, et al.'s most recent data set. Although, there are differences in the exact shape of the tidal range profile from each source, it is expected that this has no influence on the model behavior. However, quantitatively parameters for planimetry and altimetry might be different through calibration to another tidal range profile.

5.2 Bathymetric analysis

There are significant uncertainties in the bathymetric profile of the model. Based on literature, several general assumptions had to be made for the bed profile in the upstream part of the estuary, as the bathymetric data availability is limited to that of the Western Scheldt. Additionally, the cross-sections have been defined manually, determining the perpendicular of the flow direction based on visual inspection. This might mean that some cross-sections are slightly angled and overestimate the estuarine width. The method of determining the width is dependent on the data availability in the database. After the cross-sections were determined, it was noticed that some elevations exceeded 3.5m NAP at the edges, suggesting an overestimation of the average width of the estuary. This can have an effect on the calculation of the rate of convergence k in the Western Scheldt. However, the 23km obtained from the data analysis closely resembles values from other studies and quick visual inspection in Google Earth. Therefore it is not likely to have a large effect on the model outcomes.

5.3 Channel-shoal design

This study has simplified the channel-shoal system greatly, using a single channel to shoal ratio for the whole model basin and removing multiple channels and meanders. In reality the Western Scheldt shows a system of multiple meandering main ebb channels with connecting flood channels. Although this channel profile approached the shape of a compound channel, it is likely that the importance and effect of the shoals

on the tidal range is underestimated in the model due to this schematization. The used channel profile has a gradual slope toward the deep main channel in the middle of the estuary. This means that the area of shoal above -2m NAP is underrepresented in the model simulation. As is shown in the results, the tidal range is relatively more sensitive to changes of elevation in shallow areas. It is also likely to influence the horizontal deformation of the tidal wave as well as extensive shallow shoals induce flood-dominance of the tidal wave.

A difficulty that arises with relatively flat shoals, is the drying and flooding of these intertidal areas and the way this is handled in Delft3D-FLOW. Several analyses were performed with a schematized compound channel with shoals at an elevation of 0m NAP and a square main channel with a depth of 15m. The model showed large amounts of water being retained on the shoals, caused by the model not accurately drying the cells on large shoal areas. This problem was not observed with the gradual channel profile used in the current analysis.

5.4 Order of systematic analysis

The choice for the order of the systematic analysis has been based on sensitivity analyses in literature and practical considerations. In hindsight it has appeared that introducing a channel-shoal pattern can strongly influence the behavior of tidal amplification in the estuary. The current geometry is based on a uniform bed. If a channel-shoal pattern with longitudinal slope had been chosen to more accurately resemble the bathymetry in the Scheldt as a first step a very different e-folding length scale and convergence length might have been found during calibration.

The order of the analysis thus has significant influence on the value of the parameters chosen in the study. This does not mean that the qualitative behavior in the model has been influenced. It is expected that the order of the analysis might result in a parameter set with different values for planimetry and altimetry, but it is expected that it will not change the behavior of the hydrodynamic model. Even if the rate of convergence, basin length and slope length were slightly different, the effects of the channel-shoal system and local interventions would remain the same. This assumes that the planimetric and altimetric parameters determined in the analysis resemble observed physical characteristics of the Scheldt estuary.

5.5 Hydrodynamic processes

The model has shown that the tidal range is mainly affected by macro-scale changes to planimetry and altimetry. Calibration of the model using a longitudinal slope and general rate of convergence, has given adequate results of the tidal range profile. However, underlying processes are showing significant inaccuracies compared to observed values. The wave celerity and phase lag in the model are overestimated. This is likely the cause of the straight channel-shoal system with deep main channels. The impact of this inaccuracy is noticed in the relative effect of amplification through shoaling in the converging section of the estuary. However, amplification in the estuary is governed by the convergence of the lateral boundaries resulting in good estimation of the tidal amplification.

Internal behavior of the model is in accordance with the theoretical background, where as the phase lag increases the wave celerity decreases. This means that the current model can be used to assess large scale changes of altimetry and planimetry, such as changes in the rate of convergence and changes to the longitudinal slope.

However, to assess the effect of small/local altimetric changes will require a more detailed channel-shoal design.

6 Conclusion

At the start of this study 4 research questions have been formulated in order to answer the main objective, namely:

“To determine the effects of planimetric and altimetric changes on the tidal propagation and amplification in a well-mixed macro-tidal coastal plain estuary.”

This chapter will answer each of the individual research questions which are repeated below for convenience. The answers to these questions have been reached through data analysis and analysis with an idealized 2DH hydrodynamic model. The model has been set-up and validated for the case study of the Scheldt estuary based on studies by [Van Rijn \(2010\)](#), [Pieters \(2002\)](#) and [Taal, Meersschaut, and Liek \(2015\)](#).

1. *How have the tidal and morphological characteristics of the Scheldt estuary evolved over the last century?*

Historical water level data of the Scheldt estuary have shown that the tidal range at Antwerp has increased approximately by 18% from in the period of 1900 to 2000. During this time the peak of the tidal range profile has increased by 18% and the location of the peak has shifted more upstream by approximately 25km. Results of the water levels in the Scheldt estuary have shown that the estuary is predominantly flood-dominant. At Westkapelle however the tide is almost symmetrical with equal flood and ebb phase durations.

Results of the historic evolution of the bathymetry show a significant deepening going from an average bottom elevation of -8.73m NAP in 1955 to -9.33m NAP in 2005. The largest differences in depth are found in the upper part of the Western Scheldt where the width-average bottom elevation in 2005 is significantly deeper compared to 1955. Additionally, the main channels of the estuary have evolved over the last 50 years showing a decrease in surface area of the shoals and a widening of the main channels. However, the depth of the main channels has decreased slightly.

2. *How can the hydrodynamic system and morphology of the Scheldt estuary be modeled using an idealized process-based model in Delft3D?*

The tidal hydrodynamics in a coastal plain estuary can be modeled using an idealized, exponentially decreasing, funnel-shaped tidal basin implemented in Delft3D-FLOW. The implementation of a curvilinear grid improves the accuracy of the model significantly in the middle and upper regions of the estuary. The model shows distinct processes of amplification caused by shoaling, convergence of lateral boundaries and reflection, and damping through bottom friction. The model shows linear amplification in the converging section and exponential damping in the prismatic section upstream, which is in accordance with theory from other literature. The model struggles with reflection at the landward boundary of the model, which causes an amplification of the tidal range, not observed in reality. This can partly be solved by

introducing a uniform shallow depth at the end of the system and implementing a channel-shoal profile.

The model can be used to simulate tidal amplification in the lower and middle sections of estuaries where the reflection of the landward boundary plays no role. It can also be used to estimate the qualitative effects of large scale interventions such as changes in the longitudinal slope or changes in the convergence of the lateral boundaries. However, the model cannot be used for morphological evolution as the flow speeds, phase lag and wave celerity deviate significantly from observed values.

3. *How do planimetric and altimetric changes affect the tidal propagation and tidal amplification in a tidal basin?*

The tidal amplification is dependent on the combination of three basic processes:

1. Amplification through convergence of lateral boundaries
2. Amplification through shoaling
3. Damping through bottom friction

The model results show that for decreasing depths below a certain threshold, the tidal range is increased in the converging part of the estuary, but decreased in the prismatic part of the estuary. This is in line with the theory by [Savenije \(2001\)](#), which states that amplification of the tide is dependent on a combination of the depth and the rate of convergence, while damping in the prismatic part is purely dependent on the bottom friction. However, when the depth becomes shallower than a threshold depth, the tidal range is reduced throughout the estuary. The value of this threshold is dependent on the rate of convergence. As the rate of convergence increases, the threshold depth for which a basin become damping decreases. By introducing a longitudinal slope in the converging part of the estuary the tidal range is increased even more.

4. *How does the channel-shoal pattern and local interventions influence the hydrodynamic processes in a tidal basin?*

The channel-shoal system decreases the effective depth of the estuary, which causes the tidal range to increase in the converging part and decrease in the prismatic part, compared to a basin without a channel-shoal system. Although the width-averaged depth of the channel-shoal system is exactly the same as the model without a channel profile, the tidal wave is relatively more sensitive to friction on the shoals than it is to the depth in the main channel.

Local increases of bottom elevation only have significant effect on the tidal range if the bottom elevation exceeds the threshold depth, which is around -8 m NAP. However, the so-called 'bumps' only seem to affect the LW levels while HW levels remain relatively constant. Even then, the size of the intervention has to be enormous to show any significant effects on the tidal range. Changes in the HW levels can be realized by changing the longitudinal slope of the estuary as is shown by the model results of the 1955 and the 2005 smoothed longitudinal slopes.

In conclusion this research has shown that the tidal amplification in a coastal plain estuary is strongly dependent on the planimetry and altimetry of the tidal basin. Alterations of the planimetry and altimetry, caused by human interventions can be used to increase or reduce the amplification of the tidal range. Additionally, the general effects of an intervention can be estimated using a strongly simplified 2DH hydrodynamic model.

7 Recommendations

Based on the discussion, conclusions and experiences gained during this study the following recommendations are presented:

Extend research of channel-shoal system During this study a single channel profile was tested within the model. It would be interesting to extend the knowledge on how the shape of the cross-sectional profile affects the amplification and deformation of the tidal wave in a funnel-shaped estuary. This could be done by implementing channel-shoals systems with varying width for the main channels and shoals and by changing the elevation of the main channels and shoals. Additionally, the effects of meandering channels on the propagation of the tidal wave are still unknown and could lead to a better understanding of the interaction between the tidal range and the channel-shoal system.

Apply the model to other coastal plain estuaries Currently the model has been calibrated based on the Scheldt estuary. To test whether the model is robust, it should be applied to other coastal plain estuaries with a funnel-shaped basin, but with different physical characteristics.

Analysis of underlying processes Theory by [Savenije \(2001\)](#) and results from this study have shown that phase lag, wave celerity and the amplitude of flow velocities in the estuary play an important role in the amplification of the tide. A better understanding of the relationship between altimetry and planimetry, and these processes can improve model results and the ability to predict the effects of interventions in an estuarine tidal basin on the tidal range.

Extend analysis of interventions Currently the interventions have only been tested for very with a simultaneous increase of both the elevation in the main channel and the area of shoals. To better understand the effects of human interventions this could be extended by testing several effects individually and in combination

- Individual effects of local widening and narrowing of the main channel
- Locally increasing or decreasing shoal elevation
- Locally increasing or decreasing main channel elevation
- Changing the location of the interventions along the length of the estuary

Bibliography

- (RWS), Rijkswaterstaat (2017). “Getij”. In: URL: <http://getij.rws.nl/> (cit. on p. 43).
- Ahnert, F. (1960). “Estuarine Meanders in the Chesapeake Bay Area”. In: *Geographical Review* 50.3, pp. 390–401. DOI: [10.2307/212282](https://doi.org/10.2307/212282) (cit. on p. 11).
- Bolle, A. et al. (2010). “The influence of changes in tidal asymmetry on residual sediment transport in the Western Scheldt”. In: *Continental Shelf Research* 30.8, pp. 871–882. ISSN: 0278-4343. DOI: <http://dx.doi.org/10.1016/j.csr.2010.03.001> (cit. on pp. 16–18, 20, 21, 24, 32, 43).
- Brown, J. M. and A. G. Davies (2007). “Flood/ebb tidal dominance in an estuary: Sediment transport and morphology”. In: *IAHR Symposium on River, Coastal and Estuarine Morphodynamics*. DOI: <https://doi.org/10.1201/NOE0415453639-c99> (cit. on p. 11).
- Cameron, W. M. and D. W. Pritchard (1963). “Estuaries”. In: *The Sea* 2, pp. 306–324 (cit. on pp. 1, 2, 4).
- Cancino, L. and R. Neves (1999). “Hydrodynamic and sediment suspension modelling in estuarine systems”. In: *Journal of Marine Systems* 22.2, pp. 105–116. ISSN: 0924-7963. DOI: [http://dx.doi.org/10.1016/S0924-7963\(99\)00035-4](http://dx.doi.org/10.1016/S0924-7963(99)00035-4) (cit. on p. 81).
- Cleveringa, J. (2013). *Samenhang ontwikkelingen tijd- en ruimteschalen*. Report. Afdeling Maritieme Toegang (cit. on p. 16).
- Coen, L. and Y. Plancke (2015). *Sedimentstrategie Beneden-Zeeschelde: Deelrapport 1 - Opzet, validatie en scenarioberekeningen fase 1 m.b.v. een numeriek sediment-transportmodel*. Report. Flanders Hydraulics Research (cit. on pp. 18, 37, 45).
- Davies, J. L. (1964). “A Morphogenetic Approach to World Shorelines”. In: *Zeitschrift für Geomorphologie* 8, p. 127 (cit. on pp. 3, 4, 81).
- Earth, Google (2016). “Satellite Images”. In: (cit. on p. 82).
- Eurostat (2017). “Maritime ports freight and passenger statistics”. In: URL: http://ec.europa.eu/eurostat/statistics-explained/index.php/Maritime_ports_freight_and_passenger_statistics#Rotterdam.2C_Antwerpen_and_Hamburg_stayed_top_ports (cit. on p. 16).
- FOD Economie Belgie (2011). “Uw gemeente in cijfers: Antwerpen”. In: URL: http://ng3.economie.fgov.be/ni/municipalkeyfigures/NL/slide/slide_11002.pdf (cit. on p. 16).
- haecon (2006). *Actualisatie van de zandbalans van de Zee- en Westerschelde*. Report. Soresma NV (cit. on pp. 18, 85).
- Hayes, M. O. (1975). “MORPHOLOGY OF SAND ACCUMULATION IN ESTUARIES: AN INTRODUCTION TO THE SYMPOSIUM A2 - Cronin, L. Eugene”. In: *Geology and Engineering*. Academic Press, pp. 3–22. ISBN: 978-0-12-197502-9. DOI: <https://doi.org/10.1016/B978-0-12-197502-9.50006-X> (cit. on pp. 3, 83).
- Hibma, A., H. J. de Vriend, and M. J. F. Stive (2003). “Numerical modelling of shoal pattern formation in well-mixed elongated estuaries”. In: *Estuarine, Coastal and*

- Shelf Science* 57.5–6, pp. 981–991. ISSN: 0272-7714. DOI: [https://doi.org/10.1016/S0272-7714\(03\)00004-0](https://doi.org/10.1016/S0272-7714(03)00004-0) (cit. on pp. 4, 24, 32, 81).
- Jeuken, M. C. J. L. and Z. B. Wang (2010). “Impact of dredging and dumping on the stability of ebb–flood channel systems”. In: *Coastal Engineering* 57.6, pp. 553–566. ISSN: 0378-3839. DOI: <https://doi.org/10.1016/j.coastaleng.2009.12.004> (cit. on p. 37).
- Lesser, G. R. et al. (2004). “Development and validation of a three-dimensional morphological model”. In: *Coastal Engineering* 51.8–9, pp. 883–915. ISSN: 0378-3839. DOI: <https://doi.org/10.1016/j.coastaleng.2004.07.014> (cit. on p. 23).
- Levinton, J. S. (1995). *Marine Biology: function, biodiversity, ecology*. New York: Oxford University Press. ISBN: 0195085736 (cit. on pp. 1, 3).
- McDowell, D. M. and B. A. O’Connor (1977). *Hydraulic Behaviour of Estuaries*. Civil Engineering Hydraulic Series. London: The Macmillan Press LTD, p. 292. ISBN: 978-1-349-01120-9 (cit. on pp. 1–3, 5, 6, 82).
- Nichols, M. M. (2013). “Response of Coastal Plain Estuaries to Episodic Events in the Chesapeake Bay Region”. In: *Nearshore and Estuarine Cohesive Sediment Transport*. Washington, D. C.: American Geophysical Union, pp. 1–20. ISBN: 0875902561 (cit. on p. 81).
- NOAA (2017). “Tides and Currents”. In: URL: <https://www.co-ops.nos.noaa.gov/faq2.html#26> (cit. on pp. 1, 3).
- Perillo, G. M. E. (1995). “Chapter 2 Definitions and Geomorphologic Classifications of Estuaries”. In: *Developments in Sedimentology*. Ed. by G. M. E. Perillo. Vol. Volume 53. Elsevier, pp. 17–47. ISBN: 0070-4571. DOI: [https://doi.org/10.1016/S0070-4571\(05\)80022-6](https://doi.org/10.1016/S0070-4571(05)80022-6) (cit. on pp. 1, 3).
- Pieters, T. (2002). *Het Scheldegetij*. Report. Rijksinstituut voor Kust en Zee (cit. on pp. 11, 17–21, 41, 43, 69, 73).
- Pritchard, D. W. (1967). “What is an Estuary: Physical Viewpoint”. In: *Estuaries*. Ed. by G. H. Lauff. Washington, D. C.: American Association for the Advancement of Science. Chap. 1, pp. 3–5 (cit. on pp. 3, 4, 81, 82).
- Rhode Island - Office of Marine Programs, University of (2001). “Discovery of Estuarine Environments (DOEE)”. In: (cit. on p. 82).
- Savenije, H. H. G. (2001). “A simple analytical expression to describe tidal damping or amplification”. In: *Journal of Hydrology* 243.3–4, pp. 205–215. ISSN: 0022-1694. DOI: [https://doi.org/10.1016/S0022-1694\(00\)00414-5](https://doi.org/10.1016/S0022-1694(00)00414-5) (cit. on pp. 2, 4, 9, 10, 23, 35, 36, 47, 67, 74, 75).
- (2005). *Salinity and tides in alluvial estuaries*. 1st ed. Amsterdam ; Elsevier. ISBN: 0080461611 9780080461618 (cit. on p. 4).
- Taal, M., Y. Meersschant, and G. Liek (2015). “Understanding the Tides Crucial for Joint Management of the Scheldt Estuary”. In: *IAHR World Congress* 36, pp. 7–10 (cit. on pp. 1, 11, 12, 17–19, 21, 41, 63, 69, 73).
- Turrell, W. R., J. Brown, and J. H. Simpson (1996). “Salt Intrusion and Secondary Flow in a Shallow, Well-mixed Estuary”. In: *Estuarine, Coastal and Shelf Science* 42.2, pp. 153–169. ISSN: 0272-7714. DOI: <http://dx.doi.org/10.1006/ecss.1996.0012> (cit. on pp. 81, 82).
- Uncles, R. J., R. C. A. Elliott, and S. A. Weston (1986). “Observed and computed lateral circulation patterns in a partly mixed estuary”. In: *Estuarine, Coastal and Shelf Science* 22.4, pp. 439–457. ISSN: 0272-7714. DOI: [http://dx.doi.org/10.1016/0272-7714\(86\)90067-3](http://dx.doi.org/10.1016/0272-7714(86)90067-3) (cit. on p. 81).
- US Department of Commerce and NOAA (2008). “NOAA’s Noational Ocean Service Education: Estuaries”. In: URL: http://oceanservice.noaa.gov/education/kits/estuaries/estuaries01_what.html (cit. on pp. 1, 83).

- Van der Wegen, M. and J. A. Roelvink (2012). “Reproduction of estuarine bathymetry by means of a process-based model: Western Scheldt case study, the Netherlands”. In: *Geomorphology* 179, pp. 152–167. ISSN: 0169-555X. DOI: <https://doi.org/10.1016/j.geomorph.2012.08.007> (cit. on pp. 2, 18).
- Van der Wegen, M., Z. B. Wang, et al. (2008). “Long-term morphodynamic evolution and energy dissipation in a coastal plain, tidal embayment”. In: *Journal of Geophysical Research: Earth Surface* 113.F3, n/a–n/a. ISSN: 2156-2202. DOI: <http://dx.doi.org/10.1029/2007JF000898> (cit. on pp. 2, 4, 32).
- Van Rijn, L. C. (2010). *Tidal phenomena in the Scheldt Estuary*. Report. Deltares (cit. on pp. 4, 6, 7, 10, 17, 19, 24, 25, 29–33, 35, 47, 69, 73, 87).
- Van Veen, J. et al. (2005). “Ebb and Flood Channel Systems in the Netherlands Tidal Waters”. In: *Journal of Coastal Research*, pp. 1107–1120. DOI: [10.2112/04-0394.1](https://doi.org/10.2112/04-0394.1) (cit. on pp. 11, 16).
- Vandenbruwaene, W. et al. (2013). *Interestuarine comparison: Hydrogeomorphology: Hydro- and geomorphodynamics of the TIDE estuaries Scheldt, Elbe, Weser and Humber*. Report. Flanders Hydraulics Research (cit. on pp. 10, 35, 36, 54).
- Vlaams Gewest - Afdeling Maritieme Toegang (2011). *Verruiming vaargeul Westerschelde*. Report. Vlaams Nederlands Schelde Commissie (VNSC). URL: <http://www.vnsc.eu/uploads/2011/01/wbraanvraagverruimingvaargeulwesterschelde.pdf> (cit. on p. 18).
- Winterwerp, J. C. (2013). *Response of tidal rivers to deepening and narrowing*. Report (cit. on pp. 11, 12, 18).

A Estuary Classifications

Pritchard (1967) introduced a broad classification from two perspectives: one based on geologic features, and one based on water circulation. These classifications are widely used in estuarine research as a good first assessment of what can be expected in an estuary (Cancino and Neves, 1999; Hibma, Vriend, and Stive, 2003; Nichols, 2013; Turrell, J. Brown, and Simpson, 1996; Uncles, Elliott, and Weston, 1986). Another widely used classification, used in conjunction with that of Pritchard, is the classification based on tidal regime proposed by J. L. Davies (1964).

Geologic classification

The geologic classification is based on the geometry of estuaries and is directly linked to the origin of the estuaries. Most estuaries came into existence at the end of the last ice age. Due to the melting of ice sheets the sea level rose significantly inundating low lying coastal areas in the process. Four distinct categories can be distinguished according to Pritchard (1967):

Coastal plain estuary These are low lying coastal river valleys that have been inundated during the end stage of the last ice age. A process of infilling has taken place over the last 10000 years filling the inundated basin with sediments from the river or by transport from the sea. These estuaries are characterized by shallow waters and gentle sloping beds and large alluvial plains within which distinct channel patterns start to develop.

Tectonic estuary Tectonic activity can cause large scale land subsidence or cracks in the earth's surface. When located near the coast they become inundated possibly creating an estuary in presence of fresh water discharge from rivers. This type of estuary is often very deep and surrounded by mountainous areas. Their shape can also be very irregular and is often very resistant to erosion of the geometry due to the rocky characteristic of the boundaries.

Bar-built estuaries At location where rivers enter the ocean at relatively shallow coastal areas bar-built estuaries may occur. Wave action and currents along the coast can create sand bars and barrier islands. The areas between barrier islands and the coast can become permanently blocked due to sedimentation effectively creating an estuary. These estuaries have the same characteristics as coastal plain estuaries in that they are quite shallow and have gentle slopes.

Fjord estuaries Fjord estuaries are located in mountainous regions with sharp slopes and steep valleys. Fjord valleys are created by the strong erosion of moving glaciers. When then glaciers melted away the remaining valley near the coast would become inundated creating an estuary.

An example of the four different types of estuaries is given in figure A.1

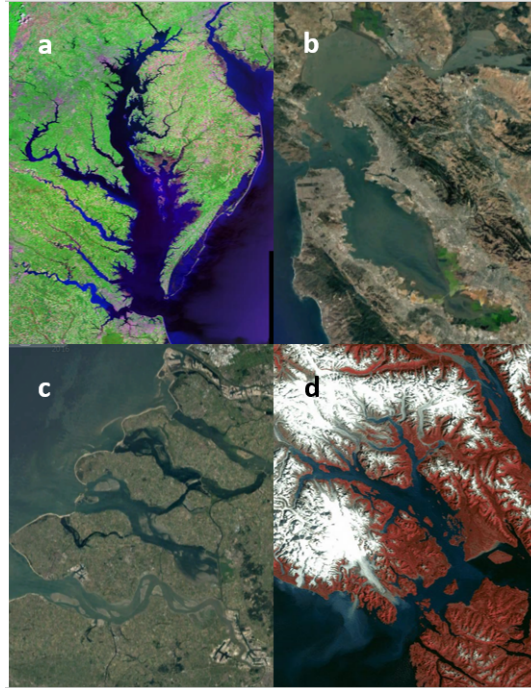


FIGURE A.1: Examples of the four estuary types across the world. a) Narragansett Bay, North-America is a coastal plain estuary, b) San Francisco Bay, North-America an example of a tectonic estuary, c) Scheldt estuary, Netherlands is a bar-built/coastal plain estuary and d) Glacier Bay, North-America an example of a Fjord estuary. (Rhode Island - Office of Marine Programs, 2001; Earth, 2016)

Classification Based on Water Circulation

Separate from the geologic classification a distinction can be made between estuaries based on the water circulation and mixing of salt and fresh water in an estuary. This distinction is an important one as the rate of stratification in an estuary has strong implications for the hydrodynamic and sediment transport processes (McDowell and O'Connor, 1977). Apart from geometry, the water circulation is also dependent on the tidal forcing and amount of river discharge. According to Pritchard (1967) there are 4 different types:

Salt wedge estuary Salt wedge estuaries are also known as highly stratified estuaries. This means that there is a distinct vertical gradient in the salt concentration through the water column. Salt wedge estuaries occur in locations where river discharge is high and salt intrusion only happens near the bottom of the estuary.

Partially mixed estuaries These estuaries are in between stratified and well mixed estuaries. There is still a noticeable salt gradient in the vertical direction of the water column, but the intrusion of salt is much further upstream compared to salt wedge estuaries. This occurs in estuaries where river discharge is still quite high compared to the tidal forcing, but is lower relative to a salt wedge estuary.

Well mixed estuaries These type of estuaries are also known as vertically well-mixed estuaries. In these estuaries the salt gradient is generally only in the horizontal direction of the estuary (Turrell, J. Brown, and Simpson, 1996). This type of water circulation happens in estuaries where the tidal forcing is

much stronger than the currents caused by river discharge. The turbulence caused by the tidal currents mix the fresh water throughout the water column.

Fjord-type estuaries Similar to salt wedge estuaries Fjord-type estuaries have a strong stratification caused by the shape of the estuary. Fjords are characterized by deep valleys with a high sill at the entrance. This traps salt sea water in the deep valley while fresh water flows over the top, regardless of the ratio between river discharge and tidal forcing.

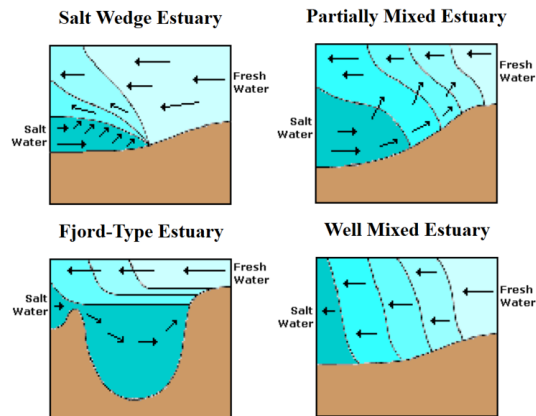


FIGURE A.2: Different types of mixing and water circulation for different types of estuaries. (US Department of Commerce and NOAA, 2008, Courtesy of Peter Cook)

Classification Based on Tidal Regime

According to Hayes (1975) there is very distinct difference between estuaries with varying tidal regimes. The effects were apparent on the distribution and presence of certain sediment grain sizes through the estuary. Based on observations three different regimes were recognized:

Microtidal estuaries Tidal ranges from 0 to 2 meter. In this type of class wave action and storm deposition are more important than in other estuaries.

Mesotidal estuaries Tidal range from 2 to 4 meter. This class has a noticeable increase in tidal-current-formed sand bodies and presence of tidal deltas.

Macrotidal estuaries Tidal range larger than 4 meter. This class of estuary often has a typical wide-mouthed funnel shape and contains more linear sand bodies than other estuaries.

B Dredging volumes

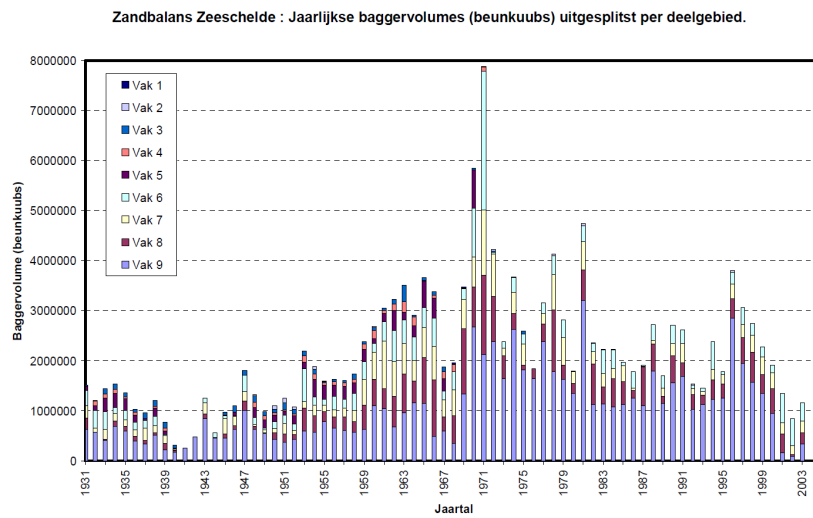


FIGURE B.1: Historical trend of dredging volume in Sea Scheldt ([haecon, 2006](#))

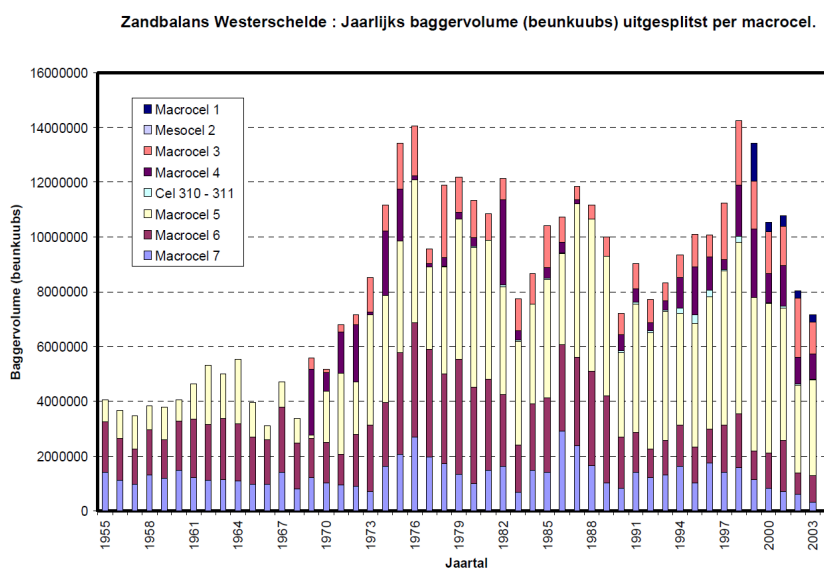


FIGURE B.2: Historical trend of dredging volume in Western Scheldt ([haecon, 2006](#))

C Van Rijn Model Validation

For the model setup first the prismatic cases by [Van Rijn, 2010](#) have been modeled and secondly the converging models have been set-up. The tidal ranges have been compared through visual inspection. Figures C.1 and C.2 show the modeled results from this study and the output by [Van Rijn, 2010](#) for the prismatic cases. This shows that the model closely resembles the output by Van Rijn. Unfortunately, the results for other variables in the model are off in some cases, as can be seen from table C.1.

The results show that flow speeds and discharge values are relatively accurate, but the phase lag at the mouth of the models varies significantly in prismatic case 2. In three of the models the phase lag is overestimated, but the results of case 1

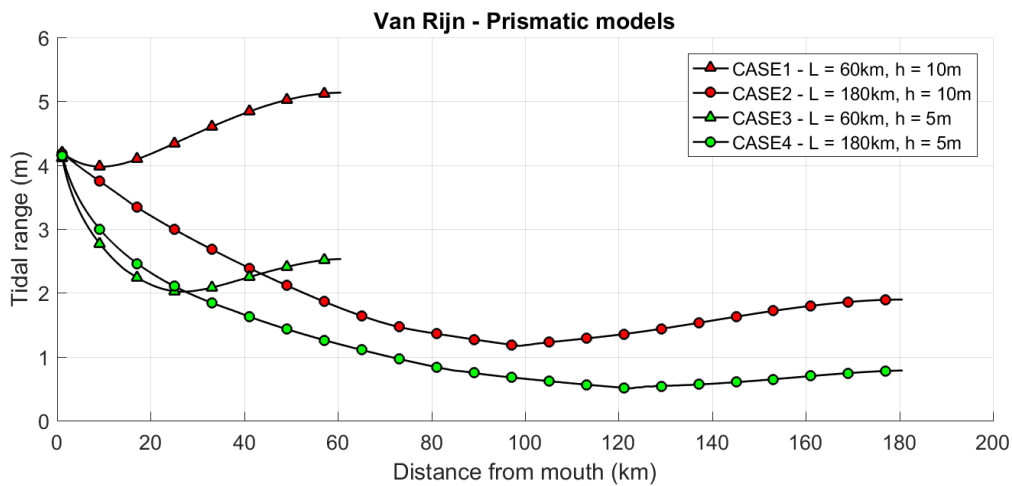


FIGURE C.1: Van Rijn prismatic cases modeled tidal range profiles

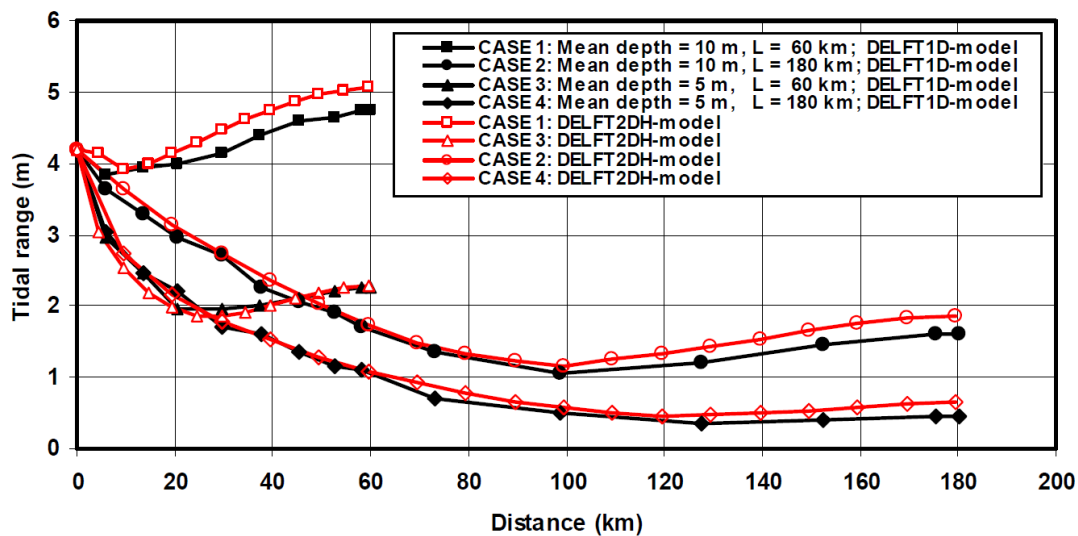


FIGURE C.2: Van Rijn prismatic cases tidal range outcome

CASE		Max flood	Max ebb	Max flood	Max ebb	Phase
		vel. [m/s]	vel [m/s]	Q [m ³ /s]	Q [m ³ /s]	lag [hours]
1	Van Rijn:	1.64	1.81	19000	17200	1.40
	Delft3D:	1.67	1.83	19222	17374	1.25
2	Van Rijn:	1.10	1.34	13200	11400	1.00
	Delft3D:	1.12	1.39	13271	11555	2.08
3	Van Rijn:	1.19	1.77	8200	6100	1.30
	Delft3D:	1.29	2,06	8799	7063	1.90
4	Van Rijn:	1.13	1.54	7600	5600	1.30
	Delft3D:	1.21	1.75	8164	6177	1.75

TABLE C.1: Results prismatic models Van Rijn at mouth of basin

show an underestimation of the phase lag. The run times of the prismatic models is relatively low (between 1 and 2 minutes) as a uniform coarse spatial grid could be used.

The converging cases by Van Rijn have also been implemented. The results are shown in figures C.3 and C.4. Similar to the prismatic cases, the water levels are in good agreement, however phase lag and maximum flow speeds occasionally show significant differences (Table C.2). The run times of the converging models are significantly longer than those of the prismatic models. Due to convergence of the lateral boundaries the cells become smaller toward the end of the system. For cases 1 to 4 this was a run time in the order of 5 to 10 minutes. However, for cases 5 and 6 the run times became in the order of 1 to 2 hours. This is caused by the increased number of computational cells, but also by the smaller time step needed to prevent numerical instability.

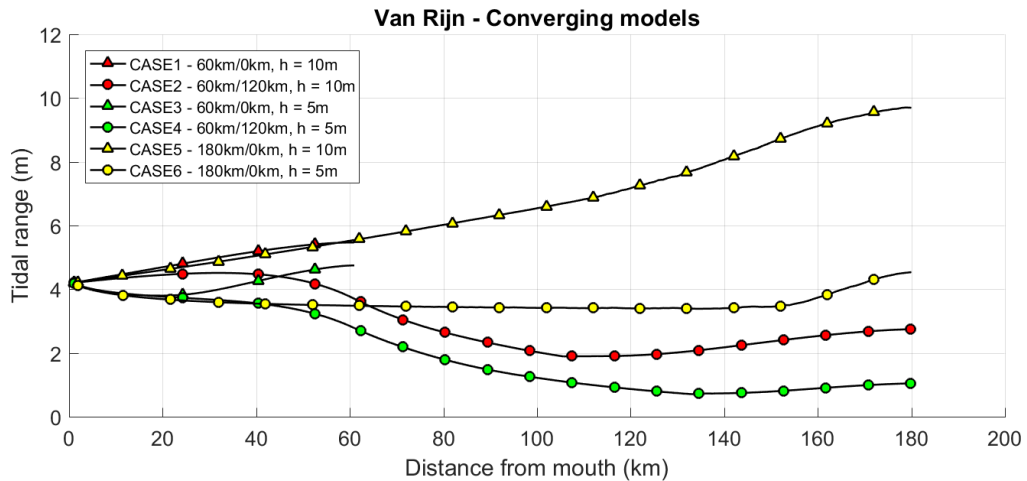


FIGURE C.3: Van Rijn converging cases modeled tidal range profiles

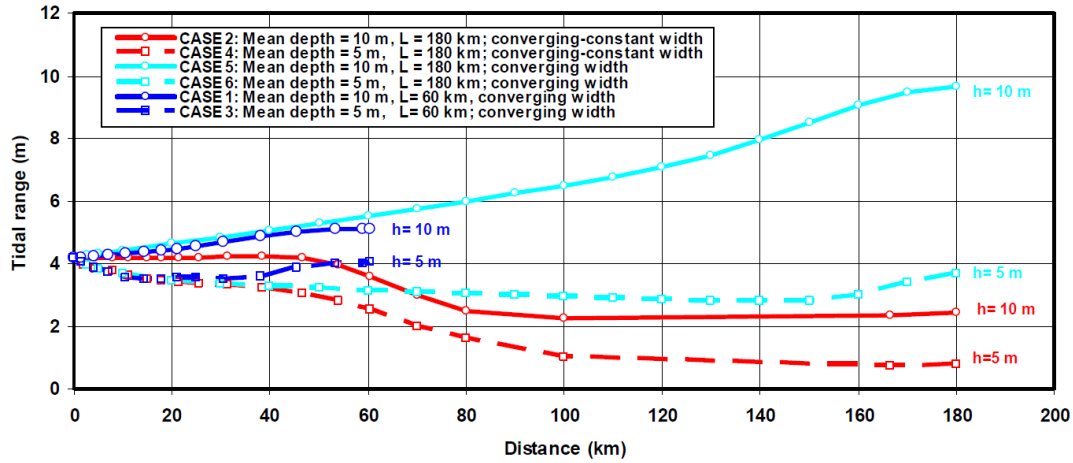


FIGURE C.4: Van Rijn converging cases tidal range outcome

CASE		Max flood vel. [m/s]	Max ebb vel. [m/s]	Max flood Q [m ³ /s]	Max ebb Q [m ³ /s]	Phase lag [hours]
1	Van Rijn:	0.83	0.72	214000	165000	3.00
	Delft3D:	0.95	0.76	236945	172355	0.00
2	Van Rijn:	0.73	0.73	192000	172000	2.70
	Delft3D:	0.83	0.78	212278	177068	0.58
3	Van Rijn:	0.99	1.24	154000	136000	2.10
	Delft3D:	1.18	1.42	176895	154076	1
4	Van Rijn:	0.97	1.15	150000	126000	2.10
	Delft3D:	1.14	1.32	171262	137288	0.83
5	Van Rijn:	0.82	0.81	215000	195000	2.50
	Delft3D:	0.95	0.86	241875	201306	0.42
6	Van Rijn:	0.96	1.16	150000	125000	1.70
	Delft3D:	1.13	1.29	170416	134677	0.83

TABLE C.2: Results converging models Van Rijn at mouth of basin

D Sedimentation and erosion maps

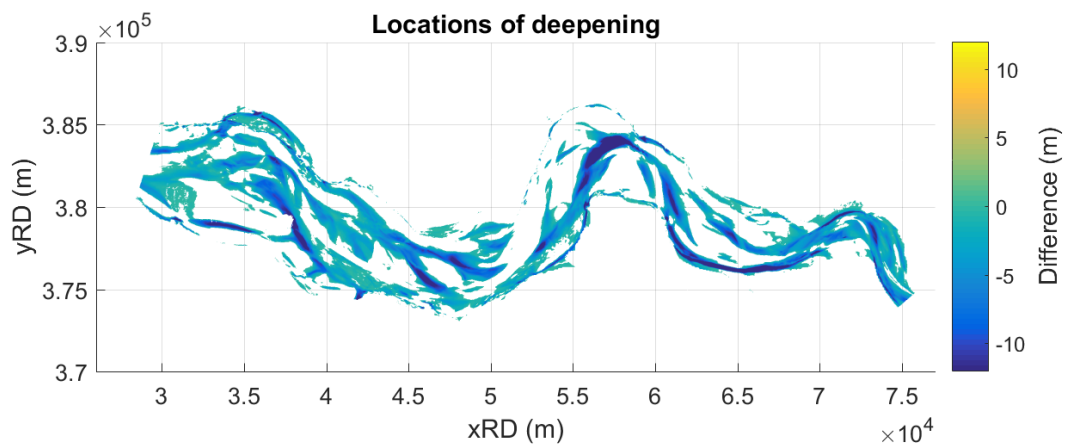


FIGURE D.1: Locations of deepening in the Western Scheldt estuary in 2005

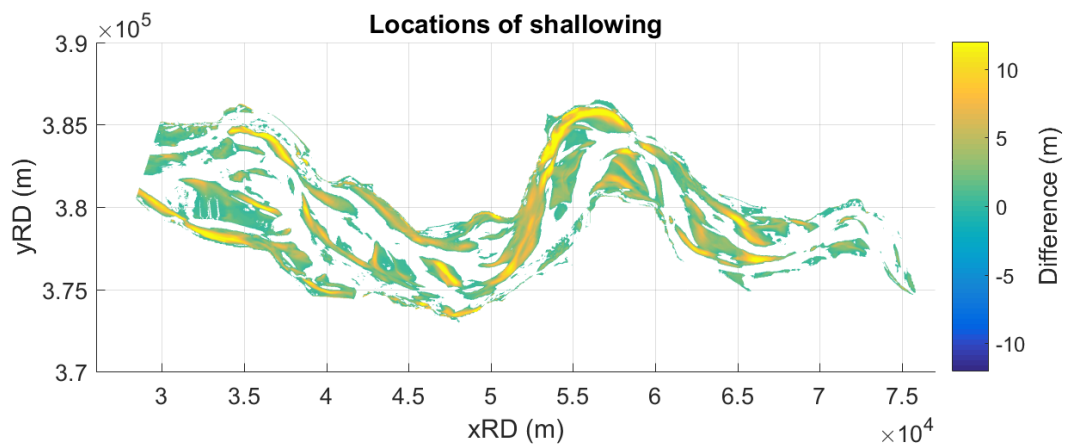


FIGURE D.2: Locations of shallowing in the Western Scheldt estuary in 2005

E Bathymetric cross-sections

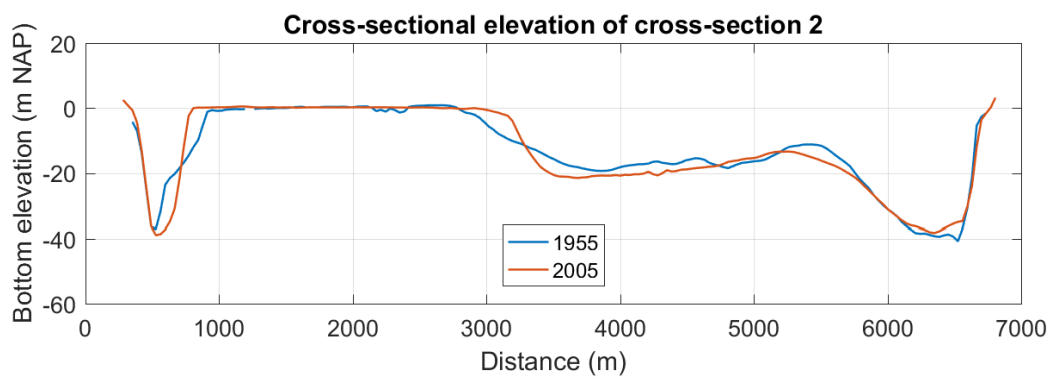
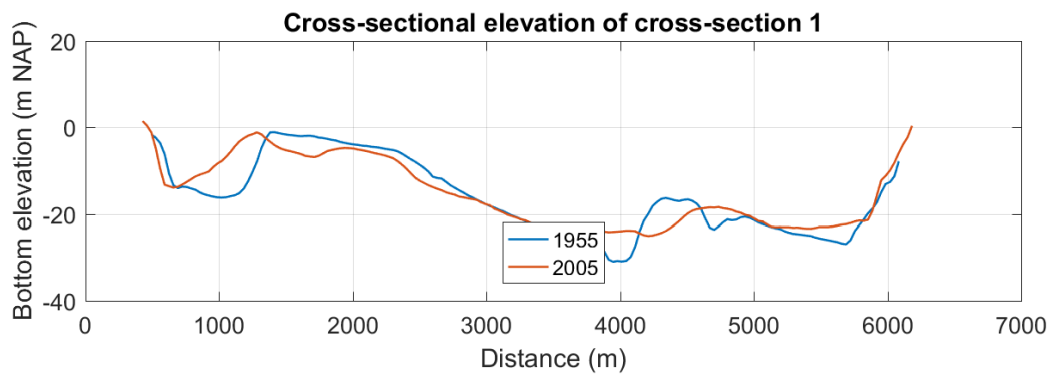
Cross section	Location [km]	Width [m]	Avg. depth [m]	Flow area [m ²]
1	2.97	5.59	16.12	90114
2	4.74	6.39	13.16	84070
3	6.83	8.78	9.07	79677
4	9.02	8.23	8.43	69330
5	11.28	5.75	15.71	90368
6	13.48	7.03	10.14	71239
7	15.41	7.30	8.68	63306
8	17.67	5.17	10.41	53810
9	20.21	4.73	10.85	51330
10	22.49	5.90	7.59	44814
11	25.56	4.41	10.65	47022
12	27.53	4.37	11.58	50570
13	29.35	4.31	9.74	41993
14	30.79	4.17	9.64	40214
15	32.06	4.62	9.19	42481
16	33.97	5.69	7.20	40976
17	35.56	4.68	8.93	41769
18	36.90	4.23	6.95	29404
19	38.27	3.58	10.59	37944
20	39.95	3.23	9.84	31813
21	41.42	4.12	7.75	31925
22	43.04	5.06	4.35	22049
23	44.43	5.02	4.46	22387
24	46.28	4.06	3.53	14359
25	48.07	3.05	4.08	12455
26	50.12	2.91	4.98	14496
27	52.35	2.68	7.19	19260
28	54.54	2.18	4.87	10609
29	55.72	1.75	5.99	10454

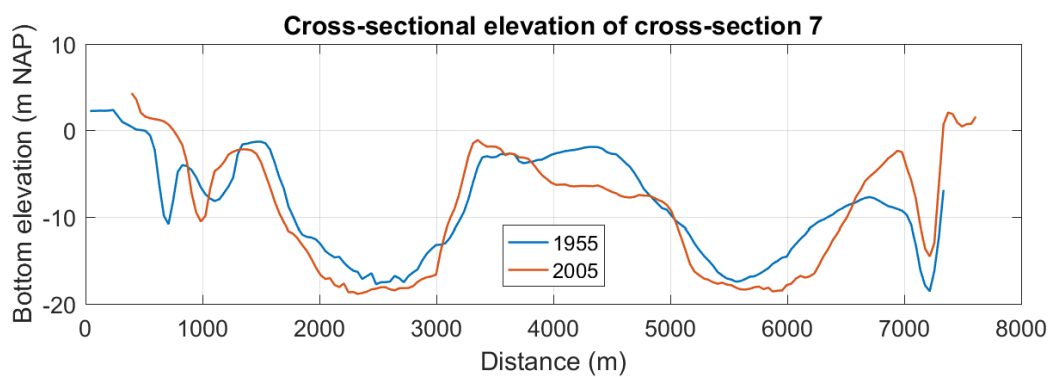
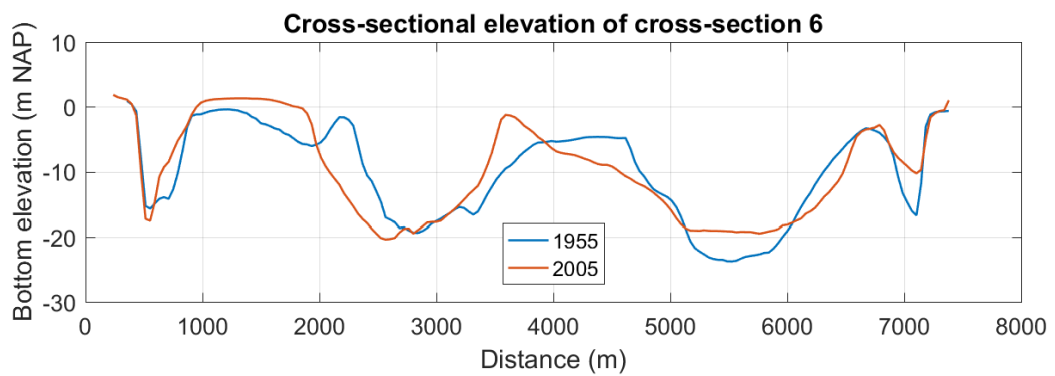
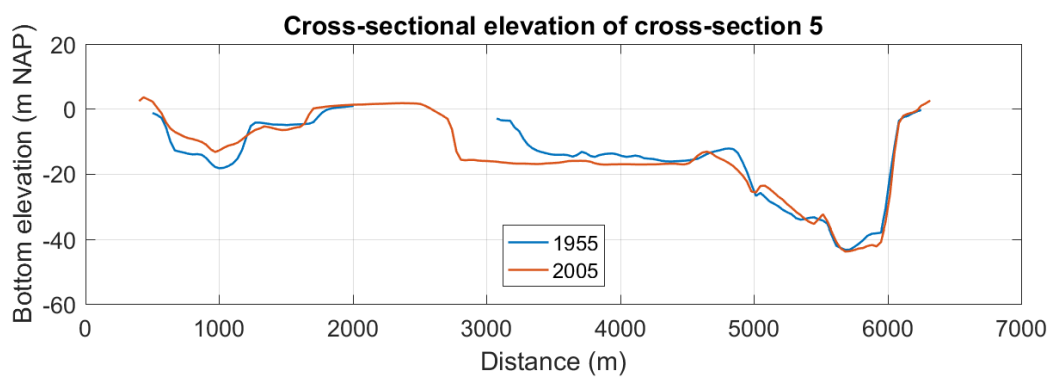
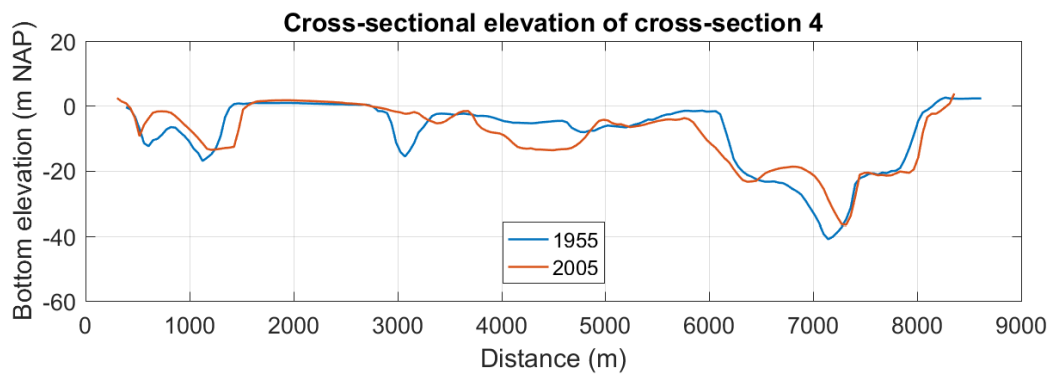
TABLE E.1: Bathymetric data cross-sections 1955

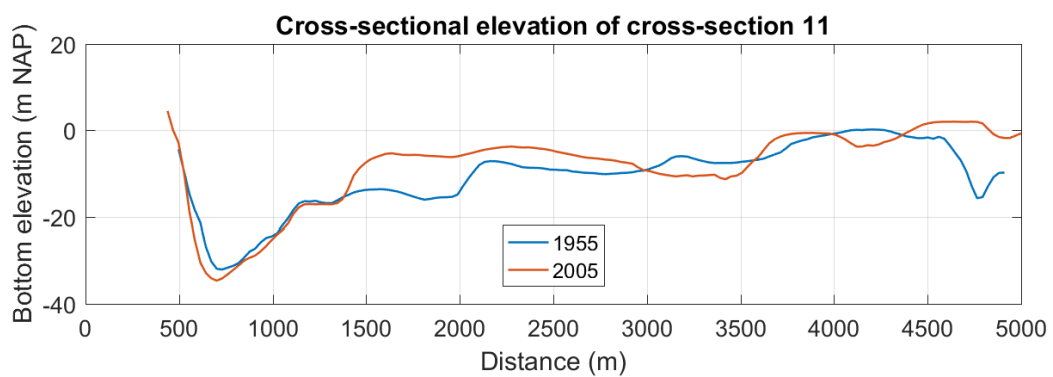
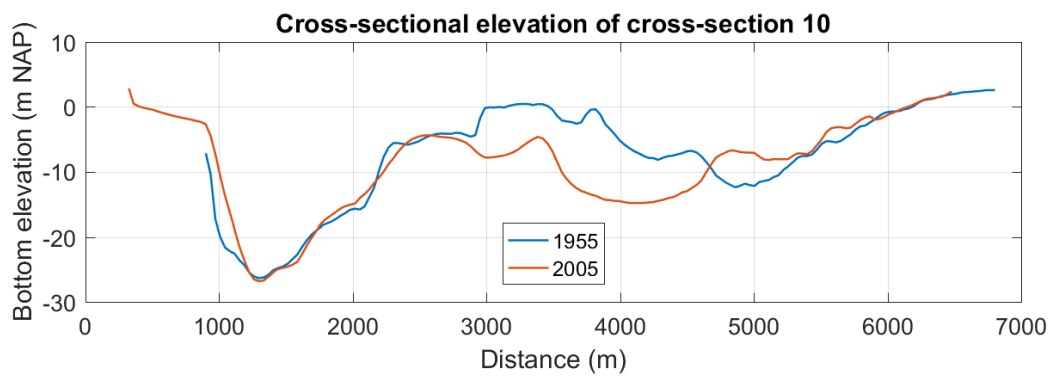
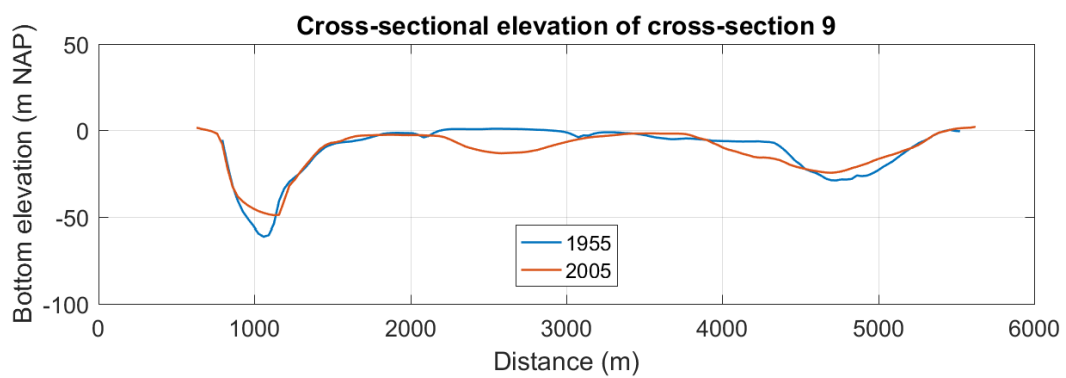
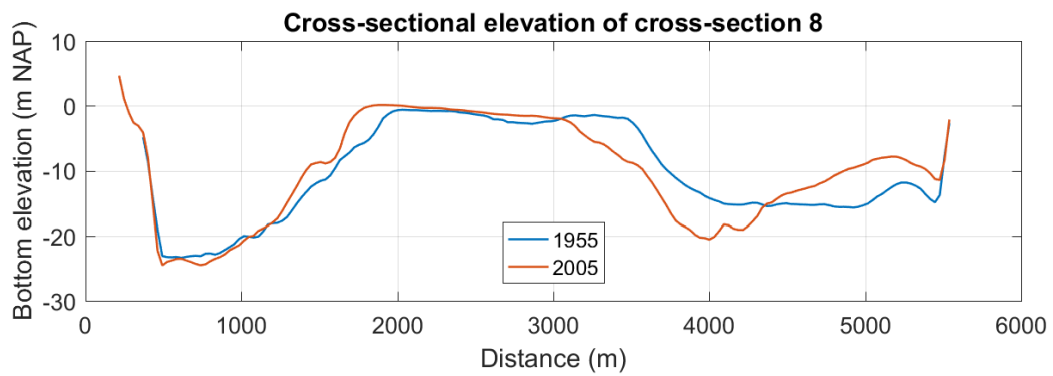
Cross section	Location [km]	Width [m]	Avg. depth [m]	Flow area [m ²]
1	2.97	5.76	15.22	87620
2	4.74	6.53	12.98	84727
3	6.83	8.51	8.83	75183
4	9.02	8.05	9.05	72898
5	11.28	5.92	13.79	81627
6	13.48	7.14	9.69	69256
7	15.41	7.30	9.23	67316
8	17.67	5.32	9.96	53035
9	20.21	5.00	11.76	58750
10	22.49	6.16	8.93	54974
11	25.56	4.56	8.27	37734
12	27.53	4.63	9.93	46014
13	29.35	4.74	8.26	39127
14	30.79	4.36	8.54	37256
15	32.06	4.84	8.40	40622
16	33.97	5.79	8.33	48211
17	35.56	4.96	6.92	34301
18	36.90	4.28	6.12	26201
19	38.27	3.76	10.08	37872
20	39.95	3.36	12.04	40434
21	41.42	4.39	7.46	32752
22	43.04	5.12	4.33	22172
23	44.43	4.66	4.90	22838
24	46.28	4.25	3.71	15764
25	48.07	3.60	5.64	20316
26	50.12	3.26	6.38	20818
27	52.35	2.87	7.88	22648
28	54.54	2.75	6.30	17317
29	55.72	2.08	7.04	14670

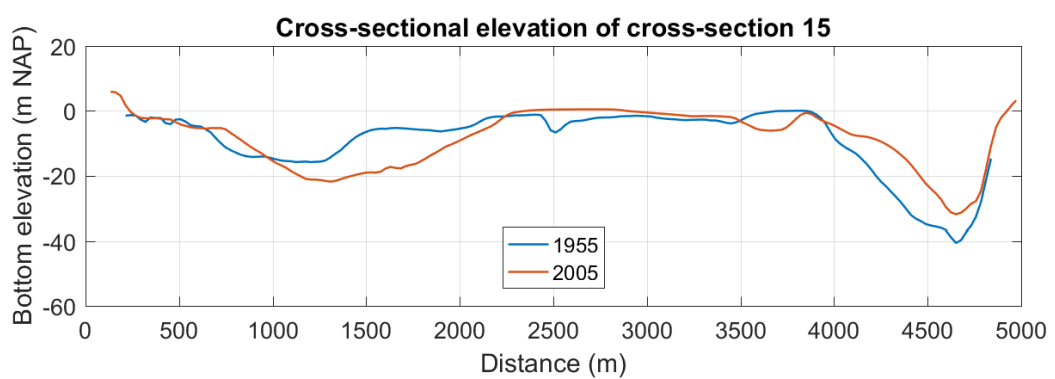
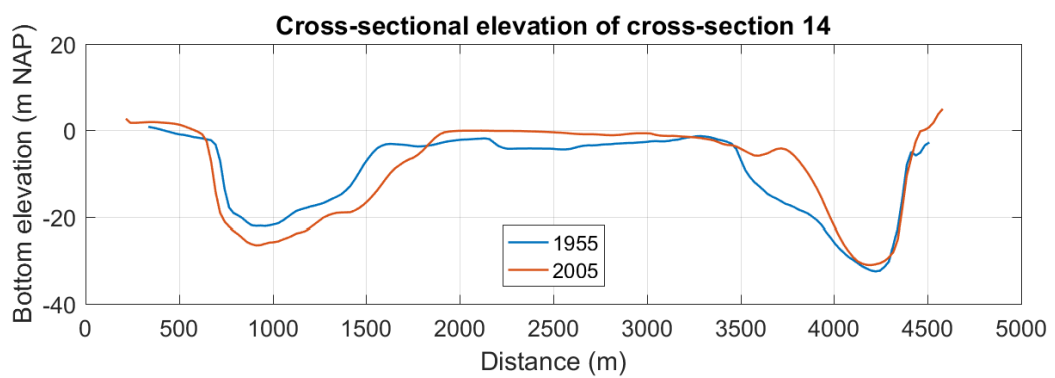
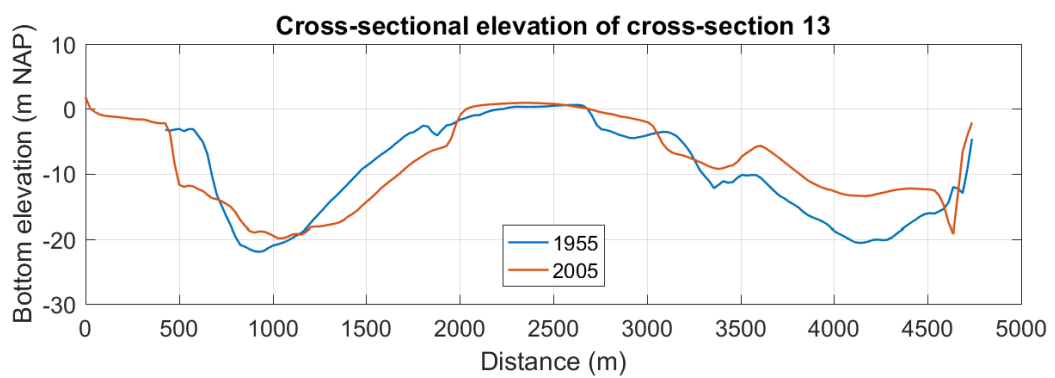
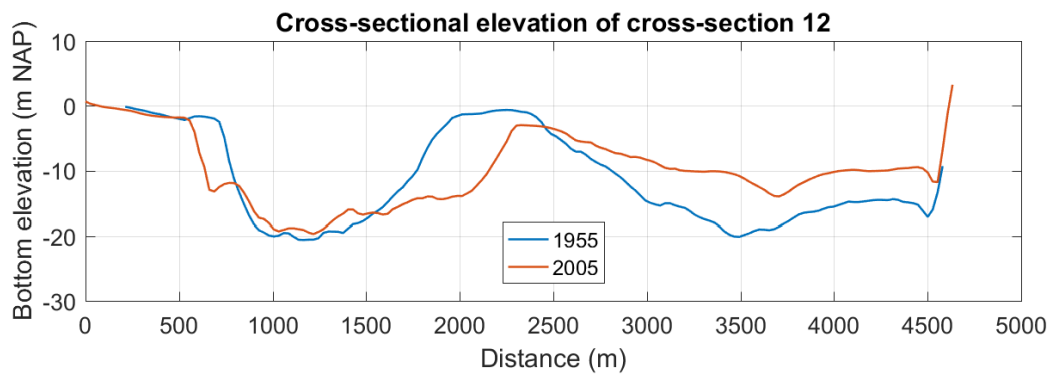
TABLE E.2: Bathymetric data cross-sections 2005

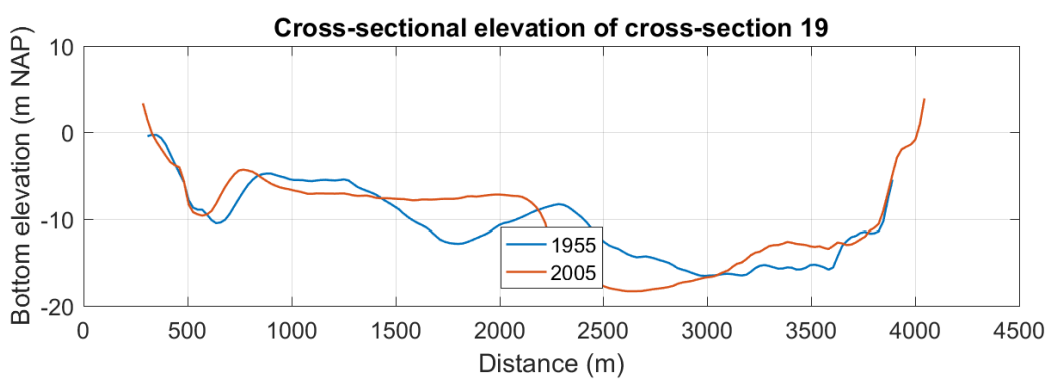
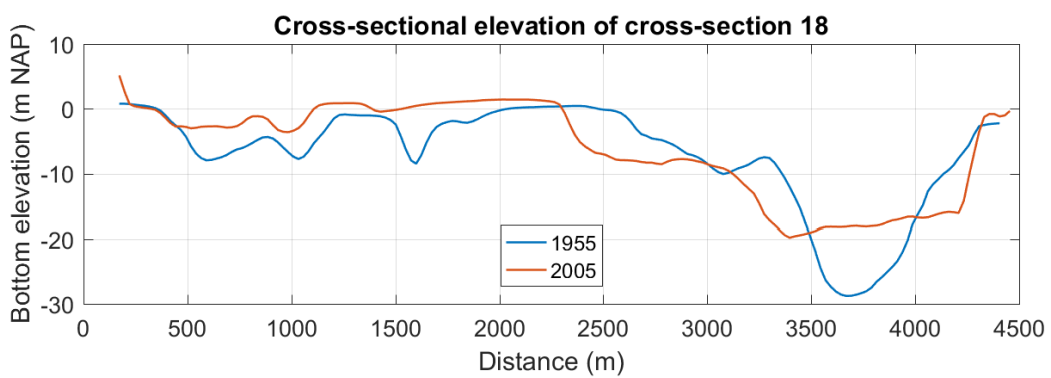
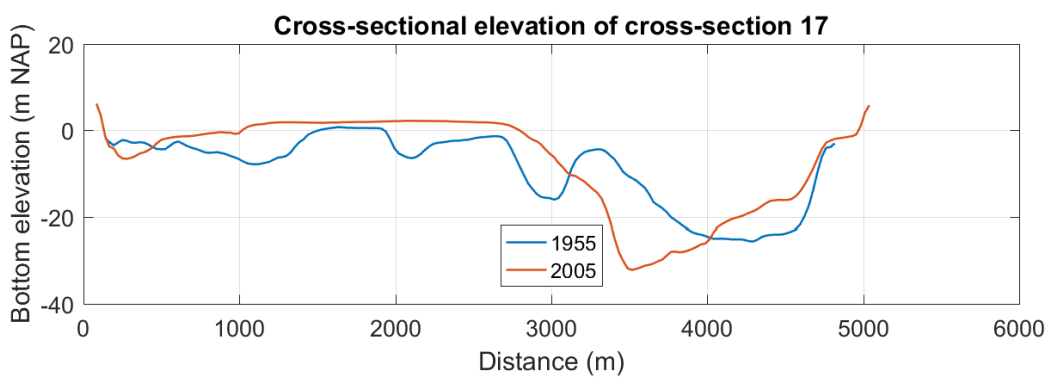
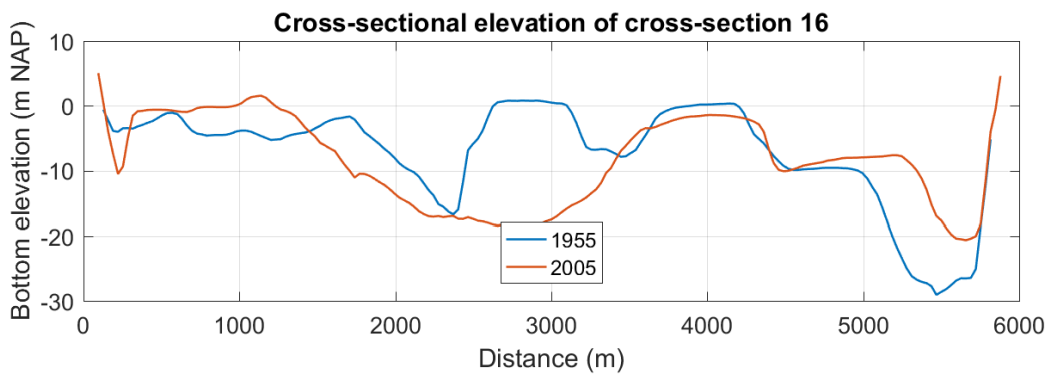
F Cross-sectional depths

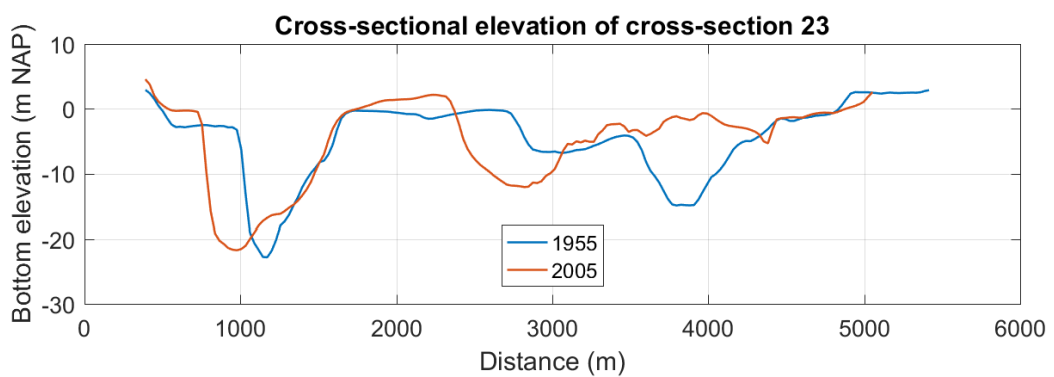
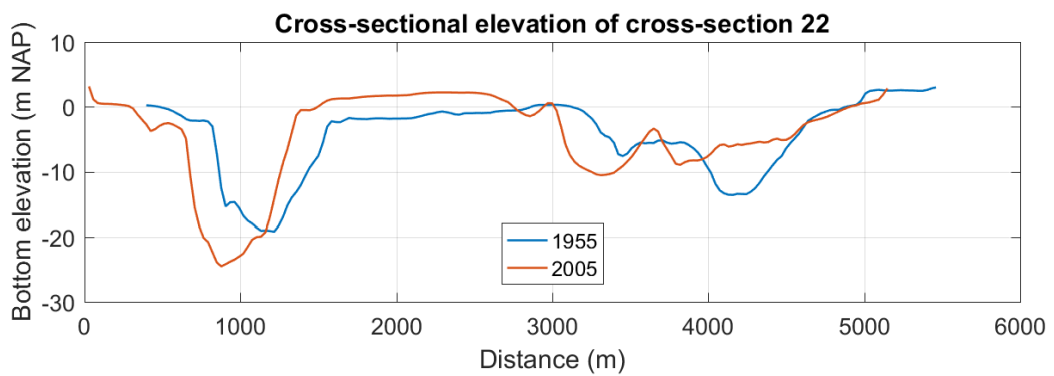
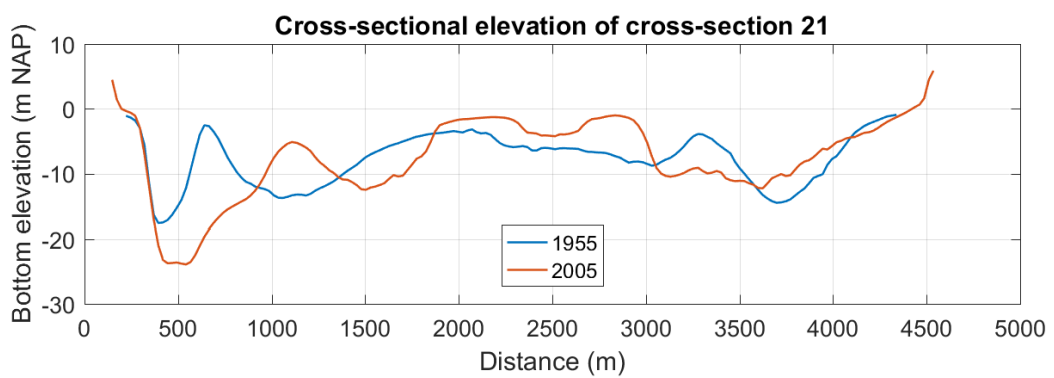
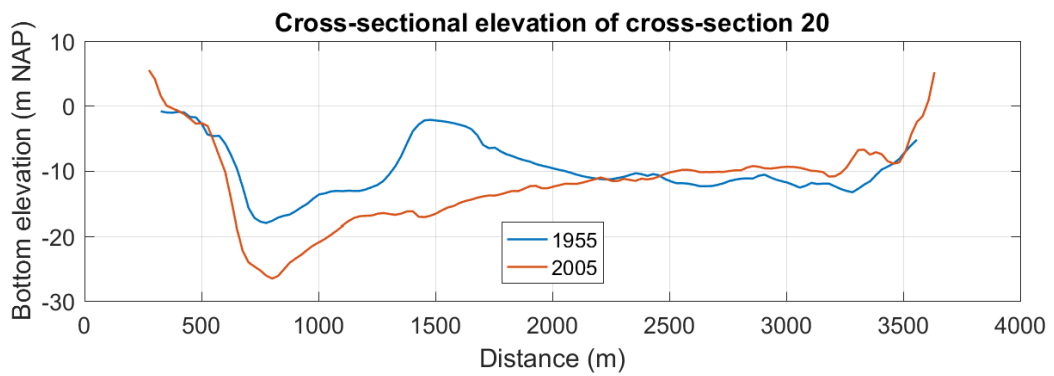


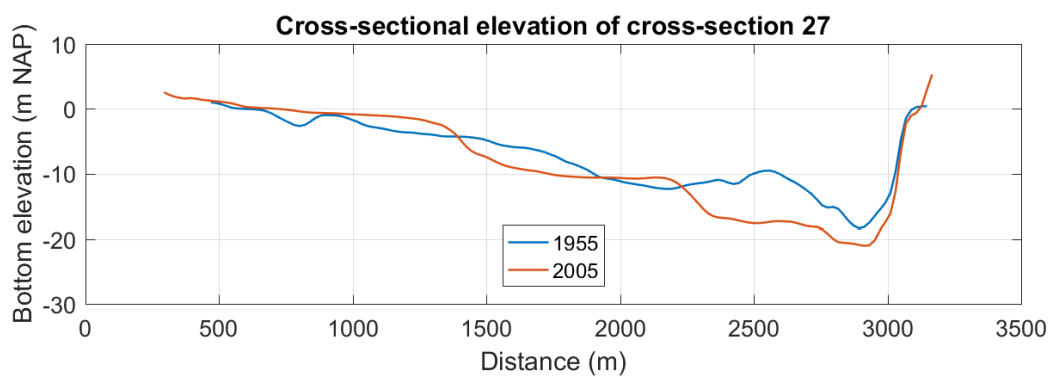
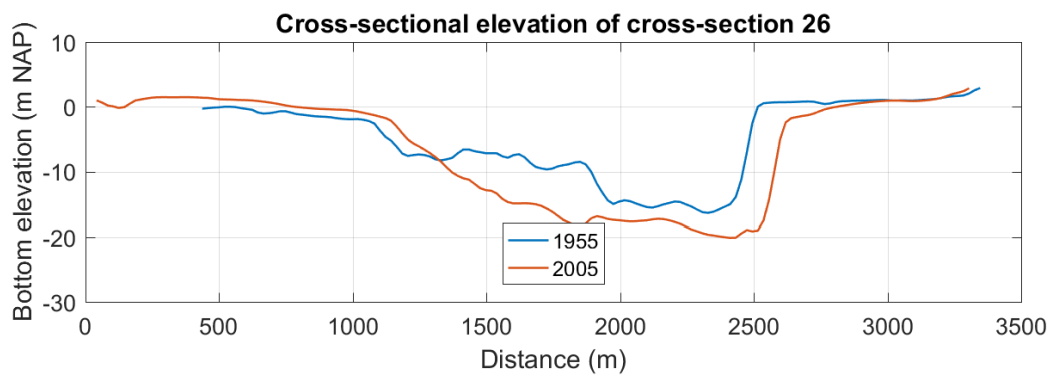
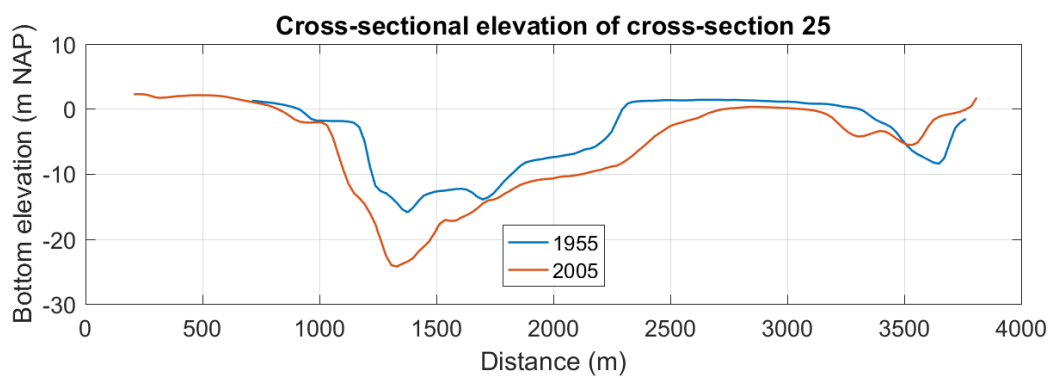
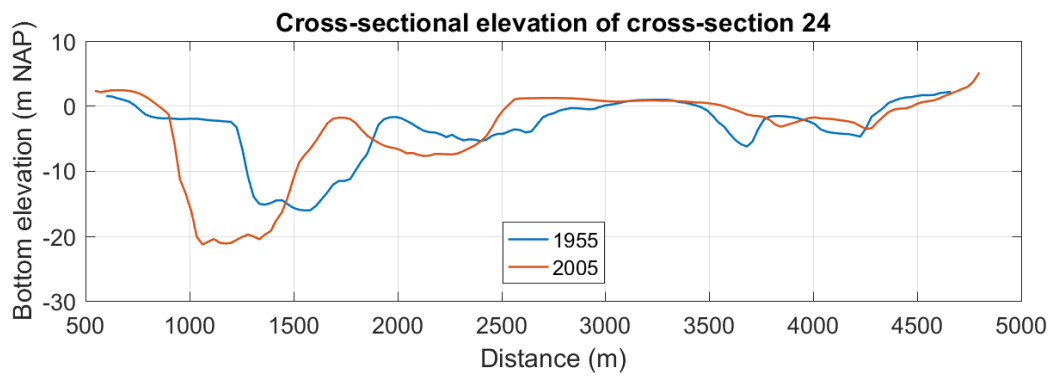


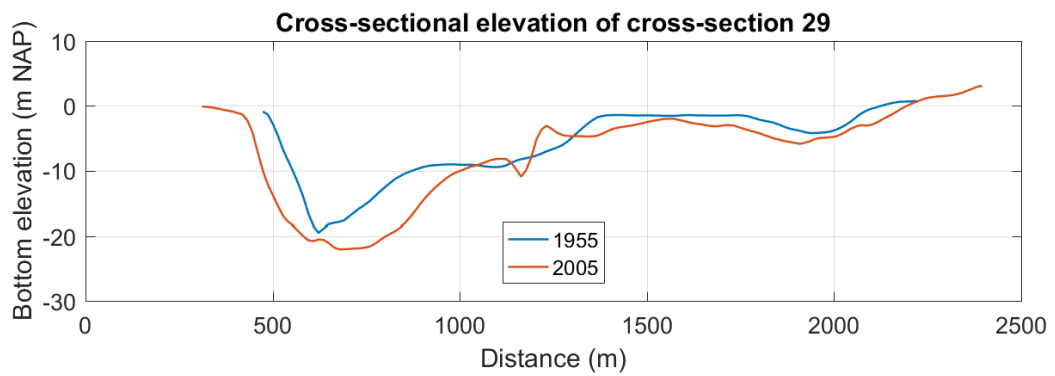
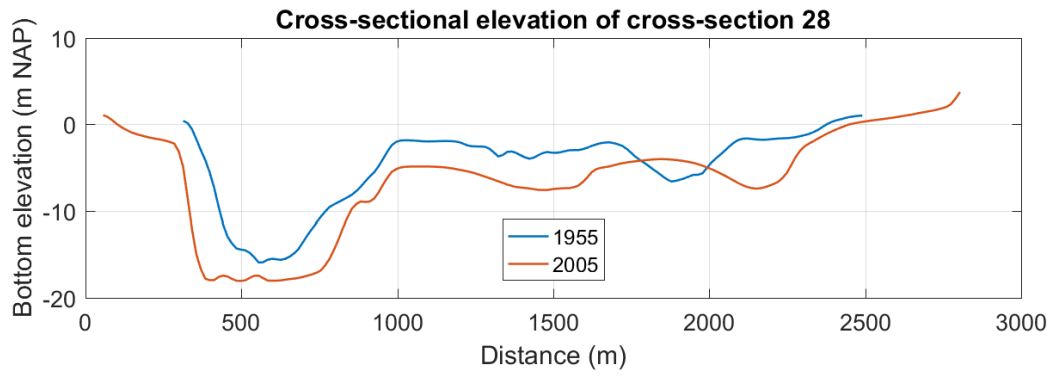












G Model output

Model	$H_{Vlissingen}$ [-]	$H_{rel,peak}$ [-]	$H_{rel,peak,x}$ [km]	RMSE	Validation peak value	Validation peak location
A11	4.38	1.042	21.87	0.597	0.722	0.240
A12	4.42	1.116	40.02	0.452	0.772	0.440
A13	4.45	1.227	62.98	0.268	0.849	0.692
A14	4.45	1.352	83.98	0.127	0.936	0.923
A21	4.37	1.038	20.91	0.600	0.718	0.230
A22	4.42	1.108	40.02	0.456	0.767	0.440
A23	4.44	1.215	62.98	0.272	0.841	0.692
A31	4.37	1.034	19.76	0.602	0.715	0.217
A32	4.42	1.100	38.92	0.461	0.761	0.428
A33	4.44	1.199	61.03	0.281	0.830	0.671
A41	4.36	1.029	18.75	0.604	0.712	0.206
A42	4.41	1.092	37.90	0.465	0.756	0.417
A43	4.43	1.186	60.02	0.287	0.821	0.660
A51	4.35	1.025	17.73	0.607	0.710	0.195
A52	4.40	1.084	36.98	0.470	0.750	0.406
A53	4.43	1.168	58.02	0.301	0.808	0.638
A54	4.43	1.282	79.98	0.149	0.887	0.879
B1	4.40	1.785	152.99	0.304	1.236	1.681
B2	4.41	1.715	152.99	0.273	1.187	1.681
B3	4.42	1.624	152.99	0.236	1.124	1.681
B4	4.43	1.519	152.99	0.196	1.051	1.681
B5	4.44	1.398	152.99	0.157	0.968	1.681
B6	4.44	1.354	83.98	0.127	0.937	0.923
B7	4.43	1.329	82.00	0.119	0.920	0.901
B8	4.39	1.282	79.98	0.150	0.887	0.879
B9	4.30	1.206	79.98	0.214	0.835	0.879
B10	4.14	1.098	76.03	0.301	0.760	0.835
B11	3.88	1.064	-9.99	0.405	-0.737	0.11
C1	4.46	1.26	73.00	0.259	0.872	0.802
C2	4.42	1.335	78.98	0.229	0.924	0.868
C3	4.46	1.304	77.98	0.168	0.903	0.857
C4	4.42	1.341	85.01	0.106	0.928	0.934
D1	4.45	1.427	83.98	0.091	0.988	0.923
D2	4.49	1.445	85.01	0.083	1.000	0.934
D3	4.38	1.392	86.01	0.211	0.963	0.945
D4	4.37	1.368	88.99	0.102	0.947	0.978

Model	$H_{Vlissingen}$ [-]	$H_{rel,peak}$ [-]	$H_{rel,peakx}$ [km]	RMSE	Validation peak value	Validation peak location
E1	4.38	1.242	74.00	0.255	0.871	0.813
E2	4.38	1.213	53.03	0.270	0.850	0.583
E3	4.38	1.202	51.96	0.303	0.843	0.571
E4	4.38	1.192	51.96	0.368	0.836	0.571
E5	4.38	1.310	79.98	0.219	0.919	0.879
E6	4.38	1.298	81.00	0.221	0.911	0.890
E7	4.38	1.271	82.00	0.226	0.892	0.901
E8	4.38	1.217	51.96	0.243	0.853	0.571
E9	4.35	1.179	88.00	0.268	0.827	0.967
E10	4.35	1.347	83.98	0.210	0.945	0.923

Model	Flood phase [hours]	Ebb phase [hours]	Wave cel. [m/s]	Phase lag [degrees]	Max flood vel. [m/s]	Max ebb vel. [m/s]
A11	5.15	6.85	13	15	1.23	1.39
A12	5.06	6.94	18	10	1.43	1.49
A13	4.96	7.04	19	8	1.68	1.50
A14	4.94	7.06	20	10	1.93	1.50
A21	5.19	6.81	12	15	1.22	1.38
A22	5.04	6.96	16	10	1.42	1.47
A23	5.00	7.00	18	10	1.67	1.49
A31	5.17	6.83	12	18	1.22	1.36
A32	5.02	6.98	16	13	1.41	1.45
A33	4.98	7.02	16	13	1.65	1.46
A41	5.17	6.83	12	18	1.21	1.34
A42	5.06	6.94	14	13	1.40	1.43
A43	4.98	7.02	15	13	1.64	1.45
A51	5.15	6.85	11	20	1.20	1.33
A52	5.02	6.98	14	15	1.39	1.41
A53	5.02	6.98	15	15	1.60	1.42
A54	4.98	7.02	15	15	1.87	1.49
B1	5.60	6.40	63	5	2.02	1.7
B2	5.46	6.54	65	5	2.03	1.69
B3	5.31	6.69	65	5	2.02	1.66
B4	5.19	6.81	38	5	2	1.62
B5	5.06	6.94	25	8	1.97	1.57
B6	4.94	7.06	20	10	1.93	1.5
B7	4.79	7.21	16	13	1.88	1.4
B8	4.65	7.35	13	15	1.81	1.27
B9	4.48	7.48	7.3	20	1.7	1.12
B10	NaN	NaN	9.2	23	1.55	1.14
B11	NaN	NaN	4.9	25	1.34	1.24
C1	4.60	7.40	14	10	1.61	1.07
C2	4.92	7.08	36	5	1.53	1.25
C3	4.71	7.29	16	10	1.67	1.19
C4	5.08	6.92	63	5	1.59	1.4
D1	5.65	6.35	29	15	1.77	1.58
D2	5.48	6.52	22	15	1.76	1.53
D3	5.69	6.31	Inf	10	1.47	1.57
D4	5.54	6.46	65	10	1.46	1.65

Model	Flood phase [hours]	Ebb phase [hours]	Wave cel. [m/s]	Phase lag [degrees]	Max flood vel. [m/s]	Max ebb vel. [m/s]
E1	4.98	7.02	34	5	1.47	1.14
E2	4.98	7.02	33	5	1.46	1.11
E3	4.94	7.06	32	5	1.43	1.30
E4	4.96	7.04	31	5	1.38	1.64
E5	4.98	7.02	36	5	1.51	1.24
E6	5.02	6.98	35	5	1.52	1.23
E7	4.98	7.02	35	5	1.52	1.46
E8	5.00	7.00	33	5	1.71	1.89
E9	5.40	6.60	57	8	1.82	2.17
E10	5.52	6.48	59	8	1.96	2.26